

AD-A039 033

TECHNOLOGY INC SAN ANTONIO TEX LIFE SCIENCES DIV
RESEARCH ON THE OCULAR EFFECTS OF LASER RADIATION.(U)
FEB 74 V E SANDERS, J A ZUCILICH

F/G 6/18

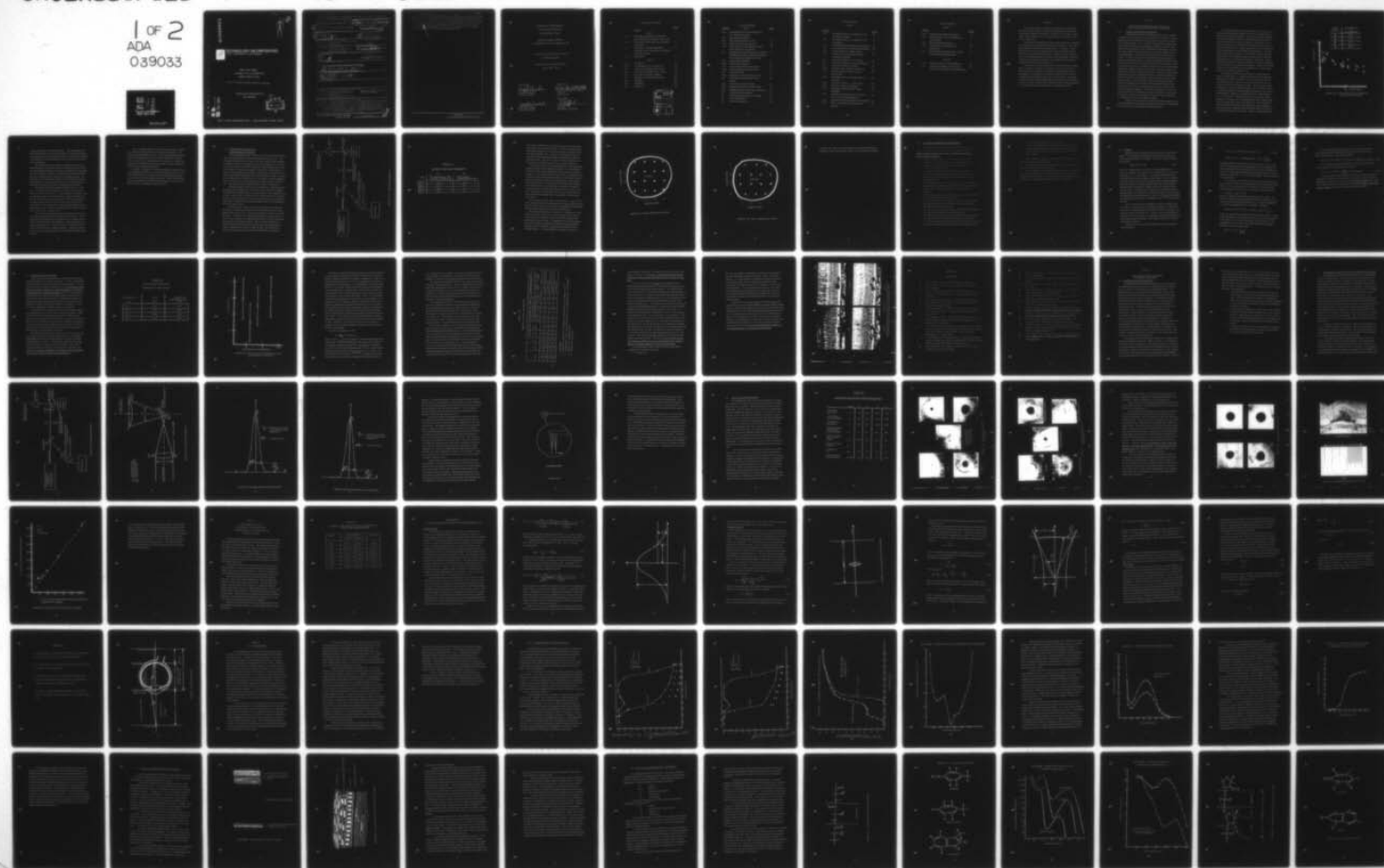
UNCLASSIFIED

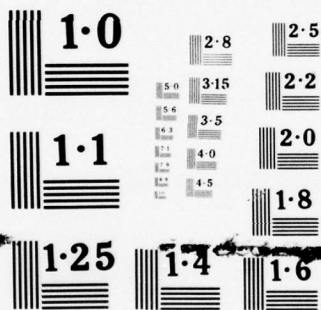
TI-74-0561-01

F41609-73-C-0017

NL

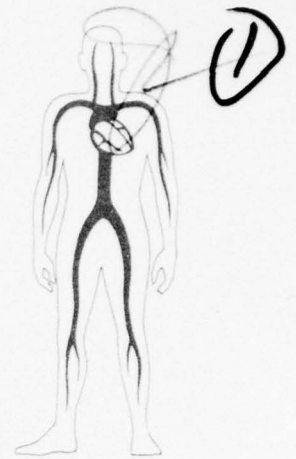
1 OF 2
ADA
039033





NATIONAL BUREAU OF STANDARDS
MICROCOPY RESOLUTION TEST CHART

AD A 039033



TECHNOLOGY INCORPORATED
LIFE SCIENCES DIVISION

ANNUAL REPORT NUMBER 1

15 FEBRUARY 1973 to 15 FEBRUARY 1974

CONTRACT F41609-73-C-0017

Approved for public release; distribution unlimited.

RESEARCH ON THE OCULAR EFFECTS OF
LASER RADIATION

AD No. _____
DDC FILE COPY



8531 N. NEW BRAUNFELS AVE. • SAN ANTONIO, TEXAS 78217

UNCLASSIFIED

SECURITY CLASSIFICATION OF THIS PAGE (When Data Entered)

| REPORT DOCUMENTATION PAGE | | READ INSTRUCTIONS BEFORE COMPLETING FORM |
|--|---|---|
| 1. REPORT NUMBER Technology Incorporated 74-0561-01 | 2. GOVT ACCESSION NO. (9) Rept. no. 1 (Annual) | 3. RESEARCH CATALOG NUMBER |
| 4. TITLE (and Subtitle) RESEARCH ON THE OCULAR EFFECTS OF LASER RADIATION. | 5. TYPE OF REPORT & PERIOD COVERED FIRST ANNUAL REPORT 15 Feb 73 - 15 Feb 74 | 6. PERFORMING ORG. REPORT NUMBER |
| 7. AUTHOR(s) (10) V. E. SANDERS Ph.D. J. A. ZUCCHICH Ph.D. | 8. CONTRACT OR GRANT NUMBER(s) (15) F41679-73-C-0017 | |
| 9. PERFORMING ORGANIZATION NAME AND ADDRESS Technology Incorporated, Life Sciences Division 8531 N New Braunfels Avenue San Antonio, Texas 78217 | 10. PROGRAM ELEMENT, PROJECT, TASK AREA & WORK UNIT NUMBERS 62202F 6301-00-34 | |
| 11. CONTROLLING OFFICE NAME AND ADDRESS USAF School of Aerospace Medicine (PAL) Aerospace Medical Division (AFSC) Brooks Air Force Base, Texas 78235 | 12. REPORT DATE (11) 15 February 1974 | 13. NUMBER OF PAGES 117 |
| 14. MONITORING AGENCY NAME & ADDRESS (if different from Controlling Office) (12) 127 P.5 | 15. SECURITY CLASS. (of this report) Unclassified | 15a. DECLASSIFICATION/DOWNGRADING SCHEDULE |
| 16. DISTRIBUTION STATEMENT (of this Report) Approved for public release; distribution unlimited. (14) TI-74-0561-01 | | |
| 17. DISTRIBUTION STATEMENT (of the abstract entered in Block 20, if different from Report) (16) 6301 / (17) 00 | | |
| 18. SUPPLEMENTARY NOTES | | |
| 19. KEY WORDS (Continue on reverse side if necessary and identify by block number) Laser-induced retinal damage/rhesus monkey Damage thresholds/wavelength dependence Lesion size vs spot size Chronological development of retinal damage UV absorption/rhesus monkey Cellular & molecular composition of the cornea. | | |
| 20. ABSTRACT (Continue on reverse side if necessary and identify by block number) This report is divided into two parts, both of which are concerned with research on the ocular hazards of laser irradiation. Part I deals with radiation in the visible wavelength range. It contains: a completed study on the size of retinal lesions induced by laser light as a function of the laser beam parameters; a study, partially complete, of the wavelength dependence of threshold retinal damage; two studies in progress on histological results; and an appendix on laser beam retinal spot size in the emmetropic eye. (Cont) | | |

DD FORM 1 JAN 73 1473

EDITION OF 1 NOV 65 IS OBSOLETE

401 650

UNCLASSIFIED

SECURITY CLASSIFICATION OF THIS PAGE (When Data Entered)

UNCLASSIFIED

SECURITY CLASSIFICATION OF THIS PAGE(When Data Entered)

AND

→ Part II deals with ocular hazards from ultraviolet (UV) laser irradiation. It contains: a summary of literature surveys on absorption characteristics and molecular composition of components of the eye; development of a preliminary quantitative model relating the extent of photochemical damage to laser beam characteristics; and suggestions for experiments to define the nature of ocular hazards from UV laser radiation and aid in the development of a quantitative model for laser-induced corneal and lenticular damage.

UNCLASSIFIED

SECURITY CLASSIFICATION OF THIS PAGE(When Data Entered)

TECHNOLOGY INCORPORATED

LIFE SCIENCES DIVISION

SAN ANTONIO, TEXAS

ANNUAL REPORT NUMBER 1

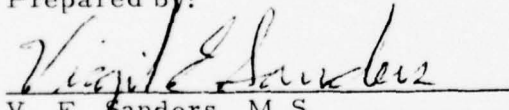
15 FEBRUARY 1973 to 15 FEBRUARY 1974

RESEARCH ON THE EYE EFFECTS OF
LASER RADIATION

USAF School of Aerospace Medicine

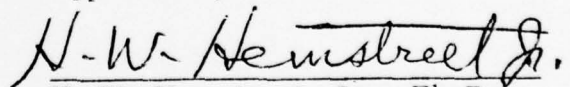
Brooks AFB, Texas

Prepared by:



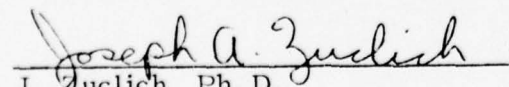
V. E. Sanders, M.S.
Associate Principal
Research Scientist

Approved by:

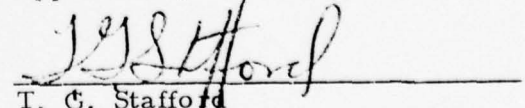


H. W. Hemstreet, Jr., Ph.D.
Manager
Laser Section

Approved by:



J. A. Zuclich, Ph.D.
Associate Principal
Research Scientist



T. C. Stafford
Manager
San Antonio Laboratory

TABLE OF CONTENTS

| | | <u>PAGE</u> |
|------|---|-------------|
| | Abstract | v |
| | PART I | |
| I-A | Wavelength Dependence on Threshold | 1 |
| | Ocular Damage from Visible Laser Light | |
| I-B | Laser Beam Retinal Spot Size vs Retinal Lesion Size | 29 |
| I-C | Two Studies Involving Histological Evaluation of the Chronologic Development of Retinal Lesions | 48 |
| I-D | Supplement I | 50 |
| | PART II | |
| II-A | Introduction | 62 |
| II-B | UV Absorption by the Primate Eye | 65 |
| II-C | Cellular Composition of the Cornea | 75 |
| II-D | Molecular Composition of the Cornea | 80 |
| II-E | Molecular Electronic Excitation | 92 |
| II-F | Summary of Proposed Experiments | 102 |
| II-G | Appendix I | 106 |
| II-H | Appendix II | 111 |
| II-I | References | 116 |

| | | |
|---------------------------------|--------------------|-------------------------------------|
| ACCESSION for | | |
| NTIS | White Section | <input checked="" type="checkbox"/> |
| DDC | Buff Section | <input type="checkbox"/> |
| UNANNOUNCED | | <input type="checkbox"/> |
| JUSTIFICATION | | |
| BY | | |
| DISTRIBUTION/AVAILABILITY CODES | | |
| DISL | AVAL. INFO/SPECIAL | |
| A | | |

LIST OF FIGURES

| <u>FIGURE</u> | <u>PART I</u> | <u>PAGE</u> |
|---------------|--|-------------|
| I-A1 | Comparable ED-50 determinations for four visible wavelengths | 3 |
| I-A2 | Experimental Apparatus | 7 |
| I-A3 | Map of exposure site on retina | 10 |
| I-A4 | Map of exposure site on retina | 11 |
| I-A5 | ED-50 values for 40 millisecond single pulse exposure to the macula | 20 |
| I-A6 | Histologically prepared sections of minimal ophthalmoscopically visible retinal damage from different wavelength laser light | 26 |
| I-B1 | Experimental Apparatus | 32 |
| I-B1a | Experimental Apparatus | 33 |
| I-B2 | Gaussian field intensity distribution | 34 |
| I-B2a | Gaussian field intensity distribution | 35 |
| I-B3 | Calibrated Probe | 37 |
| I-B4 | Funduscopy view of four lesion sizes | 41 |
| I-B5 | Chronological development of large lesions | 42 |
| I-B6 | Large lesion covering macula | 44 |
| I-B7 | Histologically prepared serial section | 45 |
| I-B8 | Retinal spot size vs laser beam divergence | 46 |
| S1 | Gaussian field distribution | 52 |
| S2 | q_1 and q_2 plane with thin lens between | 54 |
| S3 | Laser beam contour | 56 |
| S4 | Ray trace through eye | 59 |

LIST OF FIGURES

PART II

| <u>FIGURE</u> | | <u>PAGE</u> |
|---------------|---|-------------|
| II-1 | Absorption Spectra of Components of the Eye (Rhesus Monkey) | 66 |
| II-2 | Absorption Spectra of Components of the Eye (Human) | 67 |
| II-3 | Transmission Spectra of the Cornea (Rabbit) | 68 |
| II-4 | Action Spectrum for Photokeratitis (Rabbit) | 69 |
| II-5 | Density Spectra of Primate Lenses | 71 |
| II-6 | Percent of Corneal Incident Radiation Transmitted to Retina | 73 |
| II-7 | Transverse Section of Whole Cornea | 76 |
| II-8 | Transverse Section of Corneal Epithelium | 77 |
| II-9 | Molecular Structure of Protein | 82 |
| II-10 | Structure of the Aromatic Amino Acids | 83 |
| II-11 | Absorption Spectra of the Aromatic Amino Acids | 84 |
| II-12 | Absorption Spectra of Biological Macro- molecules | 85 |
| II-13 | Molecular Structure of Nucleic Acid | 86 |
| II-14 | Structure of Nucleic Acid Bases | 87 |
| II-15 | Absorption Spectrum of the Corneal Epithelium | 89 |
| II-16 | "Relative Transmission" of Protein and Nucleic Acids in the Epithelium | 91 |
| II-17 | Molecular Electronic Energy Level Diagram | 93 |
| II-18 | Three-Level Electronic Energy Level Diagram | 96 |

LIST OF TABLES

PART I

| <u>TABLE</u> | | <u>PAGE</u> |
|--------------|--|-------------|
| I-A1 | Gaussian Laser Beam Dimensions | 8 |
| I-A2 | ED-50 Values For 40 m Sec Exposures to the Macula | 19 |
| I-A3 | Thermal Model Parameters | 23 |
| I-B1 | Laser Beam and Retinal Lesion Parameters | 40 |
| I-C1 | Survival Times Associated with Lesions To Be Evaluated Histologically | 49 |

PART II

| | | |
|------|--|-----|
| II-1 | Absorption of the Corneal Epithelium | 107 |
| II-2 | Relative Absorptions of Protein and Nucleic Acid Components of the Epithelium | 109 |

ABSTRACT

This annual report is a summary of the research conducted by the Life Sciences Division of Technology Incorporated for the School of Aerospace Medicine at SAM/RAL, Brooks Air Force Base, Texas, under Contract F41609-73-C-0017 during the year 15 February 1973 to 15 February 1974.

This report is divided into two parts, both of which are concerned with research on the ocular hazards of laser irradiation. Part I deals with radiation in the visible wavelength range. It contains: a completed study on the size of retinal lesions induced by laser light as a function of the laser beam parameters; a study, partially complete, of the wavelength dependence of threshold retinal damage; two studies in progress on histological results; and an appendix on laser beam retinal spot size in the emmetropic eye.

Part II deals with ocular hazards from ultraviolet laser irradiation. It contains: a summary of literature surveys on absorption characteristics and molecular composition of components of the eye; development of a preliminary quantitative model relating the extent of photochemical damage to laser beam characteristics; and suggestions for a number of experiments which would better define the nature of ocular hazards from ultraviolet radiation and aid in the development of, as well as provide verification for, the quantitative model.

PART I-A

WAVELENGTH DEPENDENCE ON THRESHOLD OCULAR DAMAGE FROM VISIBLE LASER LIGHT

I-A INTRODUCTION AND BACKGROUND

The first decade of laser technology featured the overwhelming popularity of the helium-neon gas continuous wave laser. This resulted from the fact that the cost and the nature of this laser reasonably suited the popular uses: classroom demonstration, optical alignment, making and viewing holographic recordings, and many other applications requiring low power visible laser quality light. Now into the second decade of laser technology we find many sophisticated, increasingly popular, demands for which the helium-neon laser is not suited. A variety of commercially available high powered pulsed lasers constitutes the basic tool in the field of nonlinear optics. These high powered pulsed lasers in conjunction with such a nonlinear device as an optical parametric oscillator constitute a source of continuously tunable laser quality radiation from the near infrared through the visible region of the electromagnetic spectrum. Similarly, high powered pulsed lasers are used as optical pumps in dye lasers producing tunable laser radiation throughout the visible into the ultraviolet region of the spectrum. We now find the choice of wavelength associated with laser radiation from the infrared through visible into the ultraviolet portion of the electromagnetic spectrum well within the state of the art of laser technology. Therefore, the question of ocular hazard as a function of wavelength is no longer of academic concern only but becomes relevant and a justifiable concern of those responsible for determining laser ocular safety standards.

This part of this report is concerned with the question of laser irradiation induced ocular damage threshold as a function of wavelength in the visible region of the electromagnetic spectrum.

Many threshold damage determinations for a variety of combinations of laser light parameters have been determined and reported in the technical literature. A number of similar threshold damage determinations relevant to this wavelength question have been determined on the rhesus macaque¹⁻⁹. (The rhesus eye is a popular subject choice in this type of experiment due to its similarity to the human eye). Figure I-A1 shows several of these threshold determinations by several different investigators. The data points represented in Figure I-A1 are similar in that they involve single pulse laser irradiation exposures with minimal irradiated retinal spot size to the paramacula region of the retina. Thus, a wavelength comparison from this collection of data should partially answer the question of wavelength dependence. There is very little of this kind of comparable data in the literature for single pulses shorter than indicated in Figure I-A1.

One might conclude from the collection of data depicted in Figure I-A1 that there is a significant damage threshold difference between red and green laser light. However, there are several considerations which cause one to refrain from drawing any conclusion at all from this collection of data. The common end point, the appearance of a threshold damaged area on the retina, which is subtle and difficult to identify ophthalmoscopically, makes lesion determination a subjective determination of the "eyeball reader". G. D. Frisch et al.⁵, define their criterion for minimal retinal damage as: "the presence of an ophthalmoscopically visible opacity observed within sixty minutes after exposure". The criterion for minimal retinal damage used in this laboratory differs slightly in that there must be ophthalmoscopically visible a white or grey central region of damage to this opacity. This is a significantly more

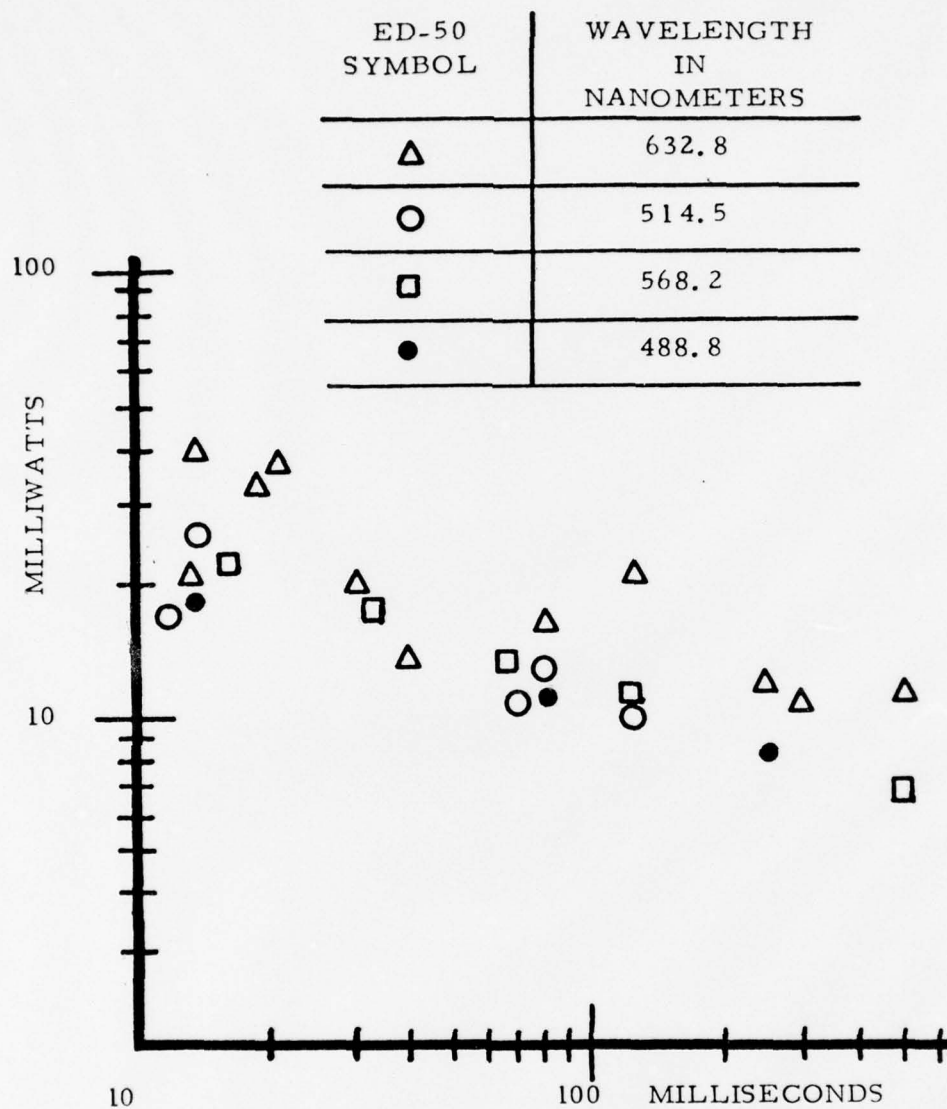


FIGURE I-A1: Comparable ED-50 determinations for four visible wavelengths

stringent definition for threshold damage. This dissimilarity and other dissimilarities among the investigators, experimental techniques and apparatuses represented in Figure I-A1 make any inference of a significant wavelength dependence not possible from the literature consideration.

We conclude from the literature consideration that a wavelength dependence investigation within a single program using similar experimental techniques, personnel, and apparatus is essential for a determination of whether a significant wavelength dependence exists for threshold ocular damage from visible laser light. The investigation reported herein addresses this threshold wavelength question within a single experimental program using the same experimental techniques, personnel, and apparatus throughout.

The experimentally determined threshold values are of two type: The first set of determinations involved four ED-50 data points associated with "worst case" laser exposure condition. (That is: minimal divergence of the laser beam, maximum dilation of the iris with the total laser beam incident on the cornea focused to a minimal retinal spot size in the macula region of the retina.) The four ED-50 data points have a common single pulse duration of forty milliseconds. The four wavelengths span the visible spectrum: 476.2, 520.8, 568.2, and 647.1 nm.

The second set of threshold value determinations involve the same four wavelengths and the same target on the retina. Two of four planned determinations are complete and are reported herein. This second set of ED-50 determinations is associated with an expanded retinal spot size. The retinal spot size diameter is measured to be 280 μ in each eye that is exposed. These four ED-50's have a common single pulse duration of two hundred and fifty milliseconds.

The wavelength dependence question should be and is considered, within the investigation, from a theoretical standpoint. The theoretical consideration is based on the assumption that the threshold retinal damage from laser irradiation is thermal in nature. That is, a given rise in temperature in the retina as a result of absorbed laser irradiation in that region results in local cell damage which is visible ophthalmoscopically.

Finally, we consider the wavelength dependence question from a histologically evaluated set of minimal retinal laser burns. A set of four photographs are presented showing histologically prepared sections of four minimal ophthalmoscopically visible retinal lesions. The four photographs presented represent lesions induced by laser light of the four wavelengths represented above.

I-A EXPERIMENTAL APPARATUS AND EXPOSURE PROCEDURE

The laser apparatus used in the first set of four ED-50 determinations in this experiment is shown schematically in Figure I-A2. The Coherent Radiation Model 52 Krypton Gas Laser shown in the schematic is capable of CW laser oscillation at the four wavelengths (476.2, 520.8, 568.2 and 647.1nm) used in this experiment, with sufficient power to induce "minimal" lesions in the subject's retina from a single pulse exposure of forty milliseconds duration. A measured cross-section of the laser beam intensity distribution showed the intensity profile to be gaussian in shape [TEM_{00} : $\exp(-r^2/2\sigma_c^2)$]. The profile measuring apparatus and an example of one of the profiles is described and given in section I-B. The results of these measurements are given in Table I-A1.

The laser output beam power was controlled by varying the current through the laser plasma tube. The power of the CW laser irradiation (40 millisecond duration) delivered to the subject eye was monitored by an SGD 444 photodiode in conjunction with a Tektronix Model 556 oscilloscope as shown in Figure I-A2. This monitoring system was calibrated daily with a Scientech model 3600 thermopile placed at the intended position of the subject's eye.

The Zeiss fundus camera shown in the schematic served to view the subject's retina and to hold the mirror that reflects the laser beam pulse into the subject's eye. The mirror swung out of place for viewing the retina. The mirror was aligned such that when it was in place, as shown in the schematic, the reflected laser beam was made coaxial with the optic axis of the fundus camera. Thus by viewing the subject's retina through the fundus camera with the mirror out of place the eye could be maneuvered in such a way that the optic axis of the fundus camera went through the spot selected on the retina for irradiation.

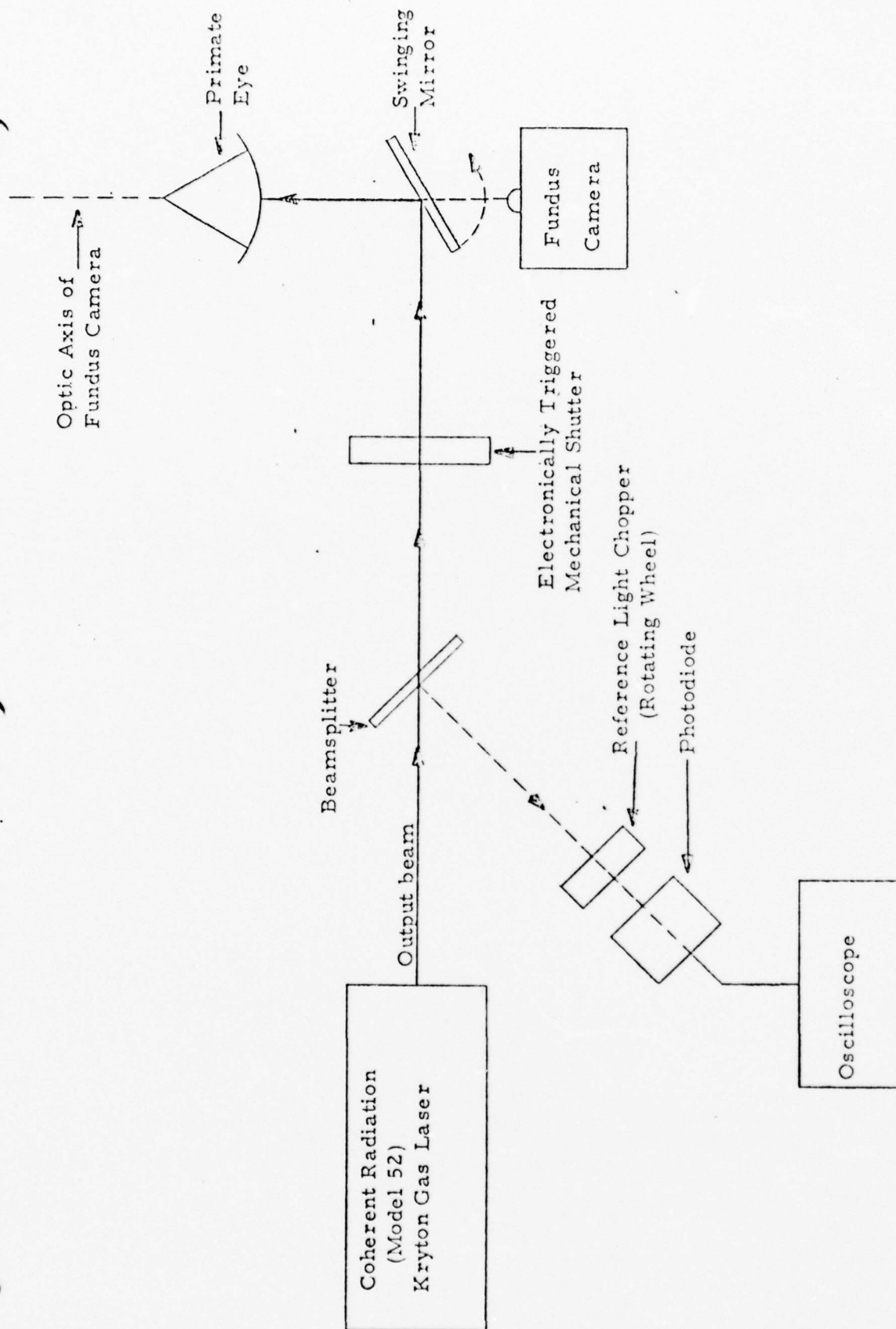


FIGURE I-A2: Experimental Apparatus

TABLE I-A1

GAUSSIAN LASER BEAM DIMENSIONS

| λ (nm) | $2\sigma_c$ | 2θ |
|----------------|--|-----------------------------------|
| | $\frac{1}{e^2}$ SPOT SIZE AT THE CORNEAL PLANE (mm) | FULL ANGLE DIVERGENCE (m rad.) |
| 647.1 | 2.47 | .80 |
| 568.2 | 2.60 | .60 |
| 520.8 | 2.87 | .54 |
| 476.2 | 2.67 | .66 |

The mirror could then be swung into place just before the laser irradiation was delivered to the eye. The laser apparatus being used in the second set of ED-50 determinations is similar to the one shown in Figure I-A2. Figures I-B1 and I-B1a in Part I-B show the similar apparatus modified to facilitate the expanded retinal spot size. We refer to Part I-B for the procedure to obtain and insure a 280 μ spot size in each eye that is exposed.

The first set of four ED-50 determinations in this experiment required sixteen laser irradiation exposures to each subject eye. The power (mW) settings associated with the sixteen irradiation exposures were symmetrically arranged about a preestimated ED-50 value in equal log intervals such that the lowest power will not create a lesion on the retina and the highest power will create a lesion on the retina. The sixteen power settings associated with the individual pulses were presented in a randomized sequence. The average time to deliver the sixteen shots was about five minutes. The exposures associated with the large retinal spot size were delivered in a similar manor except there were only fourteen of them.

The target area on the retina was the macula. Figure I-A3 is a map showing the typical arrangement of the sixteen exposure sites in the macula. Figure I-A4 shows the arrangement associated with the large retinal spot size for the fourteen exposures.

The typical threshold lesion consists of a central area of destroyed cells white or gray in color on the order of 10 μ m across. Around this area is usually a ring of reversibly damaged cells appearing dark gray in color. The appearance of a threshold damaged area is subtle and difficult to identify ophthalmoscopically, making lesion determination a subjective determination of the "eyeball reader". The determination of whether a lesion was

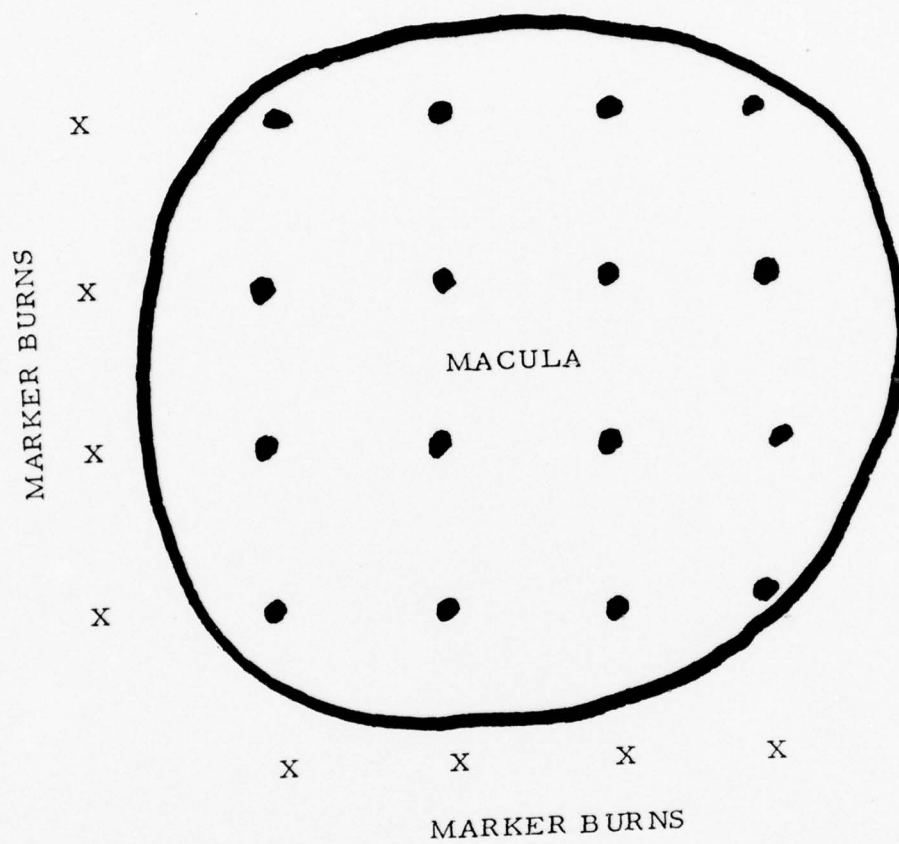


FIGURE I-A3: Map of exposure site on retina

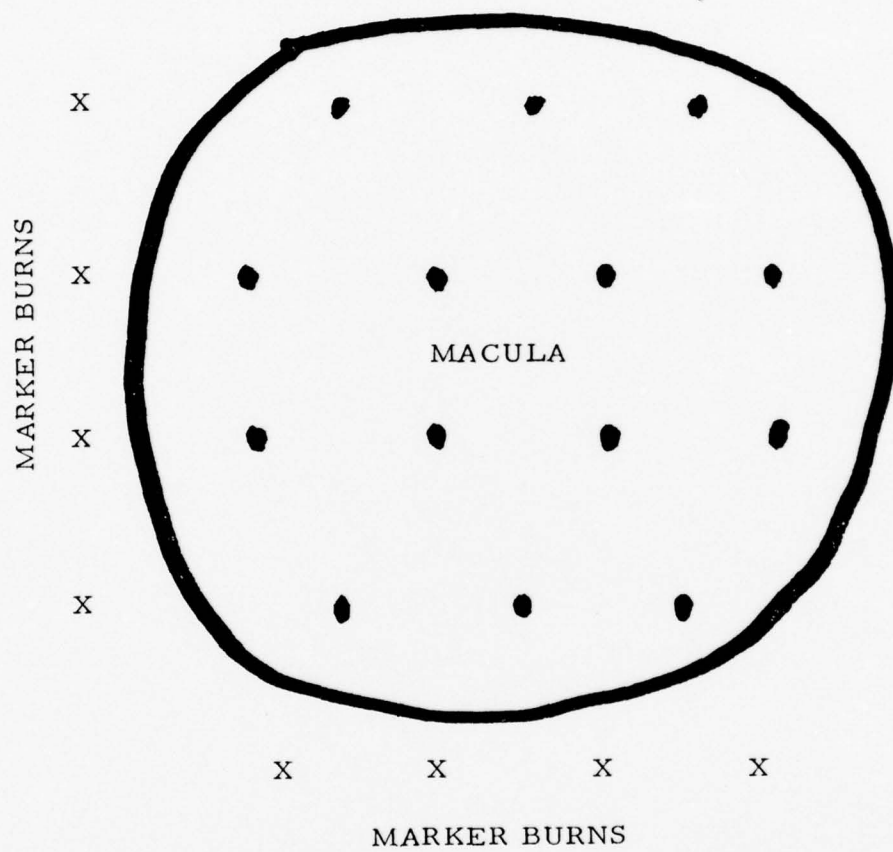


FIGURE I-A4: Map of exposure site on retina

created on the retina by a given exposure was determined ophthalmoscopically, via the Zeiss fundus camera, one hour after the exposure.

22

I-A SUBJECT PREPARATION AND HANDLING

The following list describes the chronological sequence of events constituting the clinical preparation and handling of each rhesus macaque subject before, during, and after the ocular exposure to laser irradiation:

1. Each subject's eyes were refracted to the nearest .25 diopter in each meridian. An eye with a greater than .50 diopter refractive error in any meridian was not acceptable to the experiment.
2. An intra-muscular injection of .05 cc (per kilogram weight of the subject) of ketamine hydrochloride (Ketylar), 100 mg/ml, was given prior to the administration of other anesthetic agents.
3. The pupil of each eye was dilated to a maximum (6-7mm) by the application of two drops of (1%) tropicamide (Mydriacyl) to the cornea. This application was repeated after five minutes.
4. The dilation process was followed by a retro-bulbar injection of .6 cc of lidocaine hydrochloride (2%).
5. An intra-catheter was placed in a saphenous vein for the periodic injection of .5-1.0 cc/kg of sodium pentobarbital (Nembutal) 50 mg (3/4 gr) per ml.
6. Sutures were placed in the upper eye lid to facilitate holding the eye lid open during the irradiation process.
7. During the period of exposure the subject's body temperature was monitored and maintained at a temperature of $97 \pm 2^{\circ}\text{F}$.
8. Corneal drying, during the period of exposure, was prevented by periodic application of normal saline to the corneal surface

and by manually blinking the bottom eye lid.

9. After the irradiation exposure and the determination for induced visible lesions, two drops of (1%) methy-cellulose were placed in each eye before the subject was returned to the vivarium.

These subjects ranged in weight from two to four kilograms and in age from two to three years.

No distinction is considered or discrimination made between the eyes of the male and female subjects.

These animals were maintained and the experiments conducted in accordance with procedures outlined in "Guide for Laboratory Animal Facilities and Care," U. S. Department of Health, Education and Welfare, and USAF/SAM Regulation 169-2, 26 July 1972.

I-A THEORY

The heat-conduction equation has been used by several investigators⁹⁻¹⁶ to determine temperature increase in the retina due to absorbed electromagnetic irradiation. The heat-conduction equation has the form:

$$\frac{\partial T}{\partial t} = K \nabla^2 T + A/\varphi c \quad (I-A1)$$

where T is temperature, t is time, K is thermal diffusivity, A is source strength, φ is density, and c is specific heat. T and A are functions of r , z , t , and λ where: z is the optic axis defined by the direction of the incident irradiation to the retina, r is the cylindrical coordinate radius, and λ is the wavelength of the incident irradiation. Due to the different structural layers in the retina having different thermodynamic properties an analytic solution of equation (I-A1) is not practicable. An approximate solution to this partial differential equation giving the temperature at discrete grid points associated with the independent variables (temporal, radial, and axial) in this problem was developed and used by M. A. Mainster et. al.^{10, 11, 14} to treat this problem.

It is not necessary for our purpose to treat this problem with such rigor. To determine the wavelength dependence on temperature increase in a particular layer of the retina, all that is necessary is an inspection of the source term " A ". That is to say, the magnitude of the heat source as a function of wavelength, all other beam parameters being held constant, should be a valid relative indicator of the local temperature increase.

The heat source term has the following form for a particular structural layer:

$$A(r, z, t, \lambda) = \zeta(t) h(r) H_0(\lambda) \alpha(\lambda) \exp[-\alpha z] \quad (\text{I-A2})$$

$$\text{where } \zeta(t) \text{ is a "unit step function"; } \zeta(t) = \begin{cases} 0, & t < 0 \\ 1, & 0 \leq t \leq t_1 \\ 0, & t > t_1 \end{cases}$$

indicating that the irradiation lasts from $t=0$ to $t=t_1$, $h(r)$ is a function which represents the radial distribution of the irradiation incident on that particular structural layer, $H_0(\lambda)$ is the irradiance at the center of that radial distribution at the upper surface of the particular structural layer, and $\alpha(\lambda)$ is the absorption coefficient associated with the layer.

It is of interest to express the laser beam parameters $h(r)$ and $H_0(\lambda)$ in terms of their corresponding measurable parameters at the cornea. For the convenience of this analysis we will assume the radial distribution at the cornea to be Gaussian and have the form:

$$h(\text{cornea}) = \exp[-r^2/2\sigma_c^2]$$

where σ_c represents the measured corneal spot size radius. We make the assumption in this analysis that the optics of the eye transforms any given distribution at the cornea to a similar distribution at the pigment epithelium layer in the retina. Therefore,

$$h(\text{cornea}) = \exp[-r^2/2\sigma_c^2] \Rightarrow h(\text{retina}) = \exp[-r^2/2\sigma_{PE}^2]$$

where σ_{PE} represents the retinal irradiated spot size radius. Based on this assumption, we may express $H_0(\lambda)$ in terms of the irradiance at the center of the Gaussian distribution on the cornea, H_0' , the transmittance, $T(\lambda)$, of the ocular media anterior to the pigment epithelium layer and the spot sizes:

$$H_0(\lambda) = H_0' / T(\lambda) \left[\frac{\sigma_c}{\sigma_{PE}} \right]^2$$

If we substitute these expressions for $h(r)$ and $H_0(\lambda)$ into equation (I-A2) we have the following expressions for the heat source in terms of measurable or calculable quantities:

$$A(r, z, t, \lambda) = \zeta(t) \exp[-r^2/2\sigma_{PE}^2] H_0 / T(\lambda) \left[\frac{\sigma_c}{\sigma_{PE}} \right]^2 \alpha(\lambda) \exp[-\alpha z]. \quad (I-A3)$$

For convenience and future reference, let us consider the magnitude of the heat source along the z axis ($r=0$):

$$A(0, z, t, \lambda) = \zeta(t) H_0 / T(\lambda) \left[\frac{\sigma_c}{\sigma_{PE}} \right]^2 \alpha(\lambda) \exp[-\alpha(\lambda)z]. \quad (I-A4)$$

We do not mean to imply that there is a linear relation between the magnitude of the heat source at a discrete grid point and the local rise in temperature. However, we can infer that the relative change in the magnitude of the heat source as a function of wavelength, holding all other parameters constant, is related to a relative temperature change.

I-A RESULTS AND CONCLUSIONS

There are several considerations associated with this investigation from which we may draw conclusions. The first consideration was the literature which was discussed in the introduction. We concluded from this consideration that there was no real evidence in the literature to infer a significant wavelength dependence on threshold ocular damage from visible laser light. However, the conclusion is qualified when we consider the dissimilarities associated with the data points from the literature which we considered in Figure I-A1. Likewise, the following conclusions which are drawn from the experimental results and theoretical analysis are qualified. We will discuss the qualification associated with each conclusion.

The first result to consider is the set of ED-50 determinations associated with the "worst case" laser exposure conditions. Table I-A2 list the ED-50 values and their lower 95% confidence limit. Figure I-A5 is a plot of the ED-50 values as a function of wavelength. The error bars in Figure I-A5 represent the standard deviation associated with the data sample (sixteen eyes in each case). The ED-50 value in each case is the average of sixteen threshold estimates determined from a probit analysis of each eye.

Indicated by the error bars in Figure I-A5, the variances associated with the data points are approximately equal. This implies statistically that any one of the data points is as valid a threshold determination as any other. The error bars significantly overlaps in the comparison of any two of these data points. Thus, from a statistical analysis of this data, we may conclude that there is no significant wavelength dependence for threshold ocular damage from "worst case" condition visible laser light exposures.

TABLE I-A2
ED-50 VALUES FOR 40m SEC
EXPOSURES TO THE MACULA

| WAVELENGTH (nm) | ED-50 (mW) | LOWER 95% CONFIDENCE LIMIT (mW) |
|--------------------|---------------|---------------------------------------|
| 647.1 | 12.05 | 10.96 |
| 568.2 | 11.50 | 10.69 |
| 520.8 | 10.48 | 9.80 |
| 476.2 | 11.94 | 10.97 |

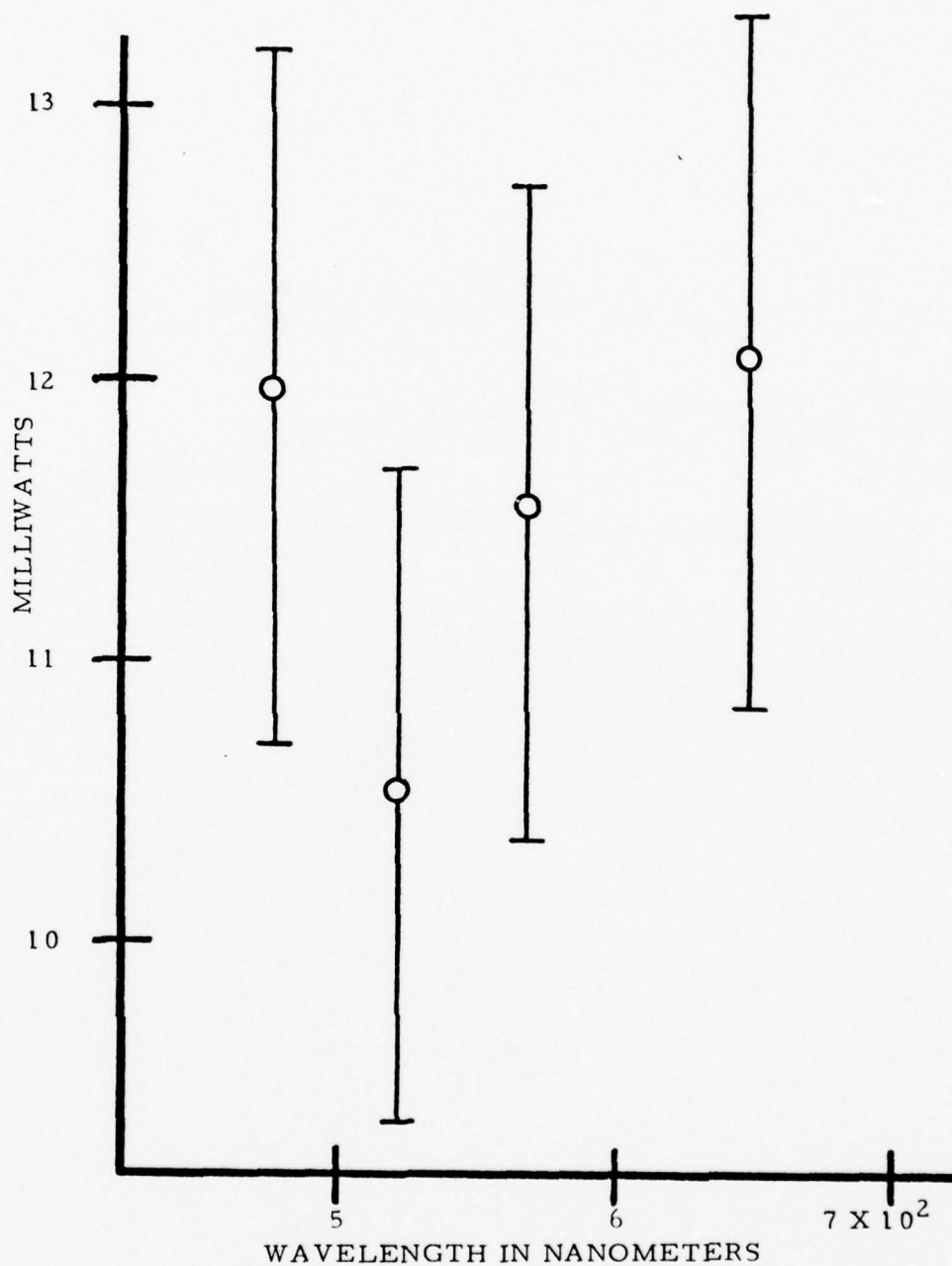


FIGURE I-A5: ED-50 values for 40 millisecond single pulse exposure to the macula

The theory associated with thermal damage to the retina suggests a correspondence between the magnitude of the heat source term in the heat-conduction equation and change in temperature. That is: the larger the heat source term, $A(r, z, t, \lambda)$, the larger the increase in temperature at any given point. It is worthwhile to note at this point that we are concerned with threshold retinal damage which implies a critical temperature to cause damage. That is: there is some critical temperature such that if the temperature of the retina is raised to that point or above, damage will result. Thus, we are interested in the maximum temperature increase from a given exposure. If we consider two sets of exposure conditions which differ only in wavelength and calculate the magnitude of the heat source as a result of these exposures, their relative magnitudes should be an indicator of the relative increase in temperature in the region of the exposure. The one with the larger maximum temperature should have the lower ED-50 value. For a Gaussian intensity distribution this maximum temperature increase will occur at the center of the retinal irradiated spot. Therefore, we consider the heat source term given in equation I-A4 as a relative indicator of temperature increase as a function of wavelength.

We see from equation I-A4 that

$$A \sim \left[\frac{\sigma_c}{\sigma_{PE}} \right]^2 \propto T \exp(-\alpha z)$$

Where σ_c and σ_{PE} are the corneal and retinal irradiated spot sizes respectively, T is the transmittance of the ocular media anterior to the pigment epithelium layer,¹⁸ α is the absorption coefficient associated with the pigment epithelium layer,¹⁷ and z is the distance along the optic axis from the front surface of the P. E. layer. We find estimates in the literature^{5, 19, 20, 21} of retinal spot size associated with "worst case" laser irradiation that range from 50 μ to

3 μ . By inspection we see that a one order of magnitude variance in the estimate of the retinal spot size results in a two order of magnitude variance in the calculated magnitude of the heat source.

We suspect a substantial variance in σ_{PE} from eye to eye for minimum irradiated spot sizes. Thus, we suspect that the variance in the data represented in Figure I-A5 is a result of this variance in minimal retinal spot size. We conclude from this that if we could insure a constant retinal spot size from eye to eye the variance associated with threshold damage may be substantially less and show a wavelength dependence.

We proposed a second set of threshold determinations as a function of wavelength involving a large measurable retinal spot size to eliminate this variance in retinal spot size. Two of the four planned threshold determinations associated with a 140 μ retinal spot size radius and 250 m sec. pulse duration are reported in Table I-A3. The numbers in the last column on the right represent the two ED-50 values and the standard deviation associated with them. We see that the variance associated with the $\lambda = 520.8$ ED-50 is equally as large a percent of the total value as those associated with the first set of thresholds determinations which involved minimal retinal spot sizes. Since the retinal spot size was measured for each eye (eighteen eyes per ED-50) and held constant throughout the experiment we are forced to conclude that the variance in the data (all ED-50 data) is not attributable to the variance in the retinal spot size. By eliminating this source of variance in an ED-50 threshold value we conclude that the variance is inherent to the nature of the damage determinations (minimal ophthalmoscopically visible lesion) and that there is a certain inherent variance to the critical temperature which will

TABLE I-A3
THERMAL MODEL PARAMETERS

| λ (nm) | α (cm) ⁻¹ | T (%) | α T exp (- αz) | | Technology Inc. Model 10, 11 | | | | Experimental ED-50 | |
|-------------------|--------------------------------|----------|-----------------------------------|-----------------------------------|---|--|--|--|---|--|
| | | | $z=0_{\mu}$ (cm) ⁻¹ | $z=6_{\mu}$ (cm) ⁻¹ | (maximum temp. per watt) | | | 40 m sec σ = minimal (mW) | 250 m sec σ = 140 μ (mW) | |
| | | | | | σ = 150 μ 40 m sec z = 5 μ | σ = 150 μ 1 μ sec z = 1 μ | σ = 10 μ 40 m sec z = 5 μ | | | |
| 647.1 | 1101 | 65 | 716 | 372 | 242 | 148 | 352 | 12.05 \pm 1.25 | 38.6 \pm 1.0 | |
| 568.2 | 1294 | 60 | 776 | 357 | 232 | 157 | 340 | 11.50 \pm 1.20 | | |
| 520.8 | 1468 | 56 | 822 | 337 | 222 | 161 | 323 | 10.48 \pm 1.18 | 37.7 \pm 3.9 | |
| 476.2 | 1622 | 50 | 811 | 308 | 203 | 157 | 295 | 11.94 \pm 1.26 | | |

λ = wavelength

α = absorption coefficient of the pigment epithelium layer via Coogen, et al.¹⁷

T = transmittance of the ocular media anterior to the pigmented layer via Boettner¹⁸

z = distance into pigmented layer

σ = retinal spot size radius

cause damage to the retina. We also see from the two ED-50 data points in Table I-A3 that there is no significant threshold damage difference for large retinal spot sizes between red and green laser light.

We now consider some temperature calculations via the Technology Incorporated model^{10, 11} for the four wavelengths associated with the experimental determinations. We consider three cases in Table I-A3 to check for an expected wavelength dependence. The first case that we consider is the laser beam parameters associated with minimal retinal spot size ($\sigma = 10 \mu$) and an exposure duration of 40 milliseconds which is relatively long compared to the thermal relaxation time. To reiterate, since we are concerned with a critical threshold temperature we are interested in the maximum temperature generated by the laser exposure. The label $z = 5 \mu$ indicates that the maximum temperature occurred 5μ into the pigment epithelium layer. This is indicative of a long exposure. The other two cases considered are for a large retinal spot size of 150μ radius, one a short exposure (1μ sec.) and one a long exposure of 40 milliseconds. We see that for the two 40 millisecond exposures the red light gives the largest temperature rise and therefore should give the lowest ED-50 value. We see that for the short exposure (1μ sec) the green light gives the largest temperature rise. This indicates a theoretical wavelength dependence associated with the length of the pulse duration. However, in each of the three cases the temperature differences are not significantly large enough to expect a wavelength dependence to show experimentally.

It is interesting to note in Table I-A3 that the calculated magnitudes for the heat source term:

$$A \sim \alpha T \exp(-\alpha z)$$

give the same relative magnitudes as a function of wavelength as does the Technology Incorporated model. That is: the column labeled $z = 0 \mu$ corresponds to a short pulse duration and has the same relative order as the Technology Incorporated model temperature calculations for the 1μ sec exposure. Likewise the column labeled $z = 6 \mu$ corresponds in the same way to the relative temperatures for the long 40 m sec. exposures. This in a sense confirms that the magnitude of the heat source term is a good relative indicator of wavelength dependence for threshold retinal damage.

Figure I-A6 is four photographs of four histologically prepared sections of four minimal ophthalmoscopically visible retinal lesions. The laser beam parameters were the same as those associated with the first four experimentally determined threshold values. The total power incident on the cornea was slightly larger than the ED-50 values given in Table I-A2 to insure an induced lesion for each wavelength. All four lesions shown in Figure I-A6 were induced in the same eye. From the comparison of these damage sites we can find no significant histological evidence of a wavelength dependence for threshold retinal damage.



YELLOW



BLUE



RED



GREEN

Figure I-A6
Histologically prepared sections of minimal ophthalmoscopically visible retinal damage from different wavelength laser light

PART I-A

REFERENCES

1. P. W. Lappin, Arch Environ. Health 20, 177 (1970).
2. P. W. Lappin and P. S. Coogan, Archives of Ophthalmology 84, 350 (1970).
3. W. T. Ham, Jr., W. J. Geeraets, H. A. Mueller, R. C. Williams, A. M. Clarke and S. F. Cleary, Arch Ophthal 84, 797 (1970).
4. I. L. Dunskey and P. W. Lappin, Vision Res. 11, 733 (1971).
5. G. D. Frisch, E. S. Beatrice, and R. C. Holsen, Investigate Ophthalmology 10, 911 (1971).
6. G. H. Bresnick, G. D. Frisch, J. O. Powell, M. B. Landers, G. C. Holstand, and A. G. Dallas, Investigate Ophthalmology 9, 901 (1970).
7. W. D. Gibbons and D. E. Egbert, Quarterly Report (Sept. -Dec. 1970), Work Unit 63010537, USAF School of Aerospace Medicine Brooks AFB, Texas (1973).
8. E. S. Beatrice, J. O. Powell, H. G. Bresnick, J. E. Chester, and C. C. Steinke, Technical Research Report, Contract AMCMS Code 5911.21.20382, Report R-1956, Frankford Arsenal, Philadelphia, Pa. (April 1970).
9. A. Vassiliadis, H. C. Zweng, and K. G. Derick, Final Report, Contract F41609-70-C-0002, SRI Project 8209, Stanford Research Institute, Menlo Park, California (January 1971).
10. M. A. Mainster, T. J. White, J. H. Tips, and P. W. Wilson J. Opt. Soc. Am. 60, 264 (1970).

11. M. A. Mainster, T. J. White, and R. G. Allen, J. Opt. Soc. Am. 60, 848 (1970).
12. J. R. Hayes and M. L. Wolbarsht, Aerospace Medicine 39, 474 (1968).
13. M. A. Mainster, T. J. White, and J. H. Tips, Appl. Opt. 9, 665 (1970).
14. M. A. Mainster, T. J. White, J. H. Tips, and P. W. Wilson, Bull. Math. Biophysics 32, 303 (1970).
15. T. J. White, M. A. Mainster, J. H. Tips, and P. W. Wilson, Bull. Math. Biophysics 32, 315 (1970).
16. T. J. White, M. A. Mainster, P. W. Wilson, and J. H. Tips, Bull. Math. Biophysics 33, 1 (1971).
17. P. S. Coogan, W. F. Hughes, and J. A. Mollsen, Quarterly Interim Technical Report (Dec. 31, 1972-March 31, 1973), Contract F41609-71-C-0006, Task No. 630105019, Rush - Presbyterian - St. Luke's Medical Center, Chicago, Illinois (March 1973)
18. E. A. Boettner, Final Report, Contract AF41 (609) - 2966, Project No. 6301, University of Michigan, (July 1967).
19. M. N. Stein and S. S. Elgin, Final Report, Contract F41609-68-C-0038, Task No. 6301, Eye Research Foundation of Bethesda, Bethesda, Maryland (Feb. 1970).
20. H. L. Mayer and F. Rickey, J. Opt. Soc. Am. 54, 678, (1964).
21. P. W. Lappin and P. S. Coogan, Investigative Ophthalmology, 9, 537, (July 1970).

PART I-B

LASER BEAM RETINAL SPOT SIZE vs RETINAL LESION SIZE

I-B INTRODUCTION AND OBJECTIVES

The following experimental determinations were a consequence of a determined need for some data to correlate laser beam retinal spot size with the corresponding size of the induced lesion. The determinations were concerned with retinal lesions and laser beam spot sizes much larger than those associated with threshold retinal damage and worst case laser irradiation. The tabulated results of this effort amount to a necessary precursor to an experiment concerning loss of visual acuity as a function of laser beam induced retinal lesion size. The particular retinal spot size and lesion size diameters of interest were on the order of 200, 500, 900 and 1500 microns. These diameters correspond to diameters of particular targets (on the retina of the rhesus macaque subject) of interest in the pending visual acuity experiment. The diameters correspond to the dimensions of the retinal fovea centralis, the fovea, approximately one-half of the area of the macula, and the macula. The tabulated results amount to the pulse duration, total power, corneal spot size, full angle divergence of the laser beam incident on the cornea, wavelength of the laser irradiation, and the retinal spot size to induce lesions of the preceding sizes.

The experiment had some goals and objectives not related to the pending visual acuity experiment. When we refer to a correlation between laser beam retinal spot size and induced lesion size, we infer a correlation between both the measured and calculated aspects of these parameters. There are two aspects to retinal spot size: the calculated size from the ocular and laser beam parameters (see Supplement I-A) and the measured size as described in the next section. There are

three aspects to retinal lesion size: the size of the lesion seen and measured with the fundus camera as is described in the next section, the size and extent of the lesion determined histologically, and the theoretically predicted size (assuming a critical temperature) via the thermal model. Thus, we are concerned with a correlation between any two of the five mentioned aspects. The following were of primary interest in this experiment:

- 1) A correlation between the measured lesion size using the fundus camera and the same determination made histologically. This should determine the extent of underlying damage not visible with the fundus camera and should eliminate the need for histological evaluation of the size of the damaged area on the retina.
- 2) Of considerable consequence is the fact that: given the data associated with this experiment (laser beam power and pulse duration, retinal image size, lesion size, etc.) in conjunction with the mathematical thermal model one should be able to calculate a critical temperature associated with retinal damage.
- 3) A comparison between measured retinal spot and calculated retinal spot size should determine whether the calculation is a reasonable estimate of the true size.

I-B EXPERIMENTAL APPARATUS AND EXPOSURE PROCEDURE

The apparatus used in this experiment is shown schematically in Figures I-B1 and I-B1a. ACW laser beam at a wavelength of 647.1 nm from a krypton gas laser was utilized in the experiment. A beam-scan analysis of this laser beam indicated a Gaussian radial intensity distribution of the beam impinging at the corneal plane. The beamscan apparatus (not shown in the schematics) consists of an EG & G-SGD100A photodiode mounted behind a 50 μ m pin hole and attached to a micrometer drive, a synchronous motor, and an X-Y recorder. The synchronous motor drives the micrometer with the photodiode attached across the laser beam while the electrical output from the photodiode indicates the intensity profile of the laser beam. Figures I-B2 and I-B2a are examples of the X-Y recorder plot of the intensity profile of the beam impinging at the corneal plane. Figure I-B2 is without the lens indicated in Figure I-B1a, and Figure I-B2a is with the lens. Note that the lens does not alter the beam profile. The vertical slashes in the plot occur every 0.5 mm to indicate the distance covered by the micrometer drive.

The power output of the laser was continuously monitored by an EG & G-SGD444 photodiode in conjunction with a Tecktronix Model 556 oscilloscope as indicated in Figure I-B1. This monitoring system was periodically (daily) calibrated with a Scientech Model 3600 thermopile placed at the intended position of the subject's eye.

The Zeiss fundus camera shown in the schematic served to view the subject's retina and to hold the mirror or beamsplitter that reflected the laser beam pulse into the subject's eye. The mirror swung out of place for viewing the retina. The mirror or beamsplitter was aligned such that when in place, as indicated in the schematic, the reflected laser beam was made coaxial with the optic axis of the fundus

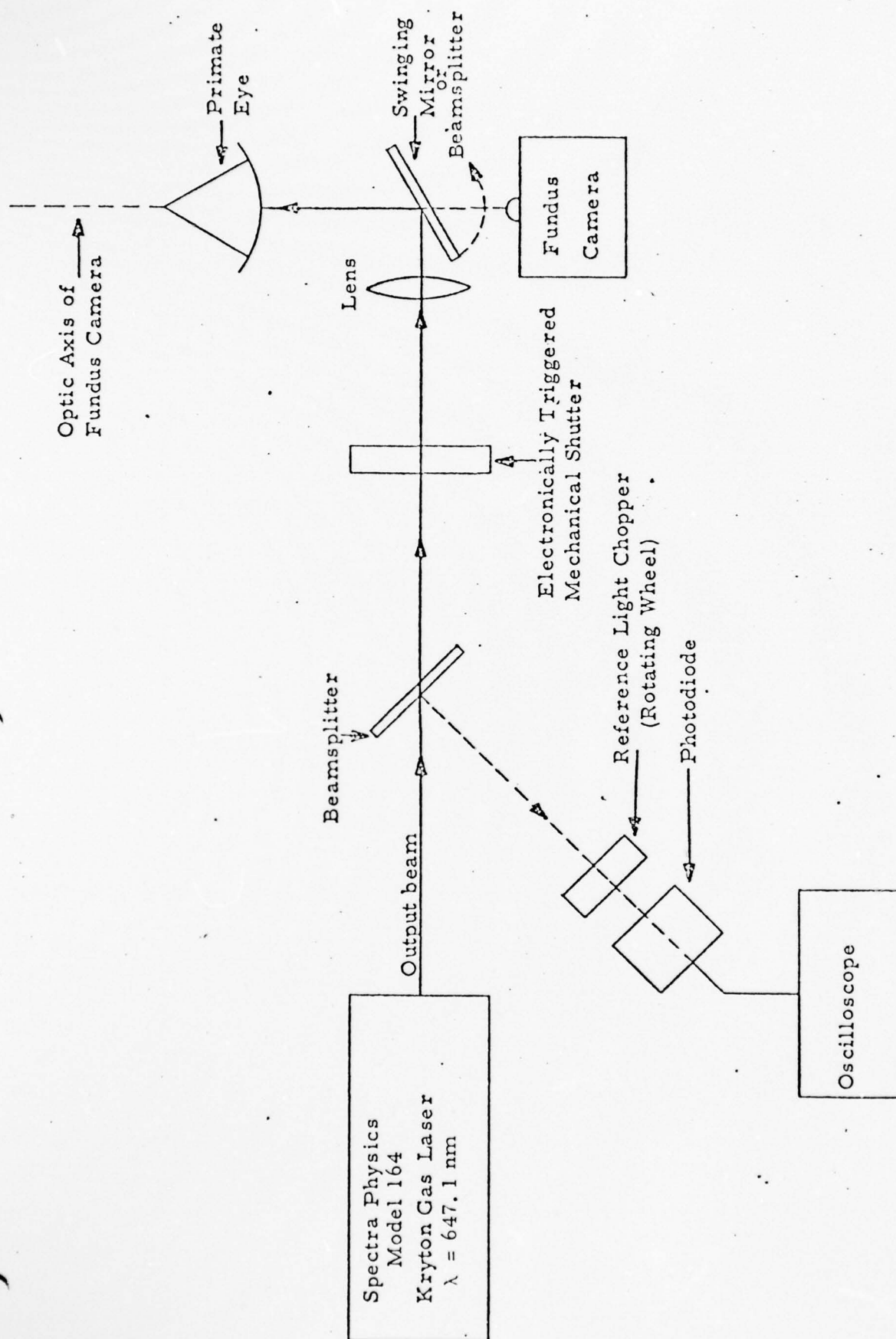


FIGURE I-B1. Experimental Apparatus

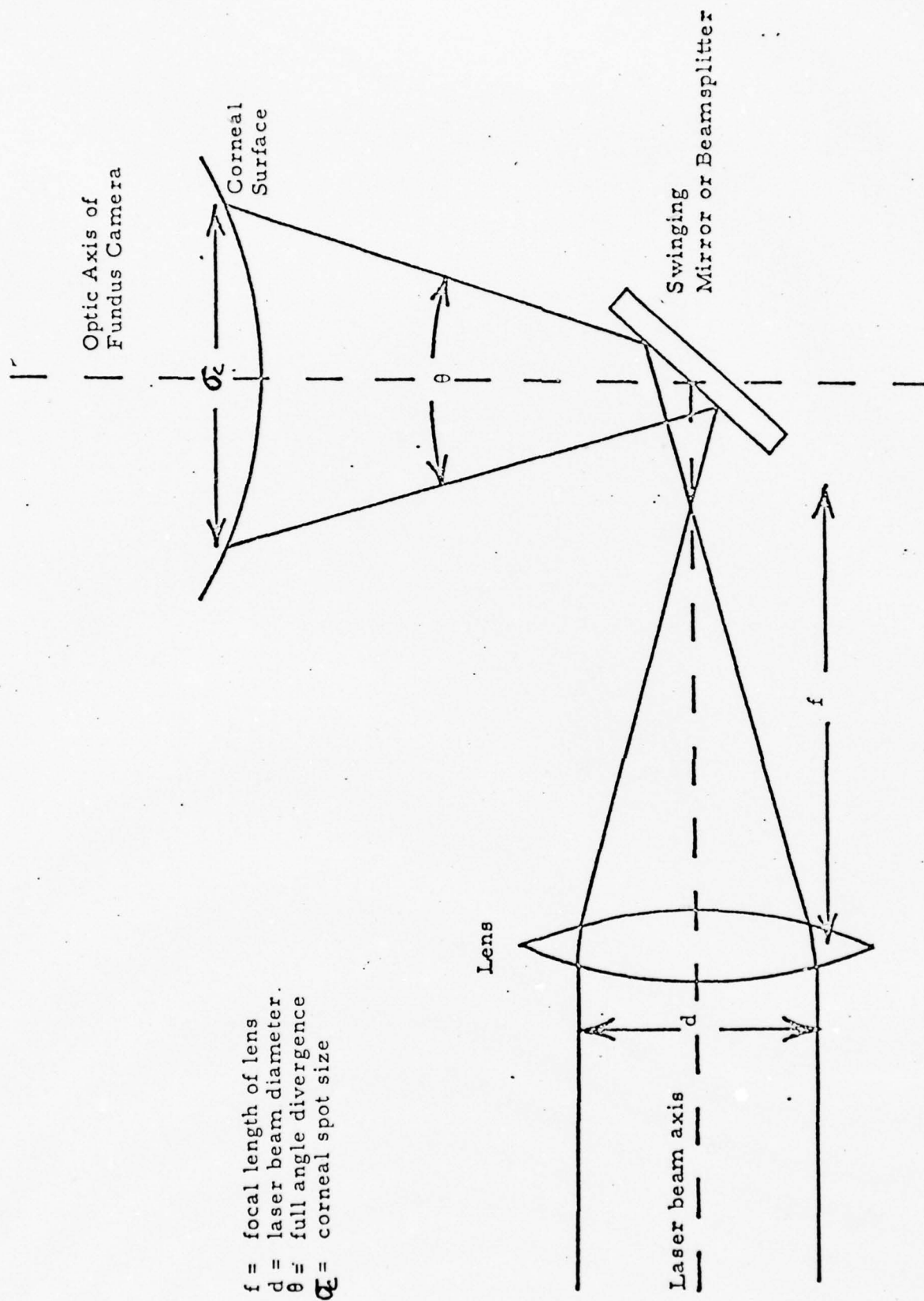


FIGURE I-Bla. Experimental Apparatus

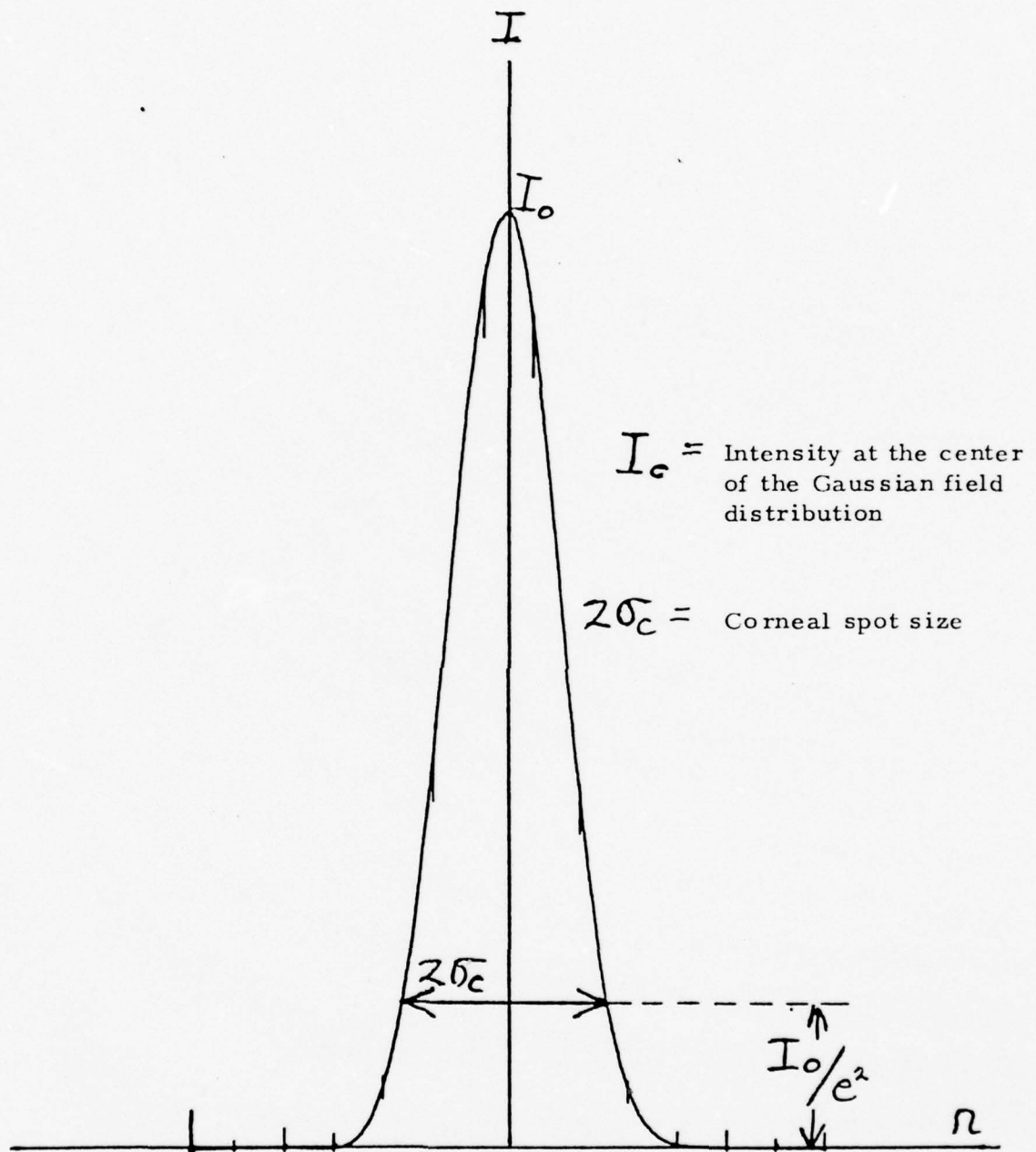


FIGURE I-B2 Gaussian field intensity distribution

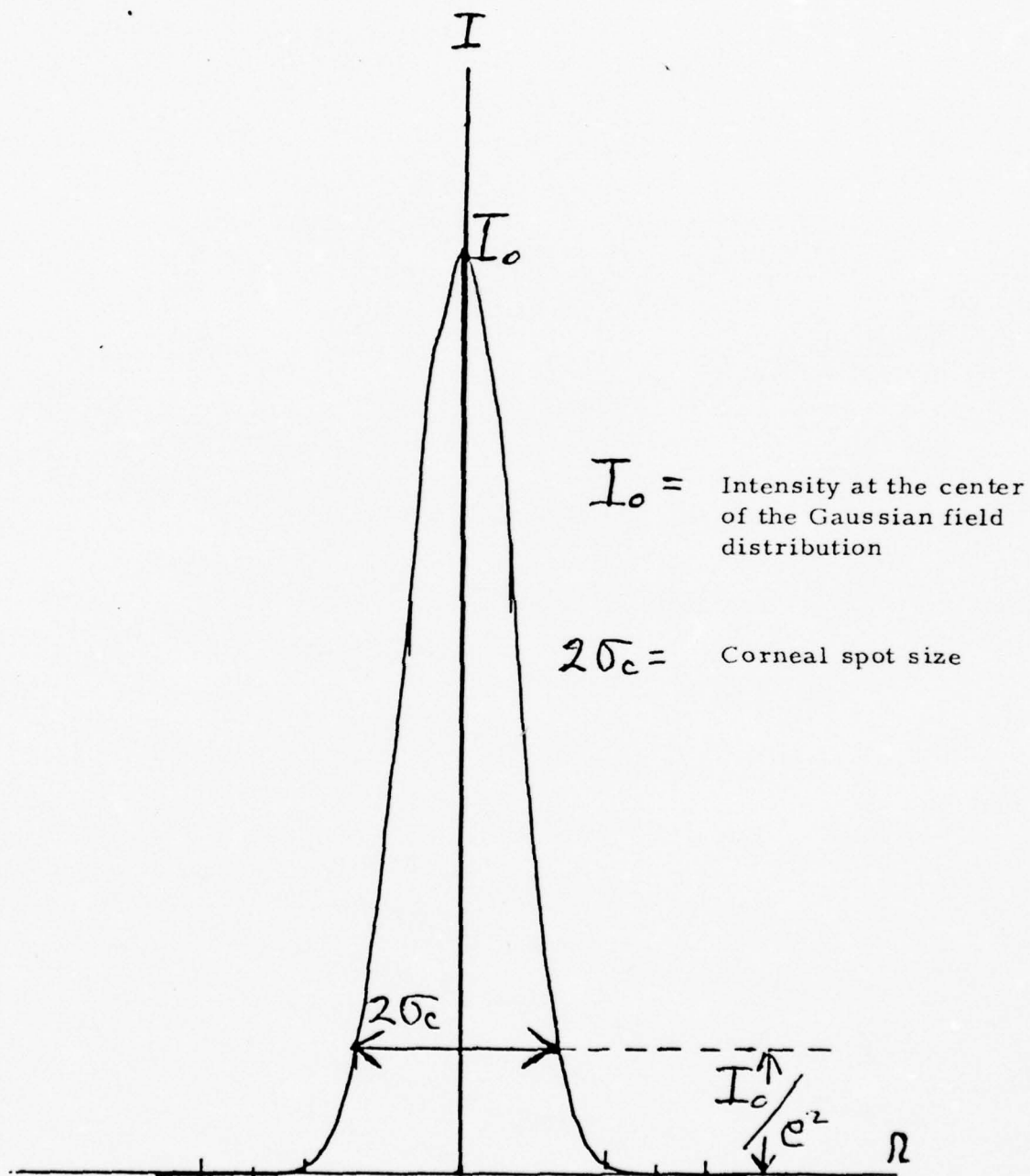
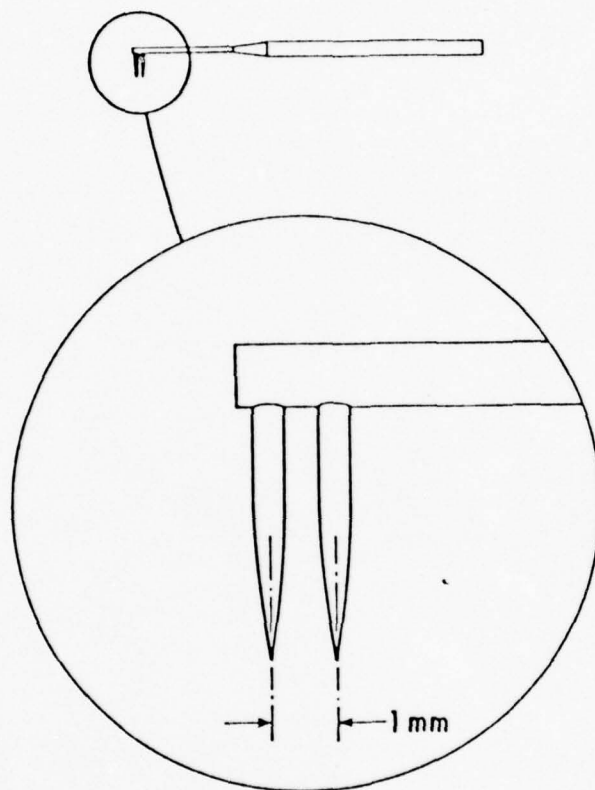


FIGURE I-B2a Gaussian field intensity distribution

camera. By viewing the subject's retina through the fundus camera with the mirror or beamsplitter out of place the eye can be maneuvered in such a way that the optic axis of the fundus camera goes through the spot selected on the retina for irradiation. Thus, the fundus camera served to select the target area to be irradiated and as an element in the laser pulse delivery system.

The fundus camera was equipped with a measuring reticle. The reticle was located directly behind the eyepiece of the camera. Thus, the view of the measuring reticle was superposed on the view of the fundus. The measuring reticle was calibrated by viewing the tips of a calibration probe [designed for this purpose (see Figure I-B3)] protruding through the pigment epithelium layer of the retina of a subject with the fundus camera, then counting the number of marks on the reticle between the tips of the probe. One division on the scale corresponded to $50\ \mu$ on the retina. The probe was inserted through the temporal region of the skull. Attaining access to the rear of the eye amounts to severe damage to the subject's skull. Therefore, the subject was killed after the calibration procedure. Six eyes were used to calibrate the reticle: two eyes with a +1 diopter refractive error, two with no refractive error, and two with a -1 diopter refractive error.

Figure I-B1a is an expanded schematic portion of the laser beam delivery system shown in Figure I-B1. The lens power was selected to give the proper full angle divergence of the beam impinging at the corneal surface to give the desired retinal image size. This choice of lens was made by arbitrarily choosing a lens then measuring the retinal image size. If the retinal image was not the desired size this process was repeated until the desired image size was obtained. The image size measurement is made with the



CALIBRATED PROBE

FIGURE I-B3.

calibrated reticle by viewing the laser beam spot on the retina (at a subthreshold lesion level) through the beamsplitter. Note that the measured spot size is not necessarily the $1/e^2$ spot size of the observed laser spot on the retina. The divergence and corneal spot size was measured and recorded with the previously mentioned beamscan apparatus.

Starting with the chosen retinal spot size, the laser beam power associated with a given lesion size was determined by an arbitrary choice of a power such that the power density at the retina was substantially less than that required to rupture the choroid and cause a hemorrhage. From this arbitrary choice of power and retinal spot size a pulse duration was experimentally determined such that the combination of chosen power, spot size, and pulse duration would produce a lesion approximately the size desired. With this determined choice of power, spot size, and pulse duration a series (at least ten) of eyes were exposed from which a statistical calculation was made, of the induced lesion size associated with that particular power, spot size, and pulse duration. The lesion size is an immediate determination.

I-B RESULTS AND CONCLUSIONS

The tabulated data referred to in the introduction is contained in Table I-B1. The laser beam parameters and the corresponding lesion sizes are given. There are two lesion sizes indicated in the table. The first lesion size is the result of a measurement made immediately after the laser exposure. The lesion size (immediate) given in the table is an average of at least ten lesions, (one lesion per eye) all induced by the same laser beam parameters. Figure I-B4 is a series of four photographs indicating the fundusoscopic view of a typical lesion of each size represented in Table I-B1. The photograph in the center of Figure I-B4 shows the fundusoscopic view of the tips of the calibration probe (see drawing Figure I-B3) protruding slightly through the fundus. The tips of the probe are one millimeter apart, thus, the photograph may be used as a scale to measure the size of the lesions in the other photographs. The standard deviation given in Table I-B1 indicates the variance associated with that immediate lesion size measurement.

The second lesion size indicated in the table was the final lesion size. In each case it is larger than the immediate determination. The size and character of the lesions dealt with in this experiment change considerably after the exposure. The diameter of the damaged area in each case grew to a final size of approximately 30% larger than the initial size of the lesion. In the case of the first size this growth takes about one hour. In the case of the largest size the growth may take two days. Figure I-B5 illustrates the fundusoscopic view of the typical change in character of a large lesion. Typically, the white area of the damaged retina grows to the final size then starts to recede leaving a gnarled

TABLE I-B1

LASER BEAM AND RETINAL LESION PARAMETERS

| | UNITS | #1 | #2 | #3 | #4 |
|--|-------|-----|------|------|------|
| retinal spot size radius | u m | 90 | 225 | 425 | 525 |
| retinal lesion size (immediate) | u m | 187 | 547 | 937 | 1328 |
| retinal lesion size (final) | u m | 231 | 683 | 1050 | 1790 |
| standard deviation retinal lesion size (immediate) | u m | 17 | 69 | 68 | 100 |
| total laser beam power corneal surface | mW | 200 | 320 | 425 | 425 |
| laser beam pulse duration | sec | .1 | .5 | 1 | 4 |
| corneal spot size | mm | 2.5 | 2.5 | 2.5 | 2.5 |
| laser beam full angle divergence | m rad | 7-8 | 33.4 | 63.3 | 78.9 |



SIZE #1



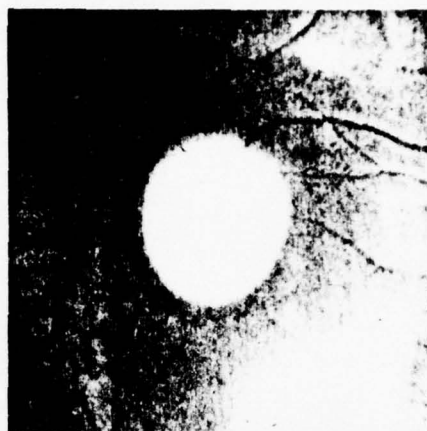
RETINAL PROBE
TIPS PROTRUDING
THROUGH RETINA
1 m m SEPARATION



SIZE #2



SIZE #3



SIZE #4

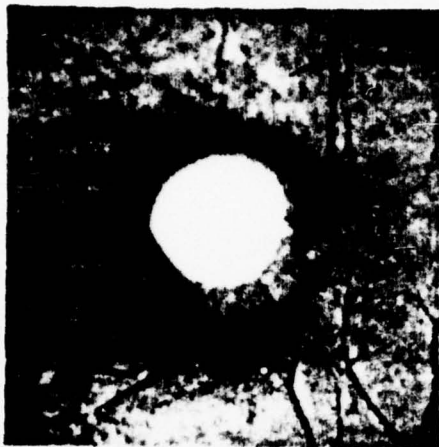
Figure I-B4. Funduscopy view of four lesion sizes.



BEFORE



TWO DAYS AFTER



IMMEDIATELY AFTER



FOUR DAYS AFTER



SEVEN DAYS AFTER

Figure I-B5. Chronological development of large lesions.

looking region on the fundus. The final observed appearance of the damaged retina, as indicated in the photograph labled "seven days after", remained unchanged for at least ninety days.

Figure I-B6 is four fundusoscopic photographs of four lesions which cover the macula. The photographs show clearly blood vessels above the white lesions.

One of the primary objectives of this effort was to obtain a correlation between the measured lesion size using the scaled reticule in the fundus camera and the size of the lesion determined histologically. Figure I-B7 shows a photograph of a one micron thick serial section (perpendicular to the plane of the retina) of a retinal lesion. The section is across the largest dimension of the lesion. Using the scaled reticule in the fundus camera the lesion measured 390 microns across. Using the scale provided with the photograph and measuring from where the pigment epithelium is broken on the left to where it is broken on the right measures 390 microns. The actual damage extends a diameter of about 470 microns. However, clearly, the fundusoscopic visible, measured damage is confirmed histologically to be the major portion of the damaged retina. The fundusoscopic view appeared similar to that labled "SIZE #1" in Figure I-B4 but slightly larger.

The above confirmed measurement lends a great deal of confidence to fundusoscopic dimensional measurements made with the calibrated scaled reticule. Figure I-B8 is the results of a series of retinal spot size measurements, with the scaled reticle, as a function of the measured full angle divergence of the laser beam at the cornea. Some of these measurements are represented in Table I-B1. The straight line on the graph represents the theoretical relationship

$$(\sigma = f \theta)$$

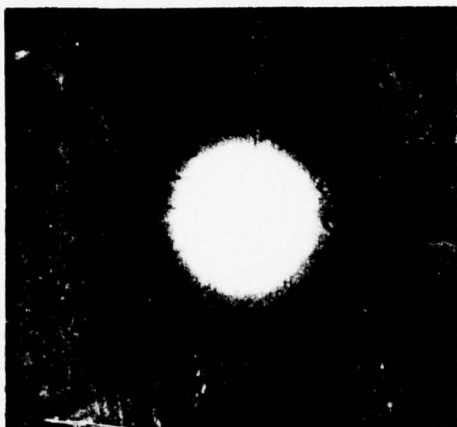
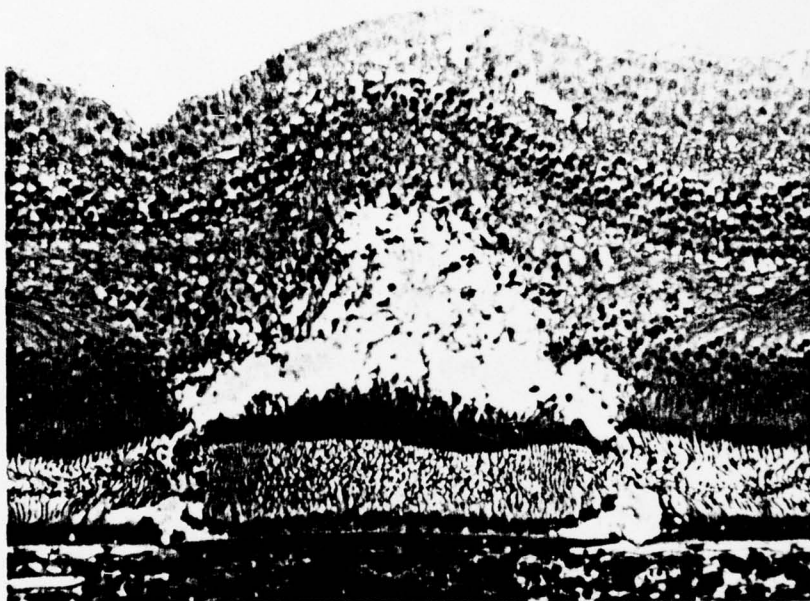
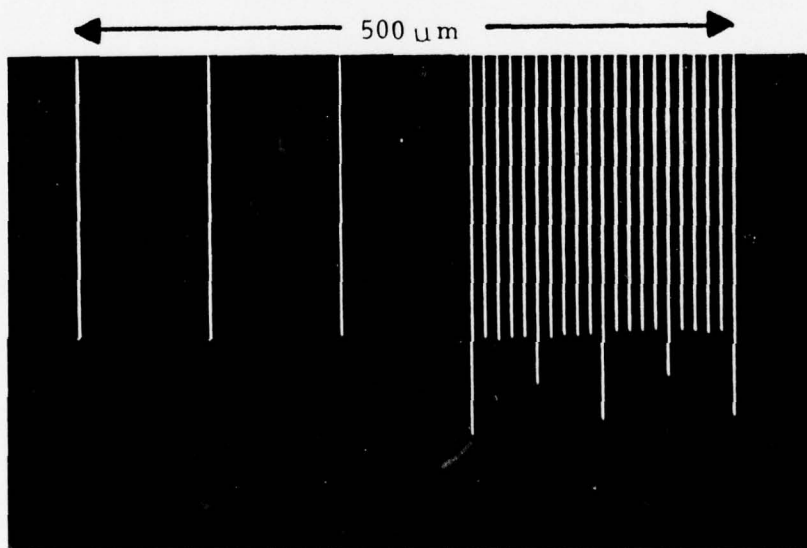


Figure I-B6. Large lesion covering macula.



- P. E.
- Coroid

RETINAL LESION



SCALE

Figure I-B7. Histologically prepared serial section

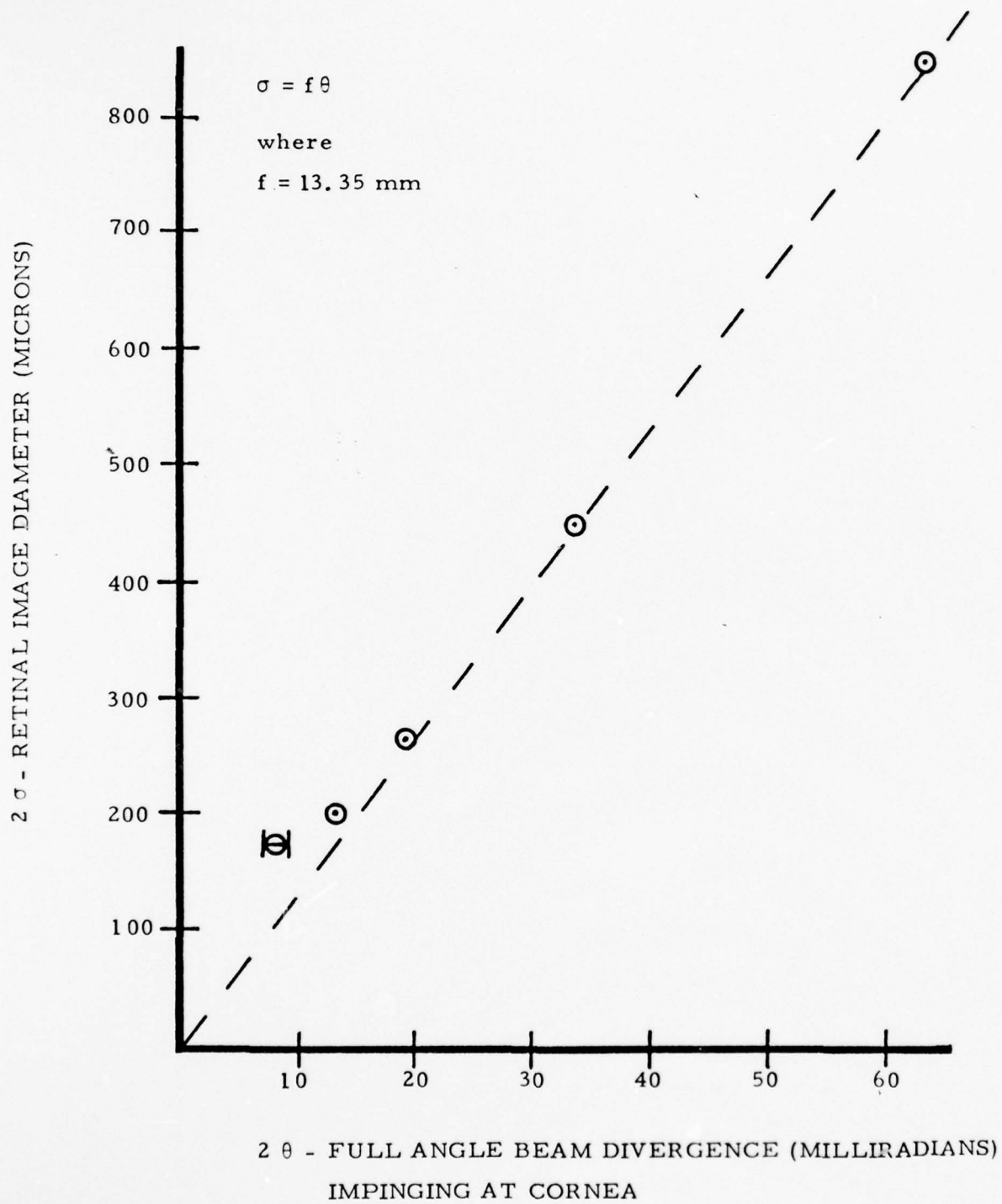


FIGURE I-B8 Retinal spot size vs laser beam divergence

for retinal spot size vs full angle divergence where σ is the retinal spot size radius, with $f = 13.35$ mm as the assumed effective focal length of the rhesus eye, and 2θ is the $1/e^2$ full angle divergence of the Gaussian laser beam impinging at the corneal surface. The points on the graph represent at least ten measurements per point (one measurement per eye) all at $\lambda = 647.1$ nm. The spot size measurement is described in the previous section. Note that the retinal spot size measurement is a subjective determination of the person making the measurement.

PART I-C

TWO STUDIES INVOLVING
HISTOLOGICAL EVALUATION OF
THE CHRONOLOGIC DEVELOPMENT OF
RETINAL LESIONS

The first study involved seven rhesus subjects (fourteen eyes). One super threshold retinal lesion was induced in each eye. The target area on the retina was the macula. The laser beam parameters were the same for each exposure: 400 mW total power incident on the cornea, 500 m sec. single pulse duration, $\lambda = 647.1$ nm, and a retinal spot size of 450 μ . The induced lesion sizes differ slightly but were all about 700 μ in diameter. The photographs of each retinal lesion (just after exposure and just before fixation) are recorded in the lab data books.

The object of this study is to determine if there is any histological evidence of repair in a super threshold laser light induced retinal lesion during a ninety day period. Table I-C1 identifies the rhesus subjects and the survival times associated with each lesion.

The second study involved one subject eye (Subject #476B-left eye). There were sixteen slightly above threshold exposures delivered to the macula region of the retina. The laser beam parameters were the same for each exposure: 18 mW total power incident on the cornea, 40 m sec. single pulse duration, $\lambda = 647.1$ nm, and a minimal retinal spot size. The exposures were placed eight minutes apart. The location in the macula and the order in which the exposures were delivered are recorded in the lab data books. The eye was fixed twenty minutes after the last exposure.

The object of this one eye study is to determine if there is any histologically observable change in a minimal visible lesion in a two hour period.

TABLE I-C1

SURVIVAL TIMES ASSOCIATED WITH LESIONS TO BE
EVALUATED HISTOLOGICALLY

| Subject # | Date of Exposure | | Date Fixed |
|-----------|------------------|-----------|------------|
| | Left Eye | Right Eye | |
| 982 | 11/30/73 | 10/30/73 | 1/29/74 |
| 786 | 10/31/73 | 11/30/73 | 1/2/74 |
| 57B | 11/5/73 | 11/19/73 | 12/3/73 |
| 59B | 11/12/73 | 11/19/73 | 11/26/73 |
| 158B | 11/6/73 | 11/12/73 | 11/13/73 |
| 186B | 11/6/73 | 11/7/73 | 11/7/73 |
| 902 | 1/29/74 | 10/30/73 | 1/29/74 |

SUPPLEMENT I

LASER BEAM RETINAL SPOT SIZE IN THE EMMETROPIC EYE

INTRODUCTION

"Laser beams are similar in many respects to plane waves; however, their intensity distributions are not uniform, but are concentrated near the axis of propagation and their phase fronts are slightly curved". ⁽¹⁾ The phenomenal and unique characteristic of light emitted from a laser is that this light is usually confined to one radiation mode. A radiation mode in a laser is a result of the nature of the amplification of the light fields by the amplifying media combined with the diffraction losses associated with propagation of the fields back and forth between the mirrors of the optical cavity. For the purpose of this discussion we are interested in the spatial distribution characteristics of the transverse fields in the radiation modes. The spatial characteristics of these radiation modes can be determined by repeated application of Huygens' principle. That is: given an arbitrary field distribution at one mirror one can calculate, using the Fresnel-Kirchhoff integral theorem, the field distribution at the other mirror. The repeated calculation yields the nature of the modes of a laser cavity.

Of particular interest to this discussion are the transverse field distributions in the modes of a confocal laser cavity. Any two curved-mirror cavity has an "equivalent" confocal cavity with the same mode structure. ⁽²⁾ Boyd and Gordon ⁽³⁾ show (via the Fresnel-Kirchhoff theorem) that the field distribution associated with a passive confocal cavity having rectangular symmetry can be approximated by Hermite-gaussian functions. (The integral theorem is solvable in closed form under this approximation.) Thus, the approximate transverse field distribution in a given mode in a plane intersecting the axis of the laser cavity at a distance z from the center of the cavity is given by:

$$E(x, y, z) = E_0 \underbrace{H_m \left[\sqrt{\frac{2}{w(z)}} x \right] H_n \left[\sqrt{\frac{2}{w(z)}} y \right]}_{\text{Hermite}} \underbrace{\exp \left[-j \left(\frac{k r^2}{2 q(z)} + kz + \Omega \right) \right]}_{\text{Gaussian}} \quad (S 1)$$

where m and n are the Cartesian mode numbers, x , y , and z are the Cartesian coordinates, $r^2 = x^2 + y^2$, k is the wavenumber of the field, and Ω is a phase shift which is constant across the wavefront (a correction of the velocity of propagation of a mode). $q(z)$ is a complex beam parameter:

$$\frac{1}{q(z)} = \frac{1}{R(z)} - j \left[\frac{\lambda}{\pi w^2(z)} \right] \quad (S 2)$$

where $R(z)$ is the radius of curvature of the wavefront that intersects the axis at z and $w(z)$ is a measure of the decrease of the field amplitude E as a function of distance from the z axis. Similarly, for a cavity having cylindrical symmetry the transverse field distributions are given by Laguerre - gaussian functions:

$$E(r, \varphi, z) = E_0 \underbrace{\left[\sqrt{\frac{2}{w(z)}} r \right]^p \frac{1}{p!} L_p^l \left[\frac{2 r^2}{w^2(z)} \right]}_{\text{Laguerre}} \underbrace{\exp \left[-j \left(\frac{k r^2}{2 q(z)} + kz + l\varphi + \Omega \right) \right]}_{\text{Gaussian}} \quad (S 3)$$

where p and l are the radial and angular mode numbers. The fundamental mode, (TEM_{00}), in each case is Gaussian in form, as indicated in Figure S 1. The parameter $w(z)$ is called the beam radius or "spot size" and is the distance at which the amplitude of E is $1/e$ times that on the axis. Note that since the intensity is proportional to E^2 , $w(z)$ is the distance from the z axis at which the intensity, which is what we can measure, is $1/e^2$ times that on the axis.

Equations S 1 and S 3 are presented to demonstrate the functional form of the spatial distribution of the transverse electromagnetic fields

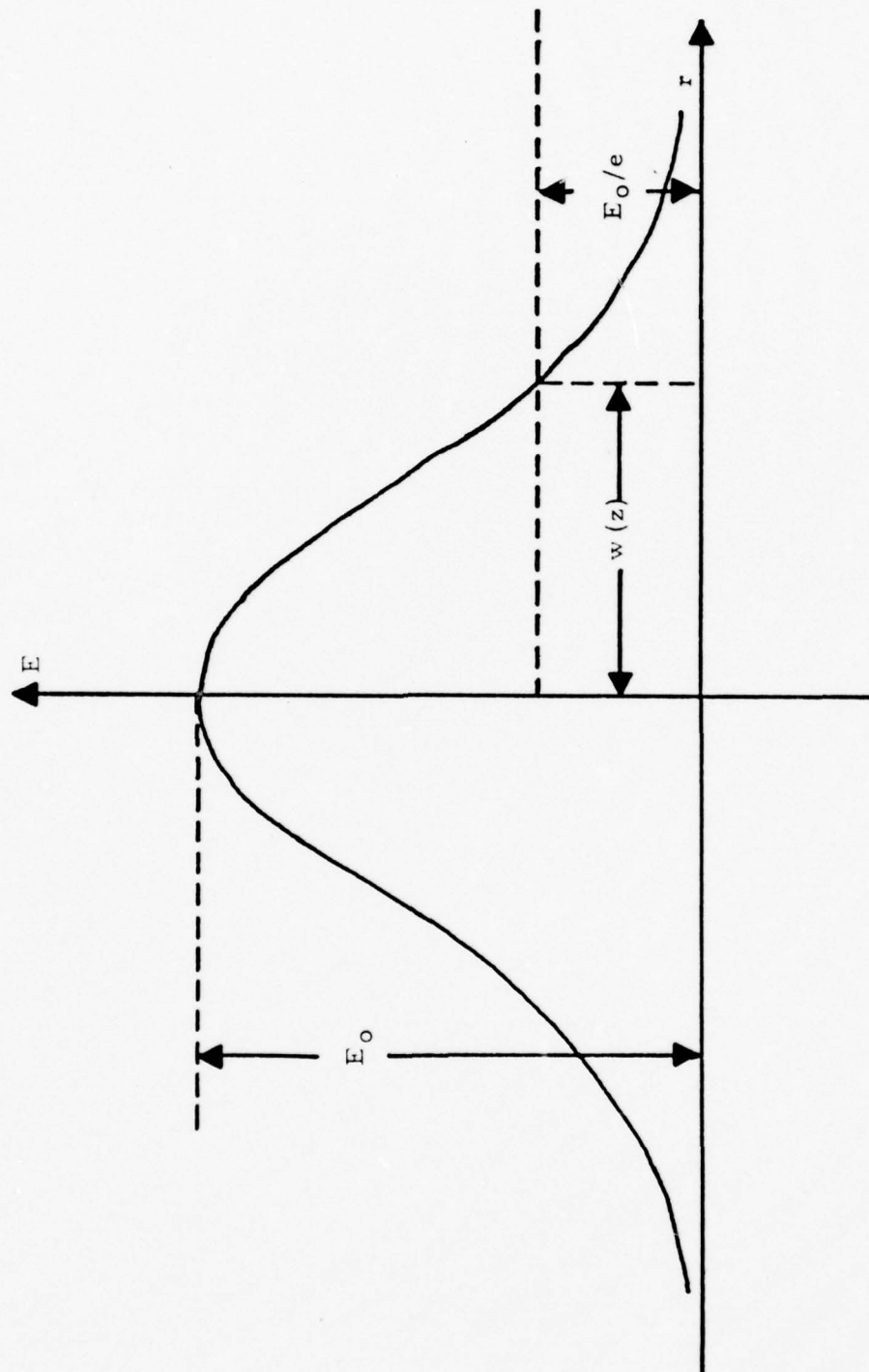


FIGURE S1. Gaussian field distribution

associated with laser beam modes. The concern of this discussion is the effect of an emmetropic eye on a laser beam mode.

GAUSSIAN OPTICS

From the definition of an emmetropic eye we may assume that the multi curved refracting surfaces which focus the light in an eye may be represented by a single thin lens placed a focal length in front of the retina. "An ideal lens leaves the transverse field distribution of a beam mode unchanged". ⁽¹⁾ Thus is the concept of an ideal thin lens in the realm of Gaussian optics. (For a general discussion of the dynamics of optical modes propagating through optical structures we refer the reader to reference #4.) However, a thin lens does change the complex beam parameter $q(z)$. It is this change we consider in determining the expected beam spot size at the retina of an emmetropic eye. Thus, the problem at hand is to determine $q(z)$ at the retina.

It serves our purpose to take from reference #4 an equation which relates $q(z)$ at one plane to $q(z)$ at another plane with an ideal thin lens between. If q_1 and q_2 are determined at a distance d_1 and d_2 from a lens with focal length f as indicated in Figure S 2, the relation between them becomes

$$q_2 = \frac{\left[\frac{f-d_2}{f}\right]q_1 + \left[d_1 + d_2 - \frac{d_1 d_2}{f}\right]}{-\left[\frac{q_1}{f}\right] + \left[\frac{f-d_1}{f}\right]} \quad (S 4)$$

Again, to suit our purpose, let d_2 equal the focal length of the lens (the distance from the effective thin lens to the retina):

$$q_2 = \frac{f^2}{f-d_1 - q_1} \quad (S 5)$$

Thus, at this point we have an expression q_2 which represents the $q(z)$ at the retina in terms of the effective focal length of the eye and q_1 ,

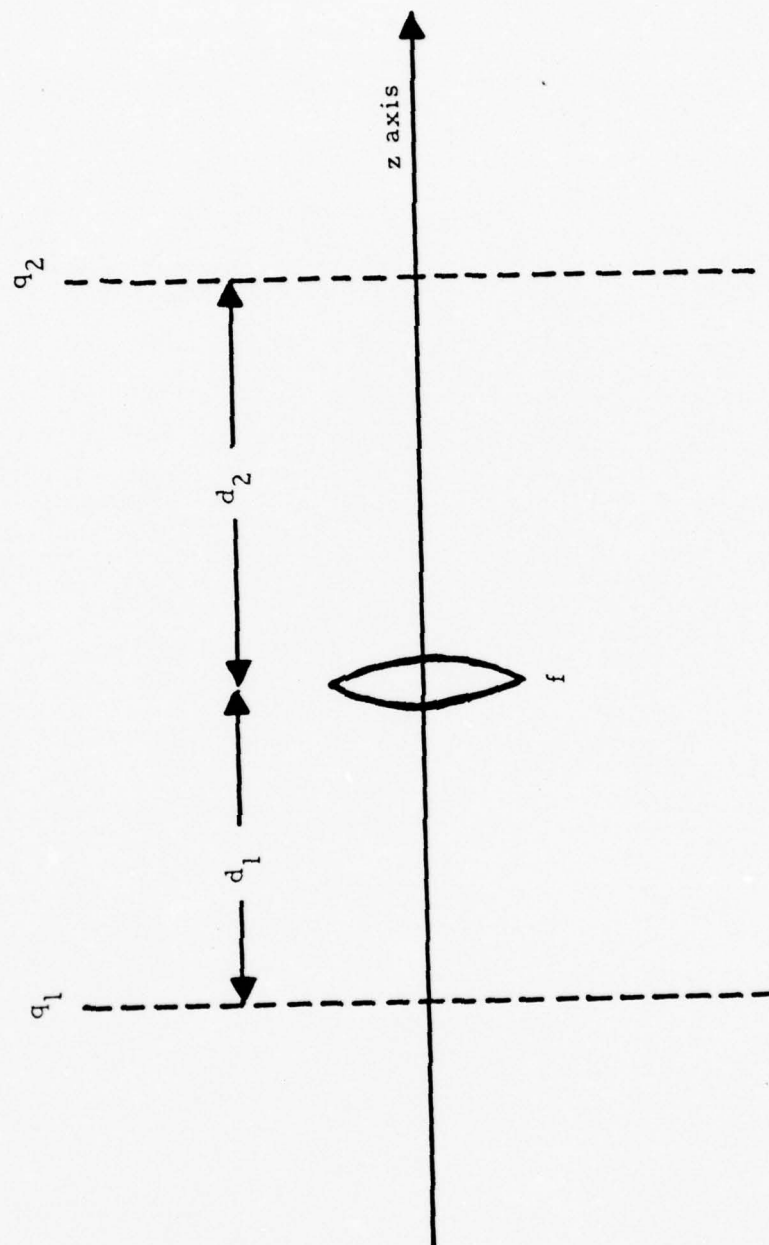


FIGURE S2. q_1 and q_2 plane with thin lens between

which we can calculate from the parameters associated with the confocal laser cavity.

We consider with particular interest the complex parameter $q(z)$ associated with the "fundamental mode" (TEM_{00}) for a confocal laser cavity. The Gaussian beam contracts to a minimum diameter $2w_0$ at the "beam waist" where the phase front is plane. Thus, $R(z)$ at the "beam waist" is equal to infinity and the complex beam parameter becomes

$$q_0 = j \frac{\pi w_0^2}{\lambda} \quad (S 6)$$

If we now substitute this expression into equation S 5 for $q(z)$ at the retina, q_2 , letting d_1 equal the distance from the "beam waist" to the effective thin lens, we have:

$$q_2 = \frac{f^2}{f - d_1 - j \frac{\pi w_0^2}{\lambda}} \quad (S 7)$$

From equation S2:

$$\frac{1}{q_2} = \frac{1}{R_2} - j \frac{\lambda}{\pi w_2^2} = \frac{f - d_1}{f^2} - j \frac{\pi w_0^2}{\lambda f^2} \quad (S 8)$$

where w_2 is the retinal spot size radius. We now set equal to each other the real and imaginary parts of the last equations which yields:

$$w_2 = f \frac{\lambda}{\pi w_0} \quad (S 9)$$

which is an expression for the retinal spot size in terms of the focal length of the eye, the wavelength of the light, and the confocal cavity "beam waist". The beam contour $w(z)$ is a hyperbola (see Figure S 3)

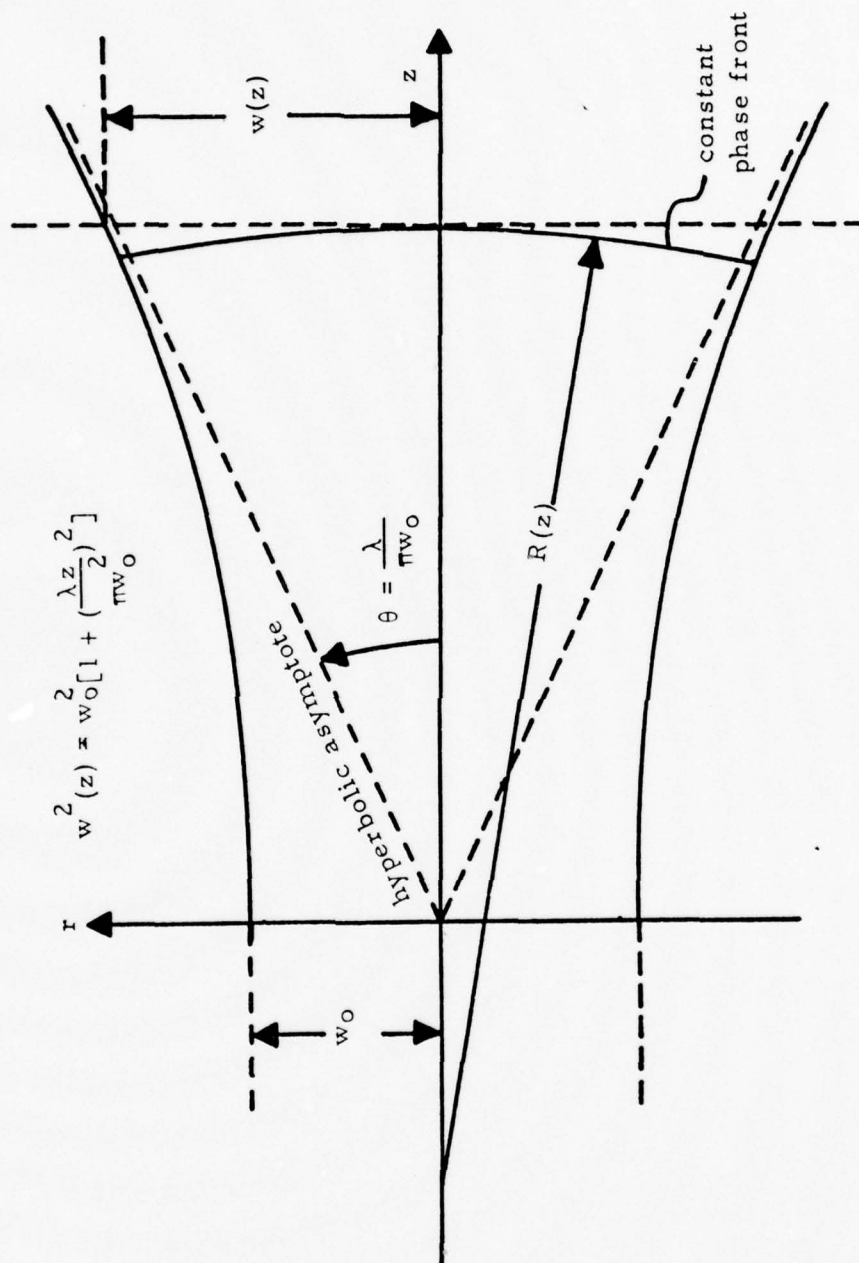


FIGURE S3. Laser beam contour

with asymptotes inclined to the axis at an angle θ where:

$$\theta = \frac{\lambda}{\pi w_0} \quad (S 10)$$

Again, for a full discussion and development of these parameters ($w(z)$, $R(z)$, θ , Ω) as they relate to the confocal laser cavity we refer the reader to any of the references listed herein. 2θ is called the full angle divergence of the laser beam. Thus, the retinal spot size radius is given by:

$$w = f\theta \quad (S 11)$$

It is important to note that the functional form of the laser beam is not changed in passing through the eye. That is to say: the functional form of the laser beam at the cornea, be it Gaussian or whatever, is the same at the retina only the real parameters $R(z)$ and $w(z)$ are changed.

RAY TRACE

The concept of a laser beam as a light ray or a bundle of light rays is void of information concerning the field distribution. Therefore, to calculate a spot size via this method we must pick a ray in the bundle of particular significance to the field distribution. That is to say, we may choose a ray that follows the $1/2$, $1/e$, $1/e^2$, etc. point in the field distribution. Thus, the spot size we calculate with the ray trace will be the $1/2$, $1/e$, $1/e^2$, etc. spot size. To be consistent with the terminology used with laser beams we choose the ray which follows the $1/e^2$ point in the intensity field distribution to define our spot size. This point in the field distribution of a TEM_{00} laser beam mode is $w(z)$ away from the z axis. In the linear region of the laser beam, which would be outside the laser cavity, this $1/e^2$ ray would essentially be the hyperbolic asymptote defined by $w(z)$ (see Figure S 3). Thus, for

the purpose of this calculation we represented the laser beam by a bundle of light rays being emitted from a point on the z axis and bound by the hyperbolic asymptote defined by $w(z)$. The retinal spot size radius we define as the distance from the z axis that the bounding rays cross the retinal plane.

As before, from the definition of an emmetropic eye we may assume that the three (see Figure S 4) curved refracting surfaces which focus the light on the retina may be represented by a single thin lens placed a focal length, f , in front of the retina. In Figure S-4 s is the distance along the optic axis from this effective thin lens to the effective point source and s' is the distance from the effective thin lens to the point source image. From the right triangles defined by the point source, point source image, optic axis, thin lens plane, and the retinal plane, we have the following two relations (see Figure S 4):

$$\frac{p}{s} = \tan \theta' \quad (S 12)$$

and

$$\frac{p}{s'} = \frac{\sigma}{s''} \quad (S 13)$$

where θ' is the angle that the bounding rays make with the optic axis, p is the corneal spot size radius, σ is the retinal spot size radius, and $s'' = s' - f$. From these two equations we get:

$$\sigma = \frac{s'' s}{s'} \tan \theta' \quad (S 14)$$

Now from the thin lens formula:

$$\frac{1}{s} + \frac{1}{s'} = \frac{1}{f} \quad (S 15)$$

which yields

$$f = \frac{s''s}{s'} \quad . \quad (S 16)$$

If we substitute this expression for f into equation S 14 we get:

$$\sigma = f \tan \theta' \quad . \quad (S 17)$$

For small θ' :

$$\sigma = f \theta' \quad . \quad (S 18)$$

Note that the two methods of calculating retinal spot size give the same equation (Equations S 11 and S 18). The calculated spot sizes are the same only if we define θ' to be the same as θ defined in equation S 10 and Figure S 3. Thus, the effective point source, ray trace calculation of laser beam retinal spot size in an emmetropic eye is dependent on how we define the bounding rays.

REFERENCES

1. H. Kogelnik and T. Li, "Laser Beams and Resonators", Proceedings of the I.E.E.E., Vol. 54, No. 10, pp 1312-1329, October, 1966
2. D. C. Sinclair and W. E. Bell, "Gas Laser Technology" Holt, Rinehart and Winston, Inc., Copyright 1969.
3. G. D. Boyd and J. P. Gordon, "Confocal Multimode Resonator for Millimeter Through Optical Wavelength Masers", The Bell Systems Technical Journal, Vol 40, pp 489-508, March, 1961.
4. H. Kogelnik, "Imaging of Optical Mode-Resonators with Internal Lenses", Bell Systems Technical Journal, Vol. 44, pp 455-494, March 1965.

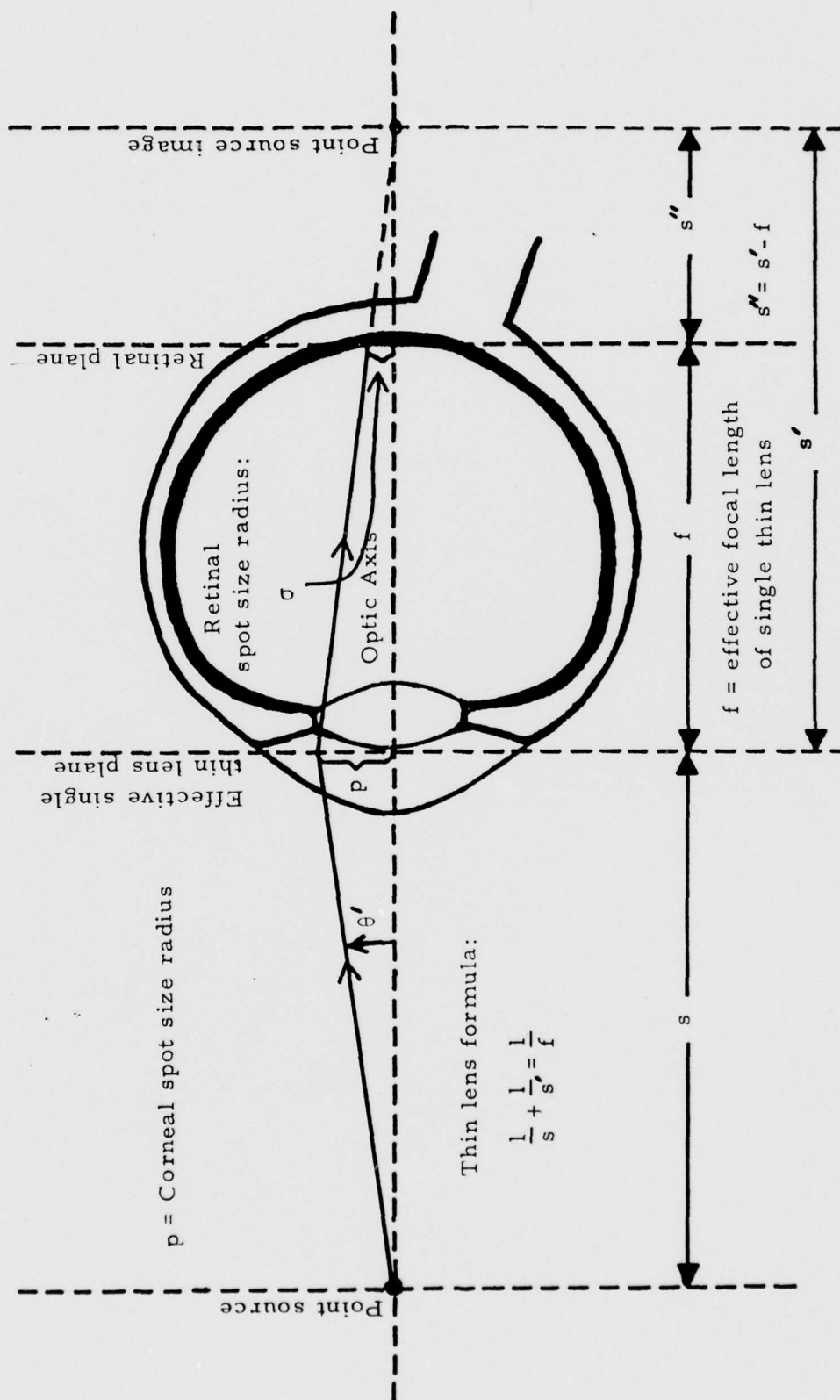


FIGURE S4. Ray trace through eye

PART II

II-A INTRODUCTION

An investigation into the effects of ultraviolet (UV) laser irradiation on ocular media was initiated during the third quarter of the contract year. A number of UV laser systems are currently commercially available and widespread use of these, and systems still under development is anticipated in the near future. Although the inherent sensitivity of biological systems to UV radiation has long been recognized, the safety standards developed for non-coherent UV sources are minimal and did not anticipate the range of parameters associated with laser systems. For example, there is little basis for meaningful safety standards for such situations as high intensity, short pulsewidth UV exposures or repetitive pulse exposures. Therefore, there is a critical need for analyzing the nature of the damage that UV lasers can cause in living matter and for providing guidelines for protection against such damage. The need is especially acute with regard to ocular exposures where grave personnel hazards are created by low damage thresholds coupled with the high potential for accidental exposure due to the victim not having any immediate physical awareness of the exposure.

The UV segment of the electromagnetic spectrum is somewhat arbitrarily divided into three wavelength regions which in common terminology are called the near UV (300-400 nm), far UV (200-300 nm) and vacuum UV(4-200 nm). This investigation will deal specifically with ocular hazards from near UV and far UV radiation. Radiation in these wavelength regions is absorbed by a number of chromophoric sites of proteins and nucleic acids. These chromophores belong to the class of "aromatic" molecules which are characterized by delocalization or sharing of electrons by several chemical bonds resulting in low-lying electronic energy levels.

The amount of energy of a single photon in the near or far UV wavelength range may be such that it can promote an electron of the absorbing aromatic chromophores to an excited energy level. The excited state which the absorbing molecule then finds itself in is a highly labile state from which the molecule may engage in any number of chemical reactions with its molecular neighbors. The resulting photo-induced products may be incompatible with the normal functioning of the exposed system and may, in time, lead to some biological damage which is observable on the macroscopic level.

The photochemical damage mechanism appears to be most efficient in the wavelength range of 260 to 280 nm where many living systems exhibit maximum sensitivity to UV radiation. This wavelength range coincides with the first absorption bands of the chromophoric absorbing sites of all proteins and nucleic acids. The photochemical mechanism is the dominant source of radiation damage only over a limited wavelength range which is tentatively estimated to be $\approx 200-340$ nm. At longer wavelengths, the energy of a single photon is not sufficient to induce excited electronic states in the normal constituents of proteins and amino acids. At shorter wavelengths, radiation is no longer selectively absorbed by the photosensitive aromatic chromophores but, rather, is absorbed by a much larger number of sites in the biological material, many of which are more photo-resistive than the aromatic molecules and may disperse the absorbed energy in a less damaging manner. At the same time at still shorter wavelengths ionization becomes the dominant form of radiation damage. Since an extensive literature is available on ionizing radiation and sophisticated models have already been developed to deal with this aspect of radiation damage, it is not considered further herein.

In this report the absorption properties of the components of the primate eye are reviewed and used to anticipate potential damage sites from radiation in the wavelength range 200-400 nm. The cellular

structure of the cornea is discussed along with the molecular composition of the various corneal layers. (UV damage over most of the 200-400 nm range is restricted to the cornea). Absorption properties of individual aromatic molecules are presented and absorption of UV radiation by living tissue is explained in terms of these molecular properties. The formulation of a quantitative model for the photochemical damage mechanism is begun through a consideration of the electronic energy level schemes associated with aromatic molecules and the kinetics involved with UV-induced transitions between the energy levels.

In the discussions of the above topics several instances are pointed out where currently unavailable experimental data would aid in the understanding of some aspects of UV radiation damage and in the quantitative formulation of this problem. The last section of this report summarizes the experiments proposed to generate the needed data.

II-B UV ABSORPTION BY THE PRIMATE EYE

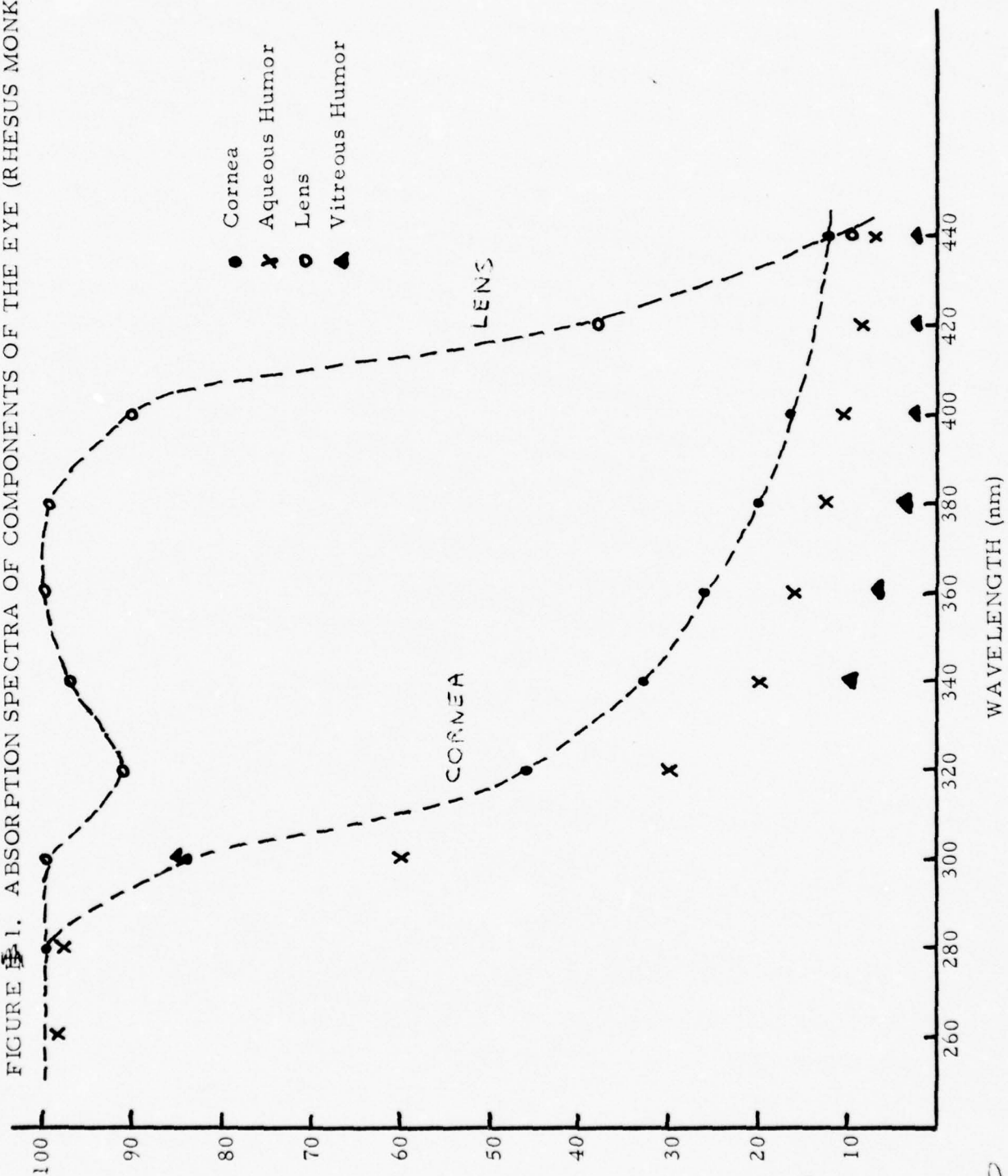
The transmission of the individual ocular media of primate eyes has been determined by Boettner¹ for wavelengths of 220 nm through 2.8 μ . Data from reference 1 has been used to plot percent absorption vs. wavelength for the cornea, aqueous humor, lens and vitreous humor of the rhesus monkey (Figure 1) and the human (Figure 2). The compositions of the rabbit, rhesus and human corneas are very similar. Unless otherwise stated, discussion of properties of the cornea will apply to all of these species.

It is seen that the cornea absorbs virtually all incident radiation below 280 nm. Above 280 nm, the cornea becomes partially transmissive but the lens continues to absorb quite strongly throughout the remainder of the UV. The low percentage of near UV radiation which is transmitted through the lens will be absorbed by the pigment epithelium layer of the retina. The aqueous and vitreous humors are relatively ineffective absorbers except at wavelengths which do not reach them due to screening by anterior components of the eye.

Ocular damage from far UV radiation is expected to be restricted to the cornea. Further, over most of the far UV lesions appear only in the corneal epithelium which comprises approximately the outer 10% of the total thickness of the cornea. Figure 3 illustrates that the epithelium layer absorbs most of the incident radiation below 280 nm.²

The action spectrum for photokeratitis in the rabbit eye due to exposure to non-coherent UV radiation is shown in Figure 4.³ No comparable data is available for exposures to coherent UV radiation. Theoretically, there is no basis for expecting differences in the interactions of UV radiation with living matter due to the property of coherence. However, it is a necessary first step to establish comparable threshold data for at least several different wavelengths to show that, in fact, the same mechanism for damage is operative in both cases.

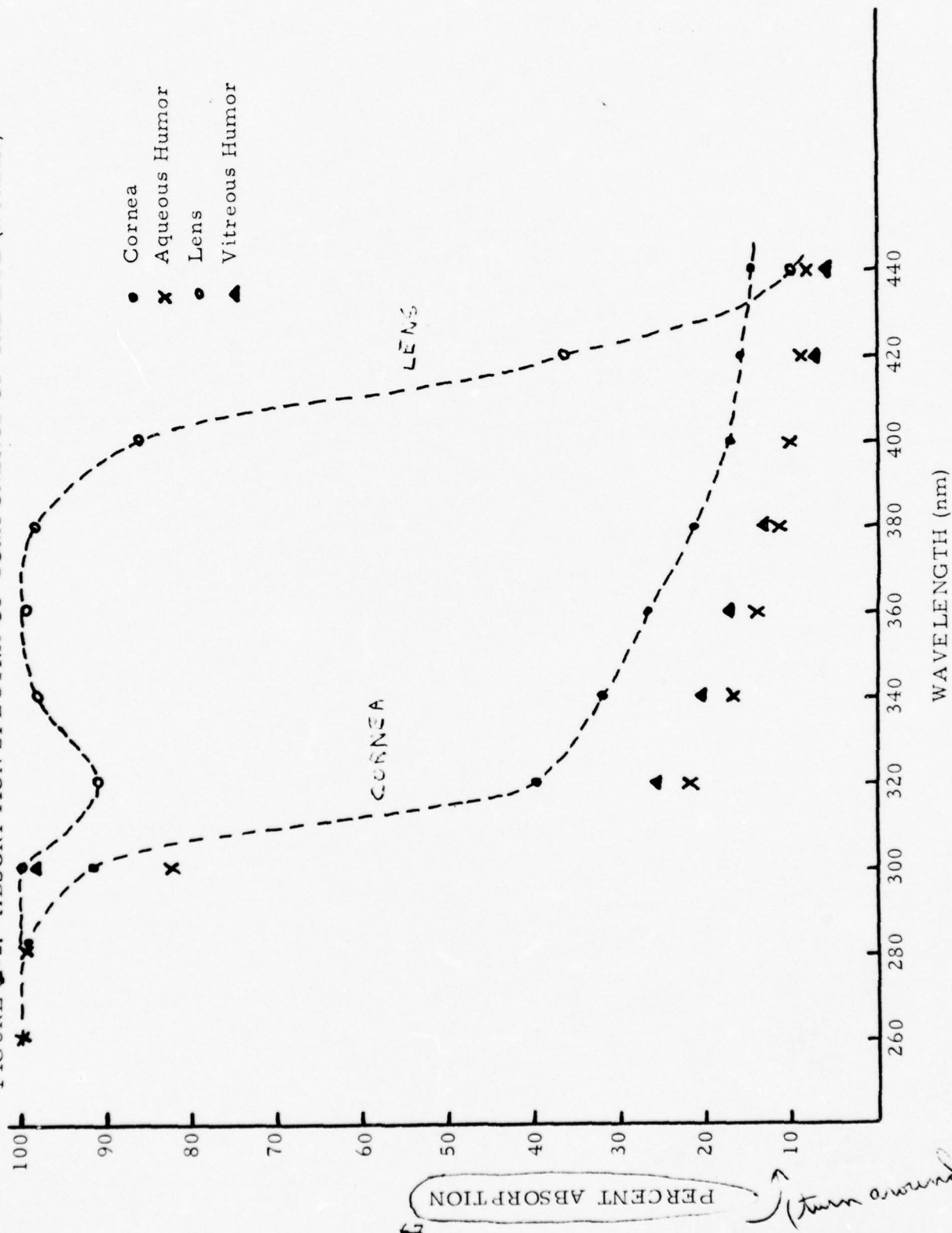
FIGURE 1. ABSORPTION SPECTRA OF COMPONENTS OF THE EYE (RHESUS MONKEY)



PERCENT ABSORPTION

WAVELENGTH (nm)

FIGURE 3-2. ABSORPTION SPECTRA OF COMPONENTS OF THE EYE (HUMAN)



PERCENT ABSORPTION

WAVELENGTH (nm)

(turn around)

FIGURE 3. TRANSMISSION SPECTRA OF THE CORNEA (RABBIT)

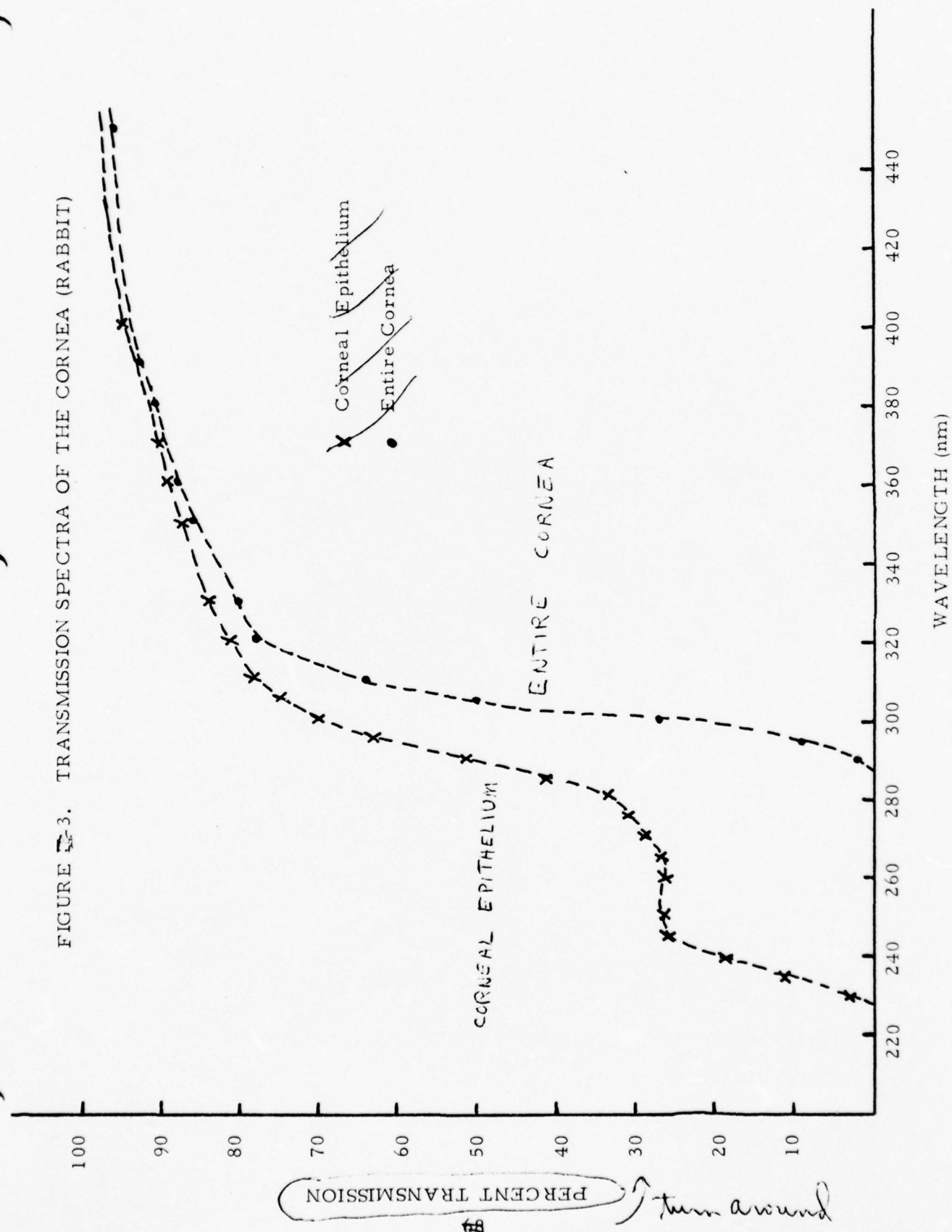


FIGURE 4. ACTION SPECTRUM FOR PHOTOKERATITIS FOR RABBITS

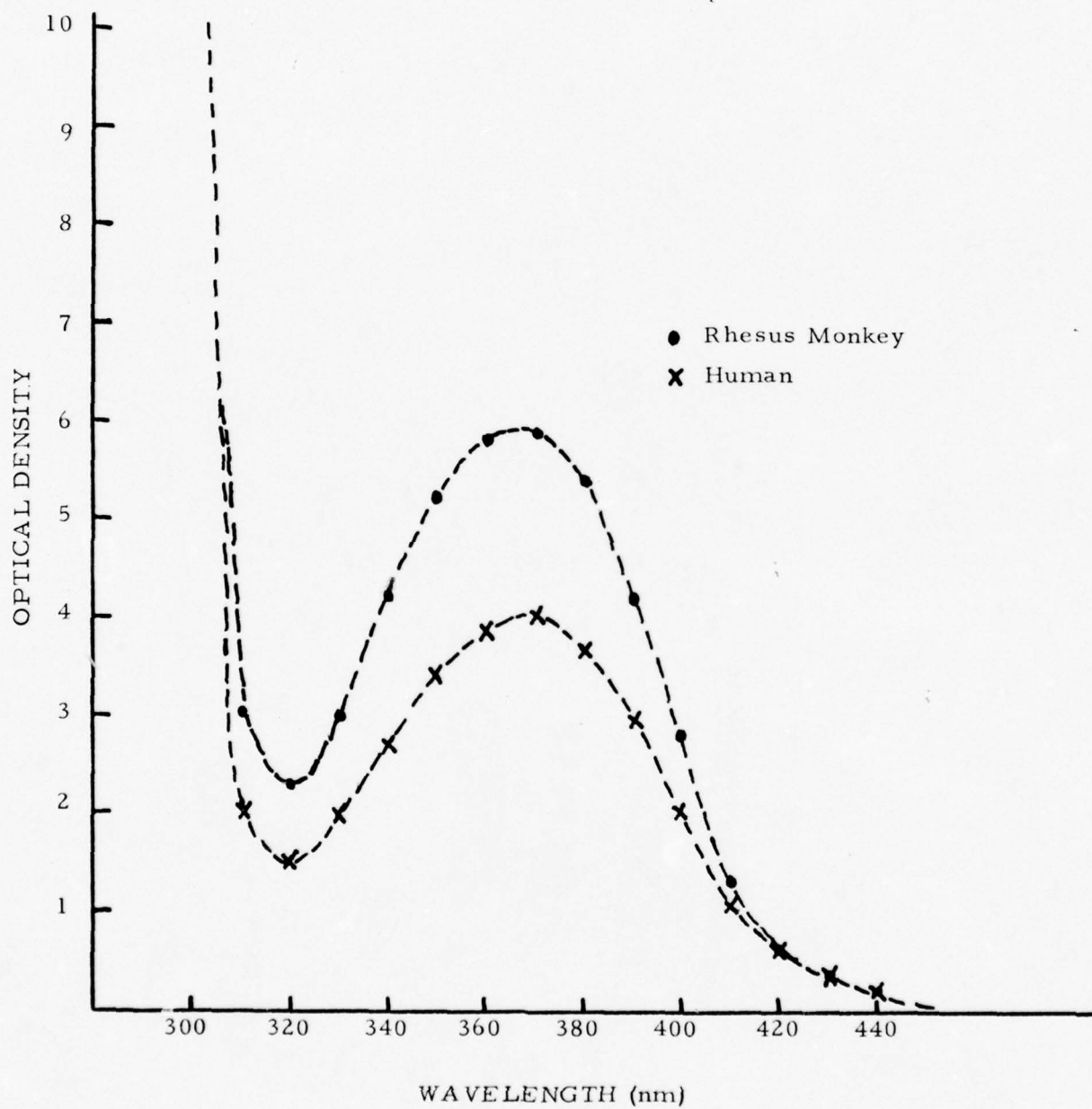


Although epithelial radiation damage may be temporarily incapacitating, it is completely repairable and full visual recovery is achieved in a matter of days. At somewhat higher intensities of incident UV radiation, lesions may also be formed in the posterior layers of the cornea. Such injury usually results in scar formation and the resulting opacities, if of sufficient size, cause permanent loss of visual acuity. Thus, at UV wavelengths where the epithelium is partially transparent, it is of considerable importance to determine an action spectrum for corneal scarring. Quantitative data for this type of damage has not appeared in the literature.

The lens will absorb most of the UV radiation which is transmitted through the cornea. In addition to the aromatic molecules found in the cornea, the lens contains a yellowish pigment which has an absorption peak in the near UV.⁴ The optical densities of the lenses of several species have been measured and the results for the rhesus monkey and the human are seen in Figure 5. Absorption maxima are found at 366 nm and minima at 320 nm. The minima allow approximately 1% of the light incident upon the cornea to be transmitted directly to the retina at 320 nm. A similar percentage of incident radiation reaches the retina at 400 nm. Above 400 nm this percentage increases very rapidly with wavelength.

Since most of the incident radiation at 366 nm is absorbed by the lens it seems reasonable to ask if the lens is the primary site of damage from radiation of this wavelength. If so, over what wavelength range is the lens the most sensitive component of the eye? Unfortunately, there is little quantitative data available on lenticular damage in the near UV. Broadband irradiation in the vicinity of 300 nm indicates comparable thresholds for lenticular and corneal damage when using a reversible lens clouding as a damage criteria.⁵ The only useful piece of data, however, is a result indicating that the threshold for cataract formation at 325 nm is roughly eight times the threshold value of 31.6

FIGURE II-5. DENSITY SPECTRA OF PRIMATE LENSES



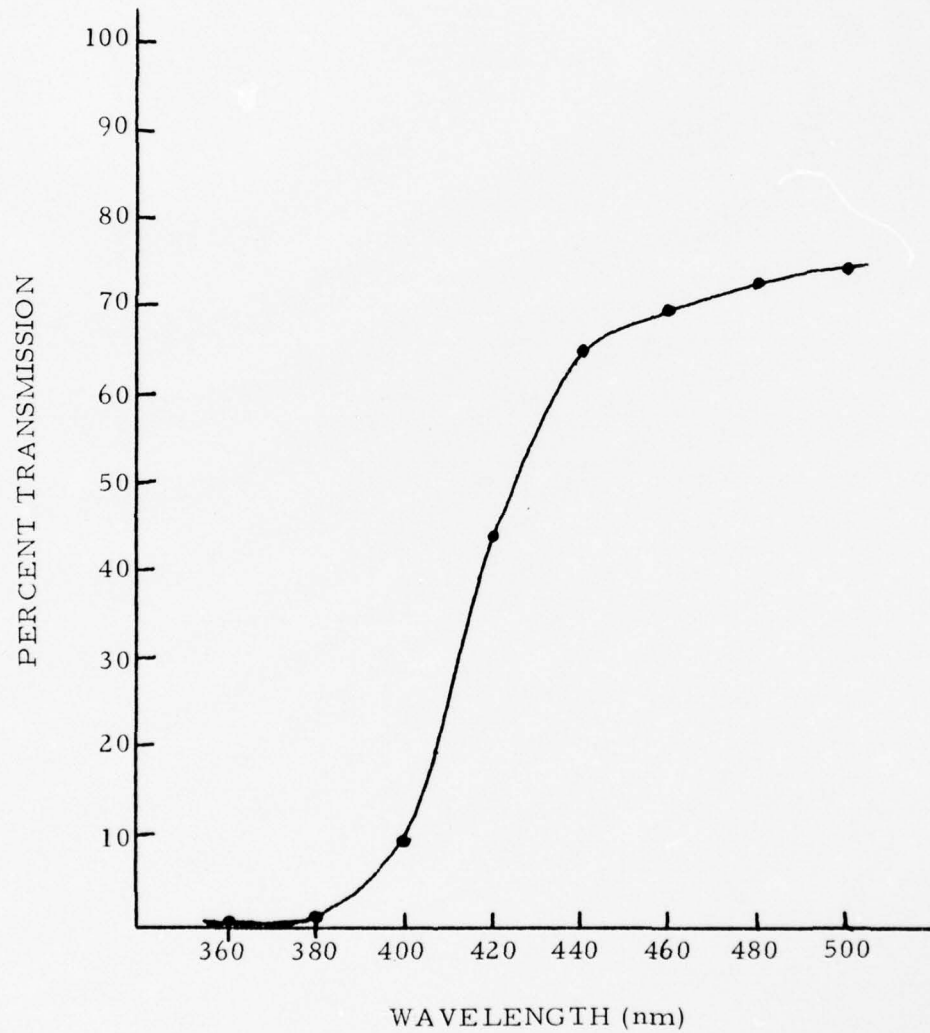
joule/cm² found for corneal damage at this wavelength.⁶

On the basis of the preliminary results for 325 nm radiation, it might well be expected that the lens will have a lower threshold for damage than the cornea at 366 nm. More of the incident radiation is transmitted through the cornea at 366 nm than at 325 nm and the radiation which reaches the lens is absorbed more strongly at 366 nm. Quantitatively the absorption characteristics (Figures 3 and 5) can be used to predict a decrease by a factor of 6.9 in the relative thresholds for lenticular to corneal damage in going from 325 nm to 366 nm. (This calculation is only meaningful if the mechanism for damage and its efficiency does not change over the wavelength range in question.)

The result mentioned above for lens damage at 325 nm represents a gross form of lens damage in that it is based upon observation of cataract formation within a matter of hours after irradiation. With lower levels of irradiation, cataract formation may not be apparent until many months after the exposure but the end result is still serious ocular damage. Thus, it seems imperative to give some consideration to the lens as a potential site for damage over part of the near UV and to establish a suitable criteria for predicting long term cataract formation.

With visible light, most of the incident radiation is transmitted to the retina and the dominant mechanism for damage is believed to be a thermal effect. As the wavelength is shortened to 400 nm and into the near UV, the percentage of radiation reaching the retina becomes severely attenuated. Nevertheless, the retina may be the most sensitive component of the eye over the nearest segment of the UV (\approx 400 nm). In any event, the threshold for retinal damage will vary considerably with wavelength near 400 nm. This may be seen from Figure 6 which shows that the percent of incident radiation transmitted through the anterior components to the retina varies radically with wavelength near 400 nm.¹ (By way of contrast it is seen that there is little wavelength dependence from 450 to 800 nm.)

FIGURE II-6. PERCENT OF CORNEAL INCIDENT
RADIATION TRANSMITTED TO RETINA



With continuously tunable UV lasers available, it seems that it would now be possible to determine the wavelength dependence of the retinal threshold level in the vicinity of 400 nm and to determine the wavelength where the retina ceases to be the most sensitive component of the eye and where the cornea or lens becomes more sensitive. The need for determining the wavelength range over which each component of the eye is the most sensitive is quite basic now that tunable lasers are commercially available. Consider that the accepted allowable exposure levels are based on the assumption of a certain mechanism occurring in a certain component of the eye. If, at the same wavelength, another component of the eye is sensitive to the incident radiation (possibly by an entirely different mechanism for damage), the safety standard may be completely meaningless or at least valid only over restricted ranges of laser beam parameters.

II-C CELLULAR COMPOSITION OF THE CORNEA

A transverse section of the human cornea is depicted in Figure 7. The human, rhesus and rabbit corneas are quite similar except for the absence of Bowman's Membrane in the rabbit.

The surface or epithelial layer comprises about 10% of the total thickness of the cornea. A close-up view (Figure 8) shows that the epithelium consists of five or six layers of cells which are divided into three categories. A single layer of basal or columnar cells lines the posterior border of the epithelium. The nuclei of the basal cells are oval in shape with their long axis perpendicular to the corneal surface. Above the basal layer are two layers of polyhedral cells which are elongated and oriented parallel to the surface. Finally, there are three layers of squamous cells which are more elongated than the polyhedral cells and also run parallel to the corneal surface.

All epithelial cells are generated from mitotic division of the basal cells. After being formed the cells are gradually pushed upward to the corneal surface, changing in shape and orientation during this process. Upon reaching the surface the cell dies (in a matter of one day or so) and decomposes, the debris being sloughed off into the tear layer. The average cell life is approximately six days.

The above considerations disclose that, in fact, there is only one type of cell in the corneal epithelium. The cells may change their positions and shapes during the six day lifetime but the molecular composition remains basically unchanged. It may be anticipated therefore that the basal, polyhedral and squamous cells will all show the same sensitivity to UV radiation.

The corneal epithelium exhibits very great recuperative powers. Even if the entire epithelium is stripped off, a complete new layer of basal cells may be regenerated within 24 hours, by multiplication of the peripheral conjunctival cells. In several weeks this single layer

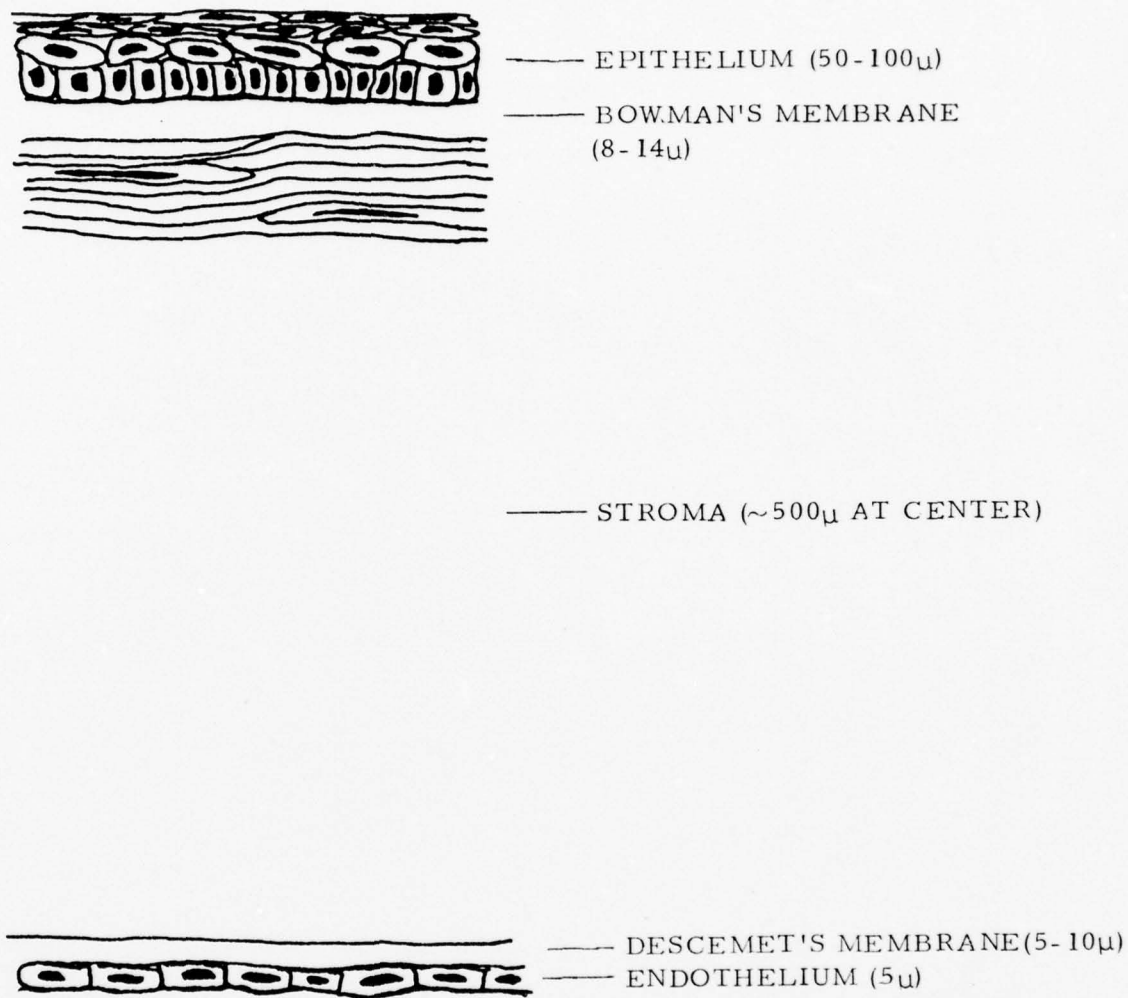


FIGURE 7. TRANSVERSE SECTION OF CORNEA

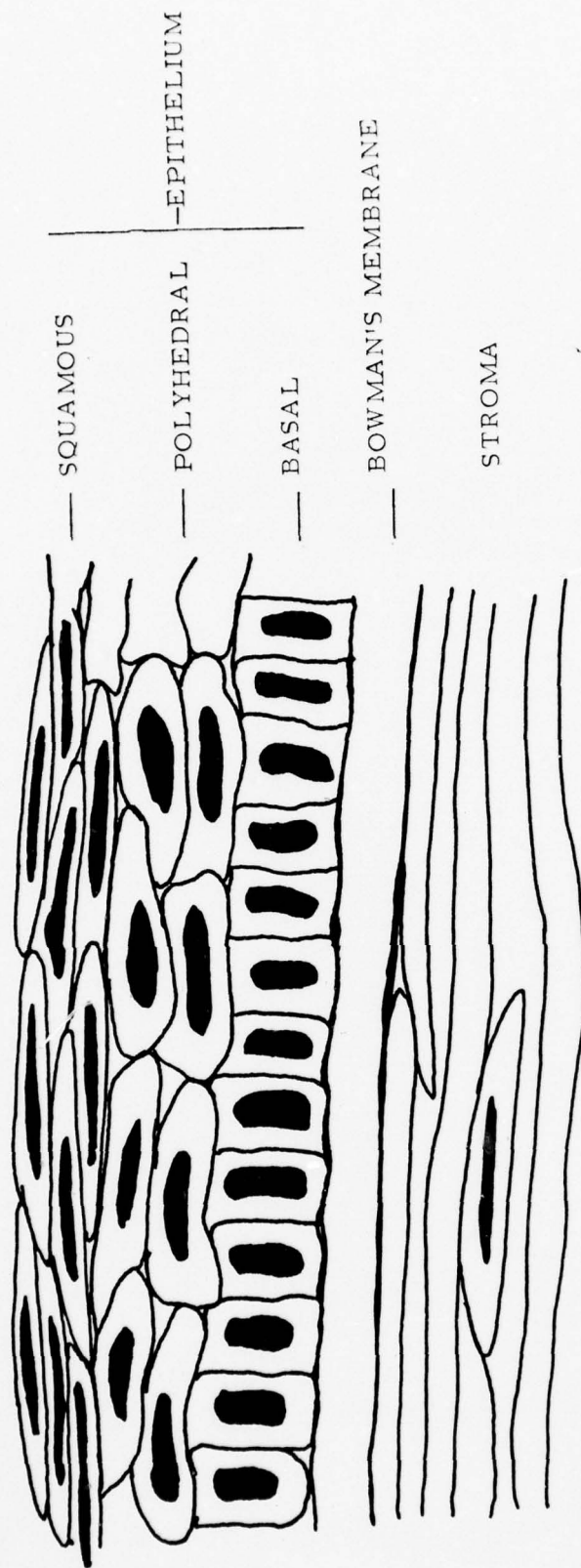


FIGURE 8. TRANSVERSE SECTION OF CORNEAL EPITHELIUM

develops into a complete epithelium.

Although no repair mechanism, per say, has been identified in the epithelium, the normal cell replacement rate must be taken into account in the consideration of repeated exposures over a period of time. The average cell life is six days, during which the cell travels from its birthplace in the basal layer to the surface where it dies and is sloughed off. Since this involves traversal of five or six layers, the cell spends roughly one day in each layer. Thus, threshold radiation damage, if restricted to the outermost layer of cells would be completely obscured within one day simply by the normal cell replacement progression. Damage penetrating the entire epithelial layer could be completely "repaired" in approximately six days by the same replacement process. If, in addition, there is a repair mechanism operative within individual cells the observed repair rate may be more rapid than the replacement rate. Any cellular repair mechanism which could be identified in damaged epithelial tissue would provide invaluable information regarding the nature of the molecular lesions which lead to observed macroscopic damage.

The stroma account for 90% of the thickness of the cornea. A cross-sectional view such as that in Figure 8 shows that the stroma is made up of lamellae or flat sheets 1.5 to 2.5 μ thick running parallel to the corneal surface. The human cornea contains over 200 such overlapping lamellae. The lamellae are composed of collagen fibres which, within any given sheet, run parallel to each other. Adjacent layers have their fibres oriented in perpendicular directions.

An occasional cell is found lying within the lamellae. These cells are usually flattened and have enlarged nuclei and "branches" which connect to neighboring cells. However, the stroma is basically a structural rather than a cellular medium and observable radiation damage appears to involve disruption of the collagen fibres rather than of the occasional cell. Destroyed collagen fibres can be replaced in the

stroma but not necessarily with the proper orientation so that a permanent opacity or scarring results.

Bowman's and Descemet's membranes are merely extensions of the stroma and also composed mainly of collagen fibres. The chief difference between the three layers lies in the ordering of the fibres within each layer. The endothelium is a single layer of cells with absorption properties similar to the anterior layers of the cornea and, hence, fairly well shielded from the most damaging forms of radiation.

From the above it is seen that for purposes of considering UV radiation damage, the cornea may be thought of as being composed of two layers: the epithelium or cellular layer and the stroma (including Bowman's and Descemet's membranes) or structural layer. Epithelial damage is apparently completely reversible while stromal damage results in permanent scarring. The action spectrum of Figure 4 shows the wavelength dependence for epithelial damage. Little is known about the wavelength dependence of stromal damage or for that matter about the threshold for stromal damage at any wavelength. While the threshold for epithelial damage may be considerably lower, it seems desirable (because of its permanent nature) to also establish a guide to radiation levels which would induce stromal damage. It is not clear that the same type of photochemical mechanism which accounts for epithelial damage will be involved in stromal damage but having comparative data would aid in specifying the nature of the mechanisms in the two cases.

II-D MOLECULAR COMPOSITION OF THE CORNEA

As mentioned in the preceding section, the basal, polyhedral and squamous cells of the epithelium all have a common parenthood and, hence, a common molecular composition. Water makes up 80% of the epithelium. Of the dry material the composition found is⁹:

| | |
|-----|-------------------------|
| 75% | protein |
| 11% | lipid (fat) |
| 5% | glycogen (carbohydrate) |
| 3% | nucleic acid |
| 1% | various salts |

The stroma which also has 75-80% water has the following breakdown of dry material¹⁰:

| | |
|-----|-------------------------------|
| 90% | protein |
| 4% | polysaccharide (carbohydrate) |
| 1% | lipid (fat) |
| 1% | various salts |

Of the stromal protein, some 70% is the collagen which makes up the array of fibres. Only a trace amount of nucleic acid ($< 0.1\%$) is found in the stroma and this is localized in the few cells interspersed within the collagen lamellae.

In view of the function of the cornea it is not surprising that it contains no pigments which absorb visible light. As will be shown below, UV absorption by the cornea is due to the absorption of certain constituents of the proteins and nucleic acids. Since the nucleic acid content of the stroma is negligible, absorption in that layer is due solely to protein. In the epithelium, the nucleic acid absorption is comparable to protein absorption over much of the UV (despite the 25:1 ratio of protein to nucleic acid).

In order to more fully characterize the interaction of UV

radiation with the cornea a brief review is presented of the molecular composition and absorption properties of proteins and nucleic acids. For further information the reader is referred to several standard texts¹¹⁻¹⁴.

A protein is a linear polymer of amino acids. The repeat sequence is illustrated in Figure 9. Some 20 amino acids are commonly found in proteins, differing only in the nature of the side chain R (see Figure 9). Of the twenty, three amino acids are aromatic in nature and account for the UV absorption of proteins. The structures of these three chromophores are shown in Figure 10. Several other amino acids begin to absorb in the vicinity of 200 nm. In the vacuum UV all of the amino acids as well as the bonds linking them together absorb quite strongly.

The absorption spectra of the aromatic amino acids are shown in Figure 11 and the absorption spectrum of a common protein (serum albumin) is included in Figure 12. This absorption curve is representative of almost all naturally occurring proteins. It is readily shown that such a protein absorption curve can be constructed from the spectra of the aromatic amino acids. The major features of the spectra (the maxima near 275 nm and 225 nm and the minimum near 250 nm) vary slightly from protein to protein depending on the relative abundance of the aromatic amino acids in each case.

A nucleic acid chain is a linear polymer of monomer units called nucleotides. As shown in Figure 13, a nucleotide consists of a sugar, a phosphate group and a "base" which is either a purine or pyrimidine derivative (Figure 14). The sugars and phosphates are transparent above 200 nm and only the bases account for the DNA absorption spectrum shown in Figure 12. There are several kinds of nucleic acids found in the cell but all have similar bases with similar absorption spectra. Therefore, the DNA curve of Figure 12 is taken as representing the absorption of all cellular nucleic acids.

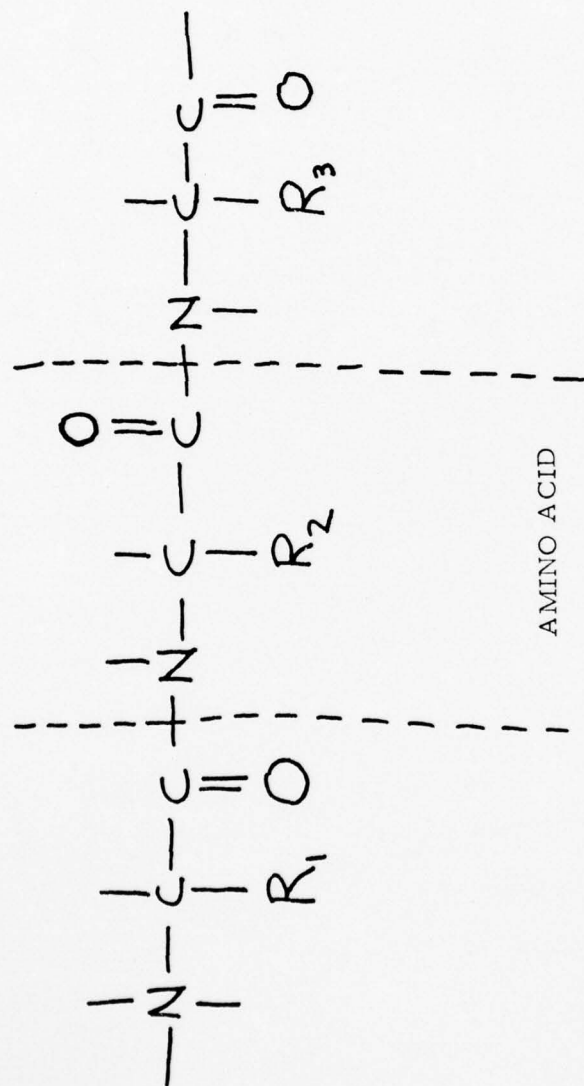
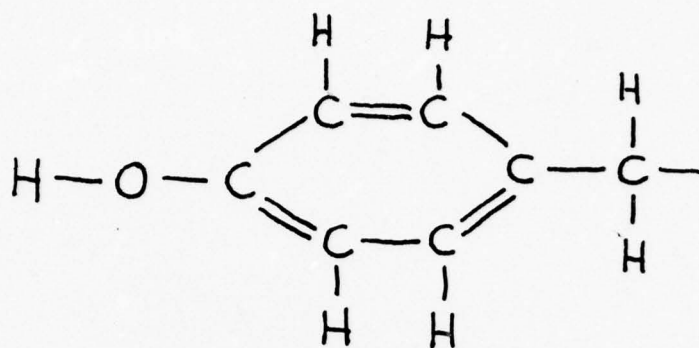
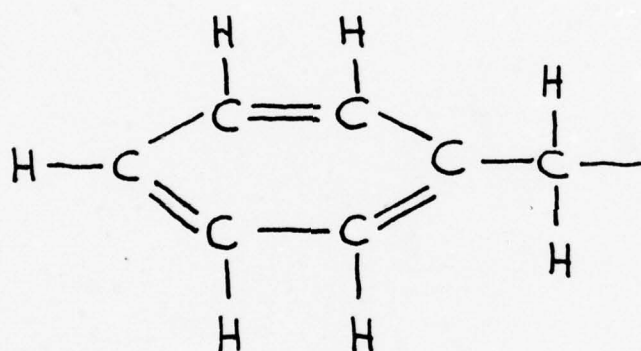


FIGURE II-9. MOLECULAR STRUCTURE OF PROTEIN

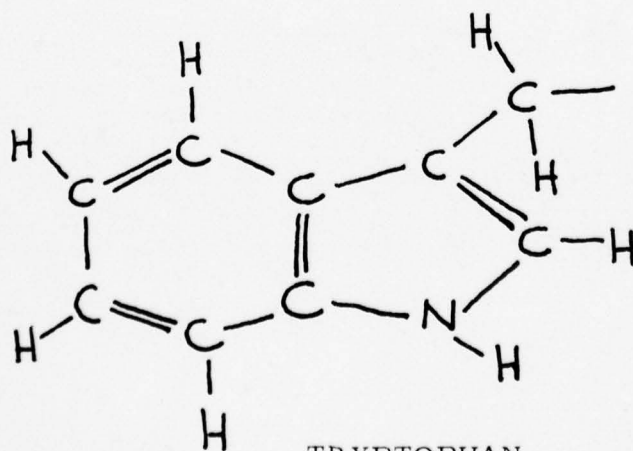
FIGURE II-10. AROMATIC AMINO ACIDS



TYROSINE



PHENYLALANINE



TRYPTOPHAN

FIGURE 11. ABSORPTION SPECTRA OF THE
AROMATIC AMINO ACIDS

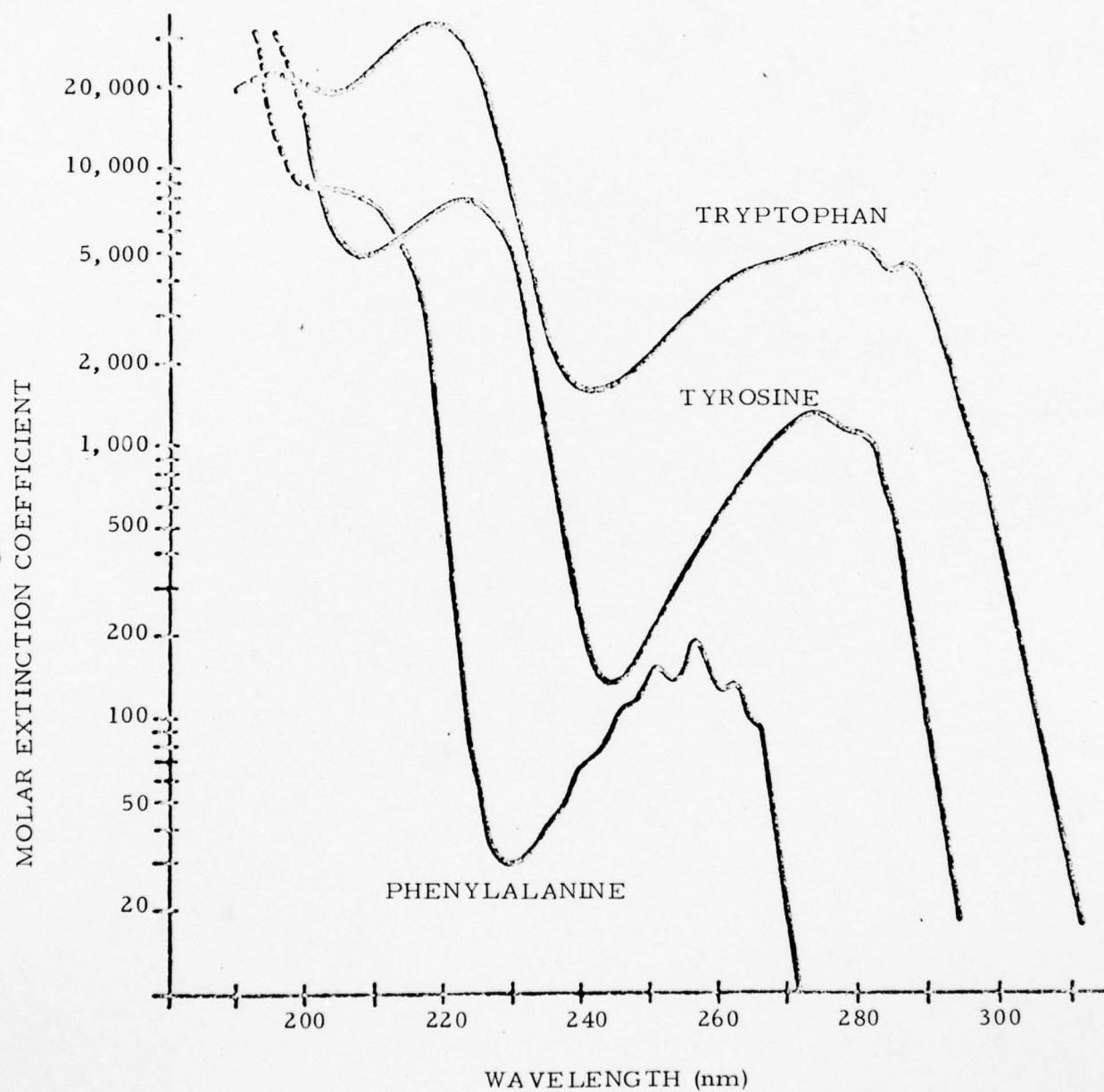
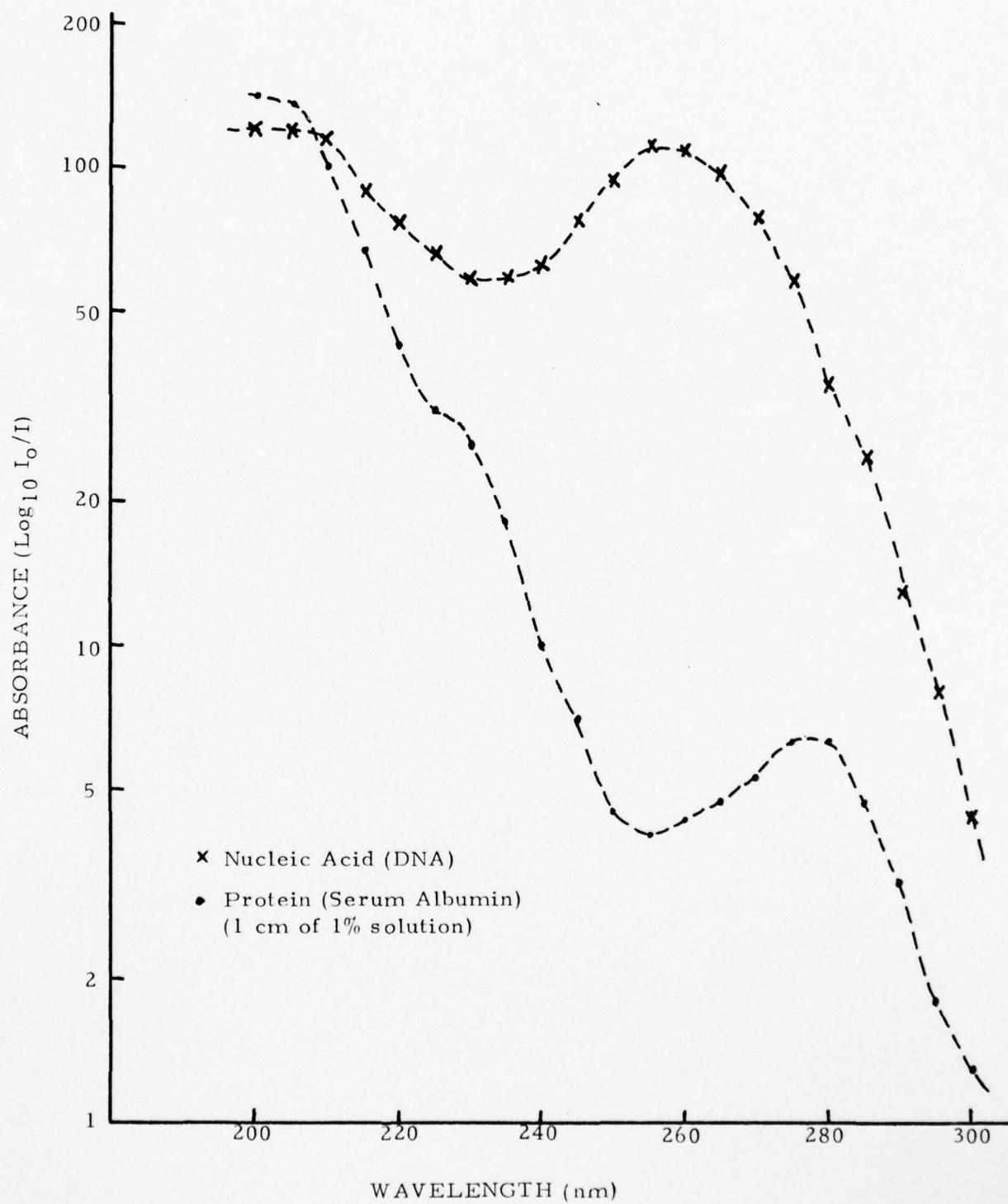


FIGURE 12. ABSORPTION SPECTRA OF
BIOLOGICAL MACROMOLECULES



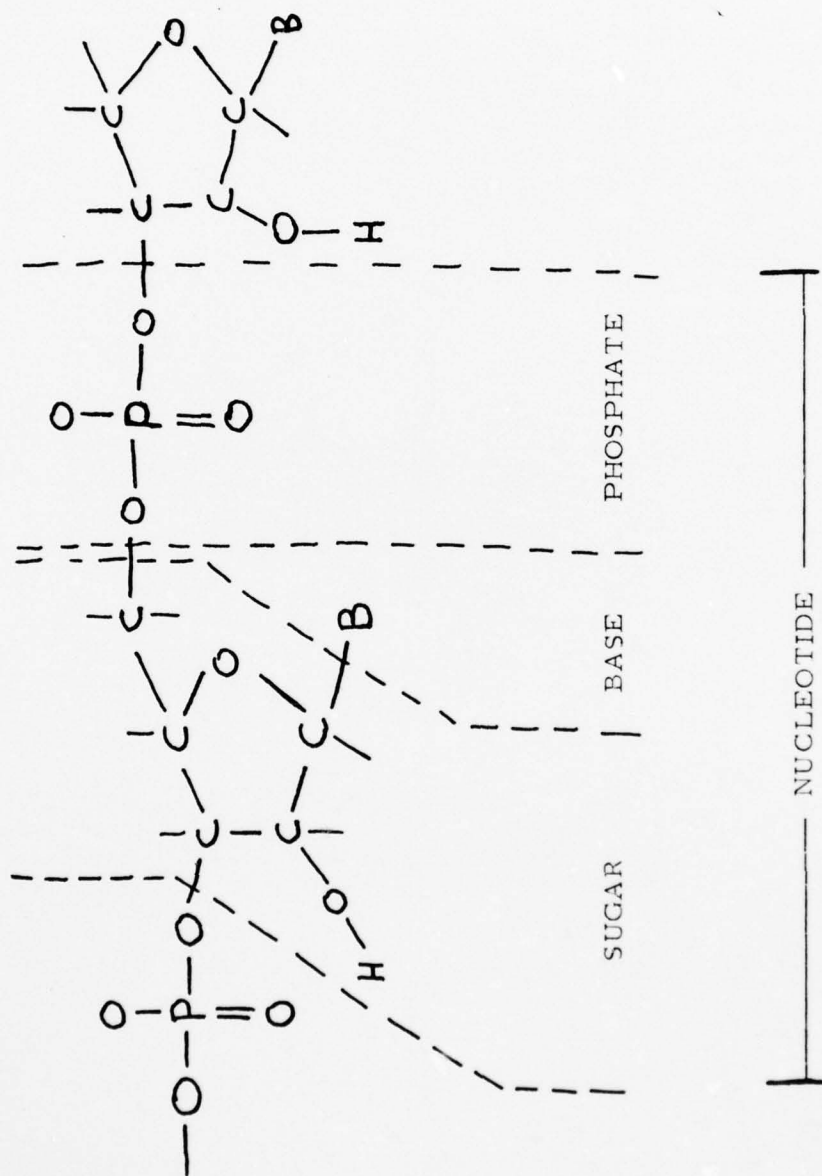
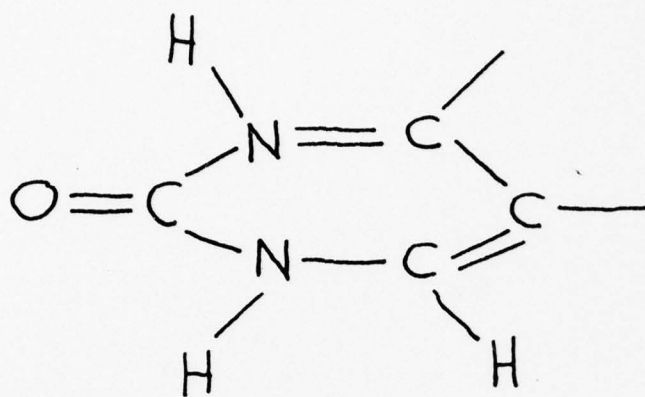
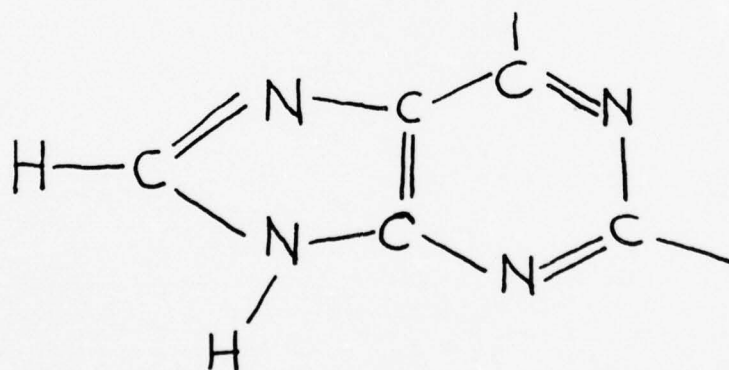


FIGURE II-13. MOLECULAR STRUCTURE OF NUCLEIC ACID



PYRIMIDINE



PURINE

FIGURE II-14. NUCLEIC ACID BASES

AD-A039 033

TECHNOLOGY INC SAN ANTONIO TEX LIFE SCIENCES DIV
RESEARCH ON THE OCULAR EFFECTS OF LASER RADIATION.(U)
FEB 74 V E SANDERS, J A ZUCILICH

F/G 6/18

F41609-73-C-0017

UNCLASSIFIED

TI-74-0561-01

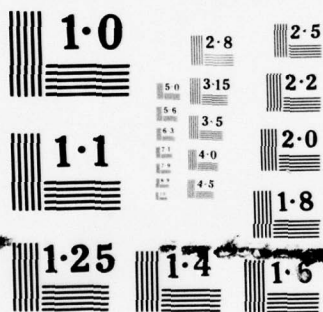
NL

2 OF 2
ADA
039033



END

DATE
FILMED
5-77



NATIONAL BUREAU OF STANDARDS
MICROCOPY RESOLUTION TEST CHART

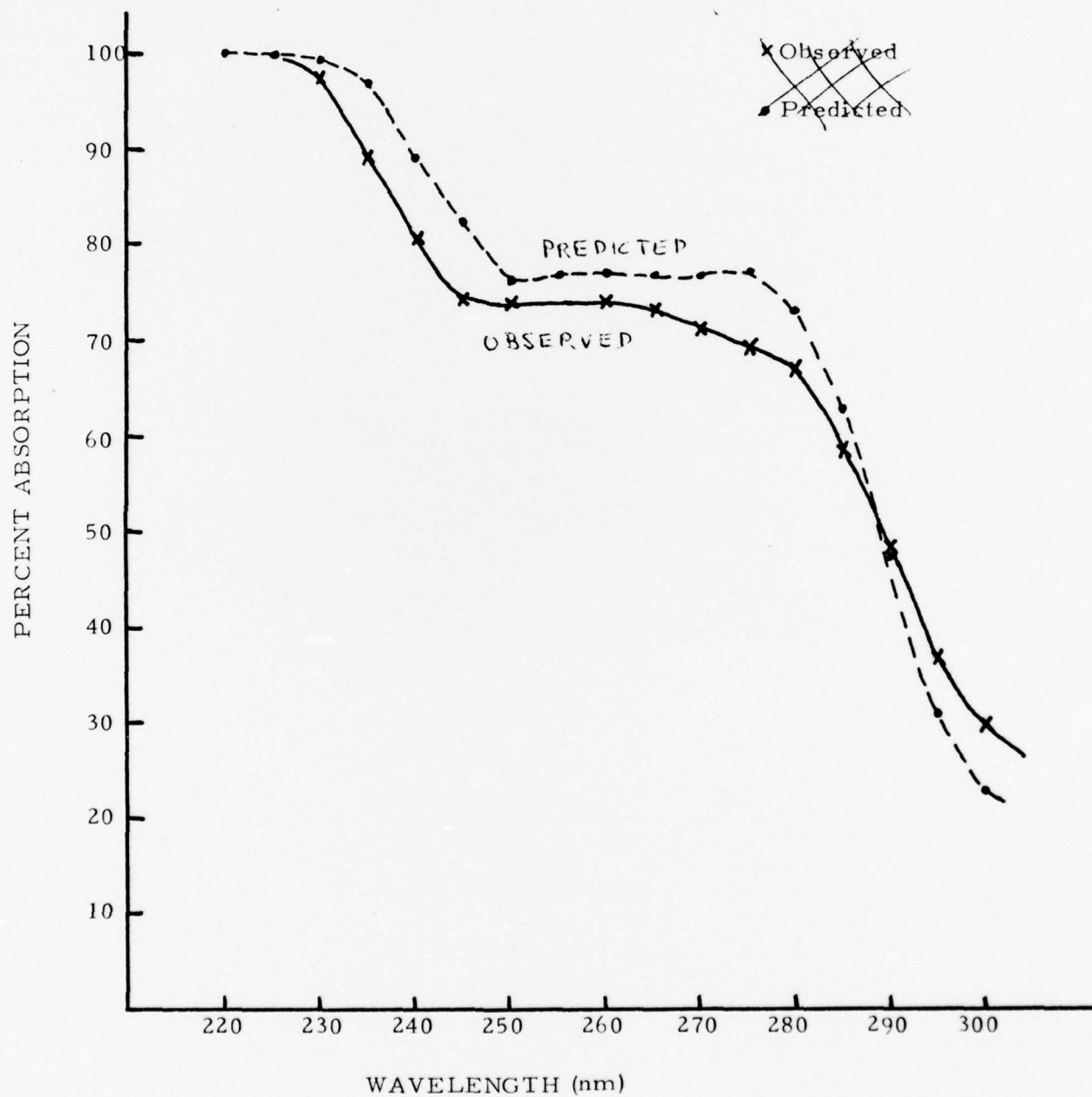
The UV absorbing species in the cornea, then, have been identified as the aromatic amino acids of proteins and the bases of nucleic acids. In order to show that these components satisfactorily explain the observed absorption spectra for the epithelium and the entire cornea, theoretical absorption curves can be constructed. The construction is straightforward and explained in Appendix I. The calculated and observed absorption spectra for the corneal epithelium are compared in Figure 15. A close fit is obtained over the entire far UV. The fact that the observed and predicted curves are not quite parallel and cross at 290 nm is probably due to choosing a particular protein containing a slightly different ratio of aromatic amino acids than the average composition for the cell.

The absorption spectrum for the entire cornea (Figure 2) is trivially reproduced by merely considering the absorption of a 500 μ thick protein solution of the proper concentration (approximately 20%). This shows a steep rise in absorption beginning about 320 nm and reaching 100% near 280 nm.

The origin of the residual absorption of the cornea above 320 nm is not clear. The extinction coefficients of proteins and nucleic acids are very low above 320 nm and have not been measured accurately. There are undoubtedly trace amounts of many other molecules in the cornea which may absorb in the 320-400 nm range. Because of the weak absorption, relatively high levels of incident radiation are required to cause observable damage in this wavelength range. Whether the dominant mechanism for damage is photochemical in nature or not is open to speculation.

Because the absorption coefficients of proteins and nucleic acids vary considerably with wavelength in the far UV, the fraction of absorbed energy actually deposited at protein sites or at nucleic acid sites is also strongly dependent on wavelength. However, the relative absorptions of each species at any wavelength are readily calculated

FIGURE 15. ABSORPTION SPECTRUM OF CORNEAL EPITHELIUM (RABBIT)



as detailed in Appendix I. Reciprocals of these absorptions which for lack of a better term will be called "relative transmissions" are plotted in Figure 16. The reciprocals are chosen so that the curves can be compared to the action spectrum for photokeratitis also shown in Figure 16. It is seen that while proteins continue to absorb more and more of the incident energy as the wavelength is lowered below 260 nm, the nucleic acid sites begin to absorb less (despite their higher extinction coefficients at shorter wavelengths) because of the greater shielding effect of the proteins. Interestingly enough the action spectrum for photokeratitis (except for the anomolous peak at 250 nm) runs roughly parallel to the nucleic acid relative transmission curve. This taken together with many in vitro and in vivo studies of photochemical damage to biological systems¹⁵⁻¹⁶ gives indirect support to the identification of nucleic acids (in particular the evidence points to the DNA of the chromosomes) as the primary sites for photochemical damage which lead to cell death.

FIGURE 16.

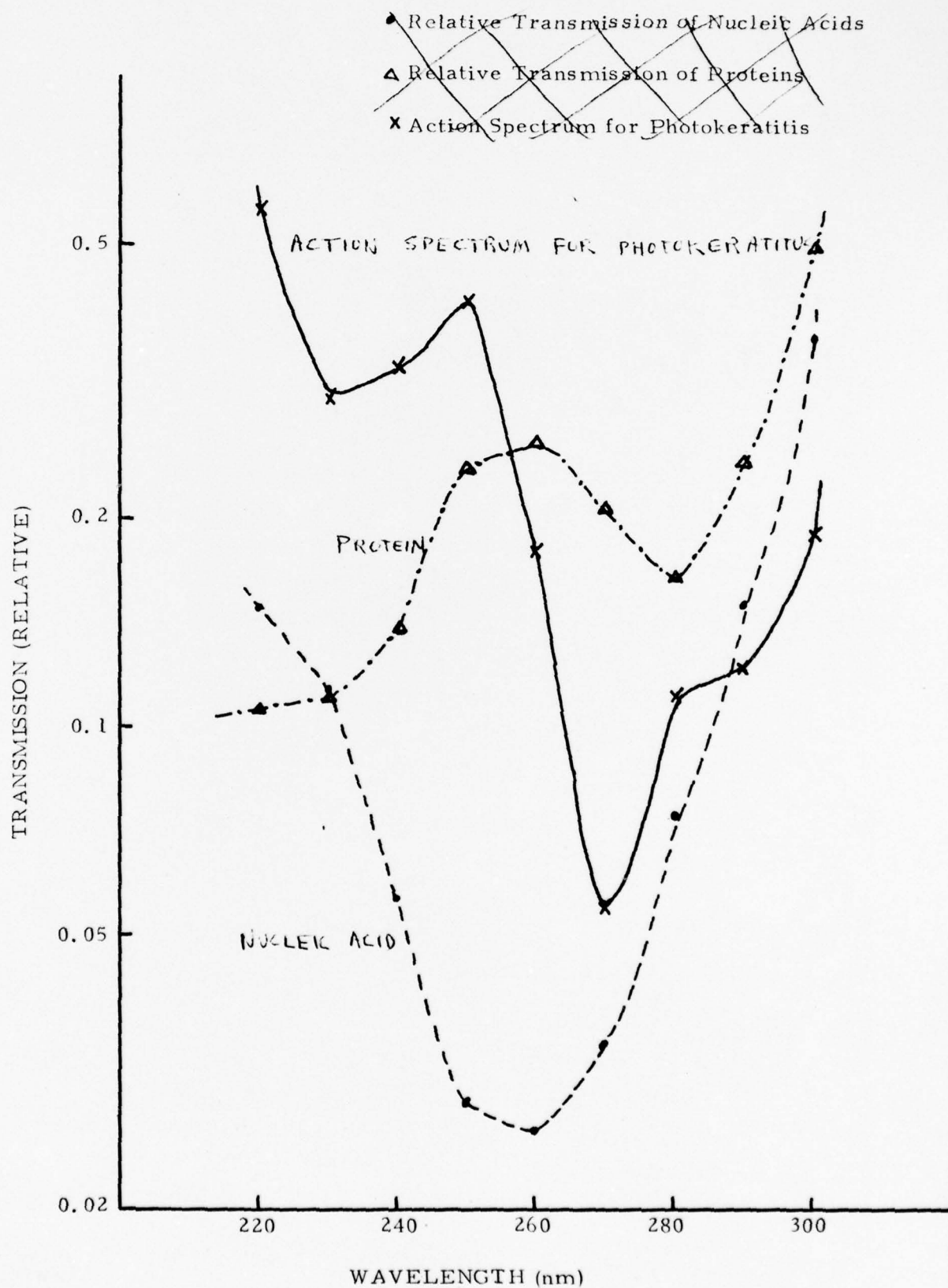


FIGURE 16. RELATIVE TRANSMISSIONS OF PROTEIN AND NUCLEIC ACID IN CORNEAL EPITHELIUM

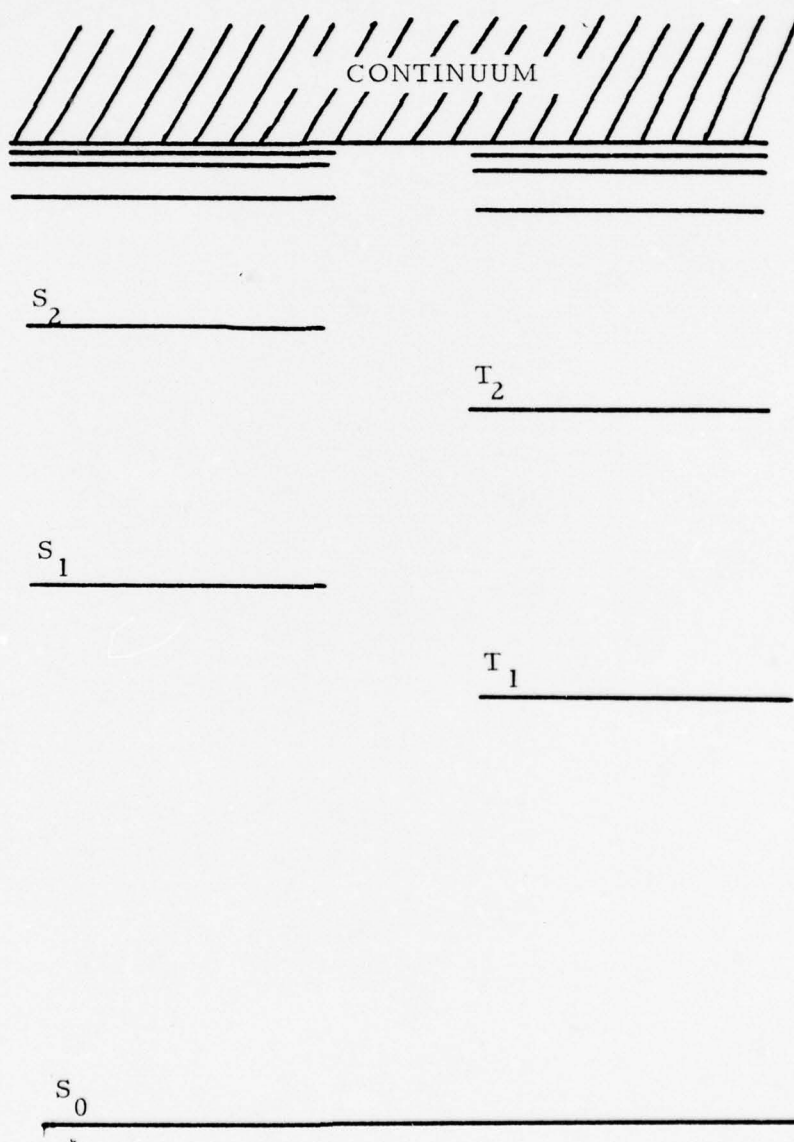
II-E MOLECULAR ELECTRONIC EXCITATION

As implied previously, radiation of wavelengths in the near and far UV can induce a variety of photochemical reactions in the cornea and possibly in other components of the primate eye. Such radiation is absorbed by aromatic chromophores found in proteins and nucleic acids and can promote an electron of these molecules from its unperturbed state to a molecular orbital of higher energy. The absorbing species then finds itself in a highly labile state from which it may enter into a chemical reaction with a molecular neighbor using its excess electronic energy, in a sense, as an activation energy for the reaction.

The number of molecular lesions formed via photo-induced chemical reactions will be proportional to the number of absorbing sites which are promoted to the labile excited states. It is the purpose of this section of the report to derive expressions for the populations of the excited states as functions of the parameters of the exciting beam.

A general molecular electronic energy level diagram is shown in Figure 17. S_0 represents the unperturbed or ground state of the molecule $S_1, S_2 \dots$ represent a series of excited electronic states of successively higher energy. $T_1, T_2 \dots$ represent another series of excited states which, unlike the S states, have a non-zero electron spin associated with them. The reason that two (and only two) series of excited states must be considered when an electron is promoted to a higher energy level is, briefly, as follows: Electron spins may be treated as vector quantities⁽¹⁾ constrained to lie along a particular molecular axis. In the ground state, S_0 , all electrons of the molecule are paired and the spins of each pair aligned in opposite directions^(↑↓) so that the net spin of the molecule is zero. When an electron is promoted to a higher energy level one pair of electrons

FIGURE II-17. MOLECULAR ELECTRONIC
ENERGY LEVEL DIAGRAM



is disengaged and no longer restricted to point in opposite directions. If the original spin configuration, ($\uparrow\downarrow$) is, in fact, maintained, the excited state is a singlet or S state, as is the ground state. However, the two unpaired electrons are now free to choose a parallel configuration ($\uparrow\uparrow$), in which case the excited state is a triplet or T state.

Figure 17 shows that at higher energies the spacings between adjacent levels becomes less and less until finally a continuum of energy states is reached. This continuum represents the unbound or ionized state of the electron. In general, the energy of a photon associated with wavelengths greater than 200 nm is not sufficient to cause ionization in an aromatic molecule. The UV absorption spectra of these molecules are due to the electronic transitions $S_0 \rightarrow S_1$, $S_0 \rightarrow S_2$, etc. Absorption may also occur from S_0 to any triplet state but the extinction coefficients for these transitions are so low that they do not contribute any measureable intensity to the absorption spectra. (Quantum mechanically these are spin forbidden transitions.)

Because the density of levels is great at higher energies, the probability for spontaneous emission is high (the energy may be efficiently dispersed in small packets) and the lifetimes of S_2 , T_2 and all higher lying electronic states are very short (picoseconds or less). If a molecule finds itself in the S_1 or T_1 state, however, there is a relatively large energy gap down to the ground state and the probability for spontaneous emission is relatively low so that S_1 and T_1 may have considerably longer lifetimes. Lifetimes of S_1 states are commonly of the order of nanoseconds and T_1 states of the order of microseconds in solutions at room temperature.

The significance of the excited state lifetimes is simply that the lifetimes of the higher lying electronic states are too short to engage in chemical reactions with the surrounding medium. (Intermolecular collision rates are diffusion controlled processes and of the order of

10^{10} sec^{-1} in solutions). Therefore, no matter what state the molecule is originally excited to (short of direct ionization) the most likely result is that the molecule will partially disperse the absorbed energy and drop down to either the S_1 or T_1 state before any other process can occur. Chemical reactions may then proceed from these states.

For our purposes, therefore, it is sufficient to consider the electronic energy level diagram to consist of three levels. This system along with the rate constants for transitions between the levels is shown in Figure 18. The absorption process is represented by a rate constant $C(\lambda)I$ where $C(\lambda)$ is the molecular cross section for absorption (a wavelength dependent term) and I is the intensity of the excitation source.

Some rate constants for excited states of protein and nucleic acid components are reported in reference 17. For these molecules k_f and k_c are of the order of 10^9 sec^{-1} and k_p of the order of 10^6 sec^{-1} . These figures are for solutions at room temperature. In rigid media k_f and k_c are usually unchanged but k_p may be several orders of magnitude less. For the most part the protein and nucleic acid constituents of cells are effectively in aqueous solutions. This may not necessarily be true for structural protein such as the collagen fibres of the stroma. In considering photochemical mechanisms in such media this wide range of possible values for k_p should be kept in mind.

The remaining rate constants of Figure 18 represent the various processes for photodamage. k_s and k_t are the rates for spontaneous generation of molecular lesions (through chemical reaction) from the S_1 and T_1 states respectively. $C_s(\lambda)I$ and $C_t(\lambda)I$ are the rates for absorption of a second photon, which may result in ionization.

Quantum yields for photodamage (i. e., the number of molecular lesions formed divided by the number of photons absorbed) are very

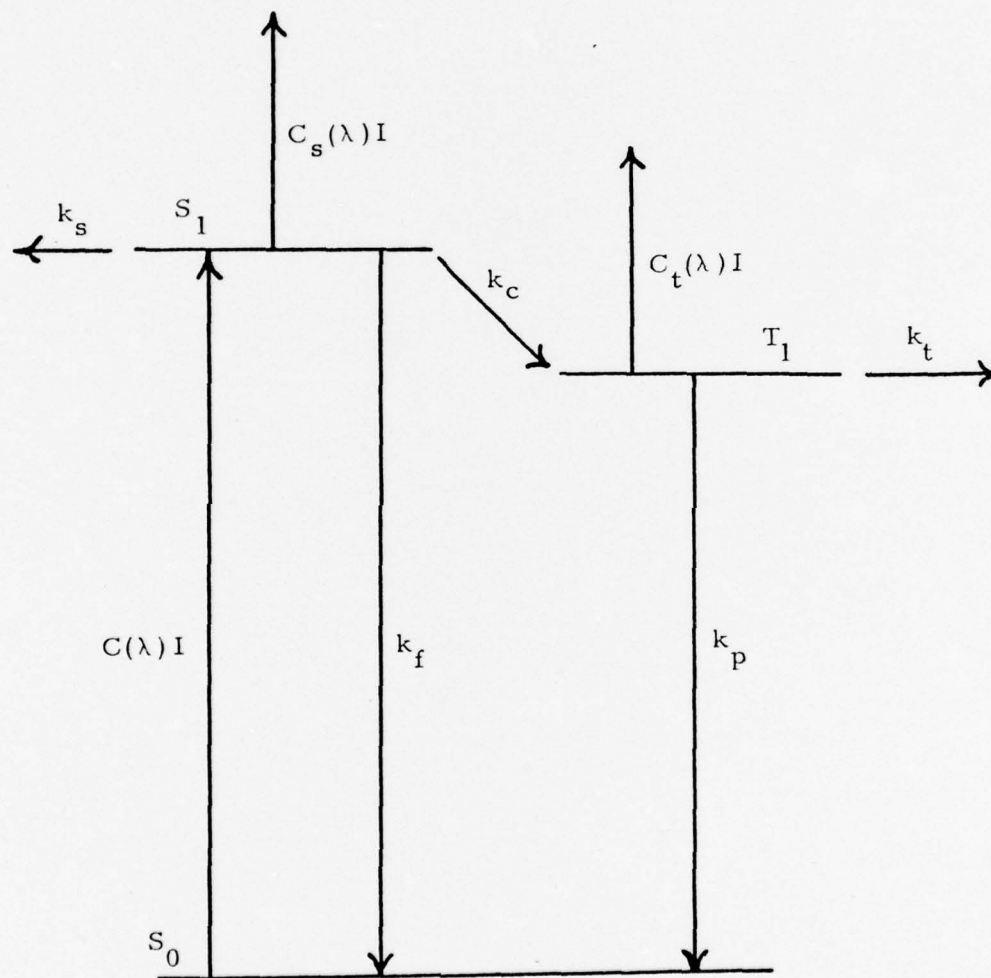


FIGURE II-18. THREE LEVEL ELECTRONIC ENERGY
LEVEL DIAGRAM

small for the cases considered here, being of the order of 10^{-3} or less for proteins, nucleic acids, and their constituents. This implies that the rate constants leading to photodamage are much smaller than the rate constants for transitions between the electronic energy levels. Therefore, these rate constants are initially neglected and later treated as perturbations to the rate equations solved below.

If $S_0(t)$, $S_1(t)$ and $T_1(t)$ are taken as the time dependent populations of the S_0 , S_1 and T_1 states respectively, the rate equations for the populations are:

$$\begin{aligned}\frac{d S_0(t)}{dt} &= -C(\lambda) I S_0(t) + k_f S_1(t) + k_p T_1(t) \\ \frac{d S_1(t)}{dt} &= C(\lambda) I S_0(t) - (k_f + k_c) S_1(t) \\ \frac{d T_1(t)}{dt} &= k_c S_1(t) - k_p T_1(t)\end{aligned}\tag{1}$$

At any given time the sum of the three populations will be:

$$S_0(t) + S_1(t) + T_1(t) = N^0\tag{2}$$

where N^0 is the total number of molecules.

This relationship can be used to eliminate one of the variables, say $S_0(t)$, from Eq. (1) to yield:

$$\begin{aligned}\frac{d S_1(t)}{dt} &= C(\lambda) I N^0 - C(\lambda) I T_1(t) - [k_f + k_c + C(\lambda) I] S_1(t) \\ \frac{d T_1(t)}{dt} &= k_c S_1(t) - k_p T_1(t)\end{aligned}\tag{3}$$

A general solution for Eq. (3) can be found by established

mathematical techniques¹⁸. The result which is discussed in further detail in Appendix II is of the form:

$$S_1(t) = c_1 e^{\lambda_1 t} + c_2 e^{\lambda_2 t} + m$$

$$T_1(t) = c_1 e^{\lambda_1 t} \left(\frac{k_c}{\lambda_1 + k_p} \right) + c_2 e^{\lambda_2 t} \left(\frac{k_c}{\lambda_2 + k_p} \right) + n \quad (4)$$

where c_1 , c_2 , n and m are constants which are determined from boundary conditions. λ_1 and λ_2 are the roots of the quadratic secular equation resulting from Eq. (3). As seen in Appendix II, λ_1 and λ_2 as well as the constants are each functions of $C(\lambda)$ and I .

If the production of photoproducts proceeds spontaneously from the S_1 and/or T_1 states the number of molecular lesions formed will be proportional to the integral over all time of $S_1(t)$ and/or $T_1(t)$. If photodamage occurs through the mechanism of absorption of a second photon the number of molecular lesions formed will be proportional to the integral over all time of $C_s(\lambda)IS_1(t)$ and/or $C_t(\lambda)IT_1(t)$ ^{19,20}. The intensity, I , is implicitly a function of time but is generally taken to be a constant for the duration of the pulse, τ , and zero otherwise.

In principal, therefore, the explicit dependence of the number of molecular lesions on the intensity, wavelength (through $C(\lambda)$) and pulsewidth (as a constant of integration) is known. As can be seen from Appendix II, the dependence on I , τ , and $C(\lambda)$ is extremely complicated. However, relatively simple expressions can be derived in certain limits which cover most experimentally interesting conditions.

It has already been pointed out that the properties of the molecules being considered here are such that k_p is much less than k_c and k_f . It will be assumed that the rate constant $C(\lambda)I$ is small

compared to each of the other rate constants. Equivalently stated, it is assumed that there is no appreciable population inversion between the ground and S_1 or T_1 states. From a brief consideration of the molecular properties, it is anticipated that this assumption will be valid outside of the Q-switched laser regime.

With negligible population inversion, the expressions for $S_1(t)$ and $T_1(t)$ reduce to:

$$\begin{aligned} S_1(t) &\approx S_1^0 \left[1 - e^{-(k_f + k_c)t} \right] \\ T_1(t) &\approx T_1^0 \left[1 - e^{-k_p t} \right] \end{aligned} \tag{5}$$

where S_1^0 and T_1^0 are the steady state populations which would be reached with constant illumination, (see Appendix II). Thus, the population $S_1(t)$ approaches the steady state value exponentially with a time constant $\frac{1}{k_f + k_c}$ and $T_1(t)$ approaches steady state with a time constant $\frac{1}{k_p}$.

With Eq. (5), the analysis for either a single pulse or a general train of pulses becomes straightforward. Consider first a single pulse having a pulsewidth, τ , much greater than $\frac{1}{k_p}$. (Generally this will mean $\tau > 10^{-6}$ sec. However, as explained above, in certain media $\frac{1}{k_p}$ may be several orders of magnitude larger.) In this case, the steady state populations will be reached and maintained throughout the duration of the irradiation. With the populations taken as constants the integrations over time become trivial. As shown in Appendix II, the number of molecular lesions formed if the photodamage occurs directly from the S_1 and/or T_1 states is then linearly proportional to the quantities $C(\lambda)$, I and τ . However, if the photodamage occurs

only after absorption of a second photon the number of lesions formed is seen to be proportional to I^2 , τ and either $C_s(\lambda) C(\lambda)$ or $C_t(\lambda) C(\lambda)$ depending upon whether S_1 or T_1 is the intermediate state. In either case, the amount of damage is proportional to I^2 for a two photon process and the wavelength dependence is more complicated by being a product of extinction coefficients for the two independent absorptions. (Experimental data for $C_s(\lambda)$ and $C_t(\lambda)$ is unavailable for protein and nucleic acid constituents.)

For a single pulse with $\frac{1}{k_p} > \tau \gg \frac{1}{k_f + k_c}$ (10^{-9} sec $\ll \tau$), the analysis is the same as above for photodamage proceeding through the S_1 state. The T_1 will likely be relatively ineffective in contributing to photodamage in this instance since little population will accumulate in T_1 with such a short pulsewidth.

For a pulsewidth less than $\frac{1}{k_f + k_c}$ (less than a nanosecond) relatively little photodamage is likely to occur unless the intensity of the radiation is sufficient to violate the assumption of negligible population inversion between S_1 and S_0 . While the mathematical solution of the problem may still be tractable without this assumption, there seems little incentive to pursue the more complicated analysis unless it can be experimentally demonstrated that the approximate solutions derived above do, in fact, break down in this limit.

If instead of a single pulse, the exposure consists of a train of n pulses of intensity I_i and pulsewidth τ_i the total number of molecular lesions formed by the train will be proportional to $\sum_{i=1}^n I_i \tau_i$ for damage occurring directly from the S_1 or T_1 states and proportional to $\sum_{i=1}^n I_i^2 \tau_i$ for lesions occurring following absorption of a second photon. The only requirement on the time interval between successive pulses is that it be long enough ($\gg \frac{1}{k_p}$) for all excited molecules to return to the ground state following each pulse.

A simple experiment may be proposed to distinguish between the two mechanisms discussed above. Let the wavelength and the pulsewidth be fixed and I_{TH} be the intensity required for threshold damage from a single pulse at the given λ and τ . Then for a sequence of n identical pulses the intensity required for threshold damage will be I_{TH}/n if the mechanism for photodamage is that of generation of molecular lesions directly from the S_1 and/or T_1 states. If the mechanism is that of absorption of a second photon, the threshold intensity for a sequence of n pulses will be I_{TH}/\sqrt{n} . This analysis will be valid at any wavelength where photochemistry is the dominant damage mechanism. In fact, even for more closely spaced sequences of pulses, the dependence of the number of lesions formed on I will be the same as above. The dependence upon the pulsewidths will be considerably more complicated since τ will appear in the exponential terms of Eq. (4) after the integration over time is carried out.

II-F SUMMARY OF PROPOSED EXPERIMENTS

Figure 4 illustrates an action spectrum for threshold damage in the corneal epithelium caused by a non-coherent radiation source. It covers the far UV wavelength range. No comparable data is available for damage from coherent radiation sources. Further, little quantitative data is available for ocular radiation damage in the near UV and it is not clear which component(s) of the eye have the lowest damage threshold in this wavelength range. Where studies have been published of ocular damage from UV radiation, no more than brief speculation is provided as to the nature of the mechanisms involved.

It is suggested that a suitable starting point for the experimental aspects of the current program would be the generation of data for epithelial damage from UV lasers which would be comparable to the data for non-coherent radiation represented by Figure 4. This is the first on the list of proposed experiments which follows. The remaining experiments are placed in the order in which they were referred to in earlier sections of the report with no priorities implied by the ordering.

- 1) Corneal epithelial damage from UV lasers; comparison with non-coherent UV radiation: Experimentally it must be established whether or not the physical appearance of the lesions caused by far UV lasers is similar to that for non-coherent UV radiation, whether the same end points can be used to define threshold damage in the two cases and whether the measured threshold exposure levels are similar. Preliminary experiments while comparing the two cases would also attempt to identify the end point which was most quantitatively reproducible for the case of coherent radiation. Once a suitable end point is established, threshold determinations should be made for several different wavelengths in the far UV to

compare the wavelength dependence to that shown in Figure 4.

2) Corneal stromal damage from UV lasers: Because of the permanent nature of stromal lesions, it is desirable to establish a guide to threshold levels for the stroma. Preliminary experiments would try to define a suitable end point for this type of damage. Eventually it is desirable to establish the wavelength dependence for stromal damage for comparison with that for epithelial damage. Because of the difference in composition of the two layers this comparison could help to resolve the question of which type of molecular lesion (protein or nucleic acid) leads to the observed macroscopic damage in each case.

3) Lens damage from UV lasers: As discussed earlier the lens may be the most sensitive component of the eye over part of the near UV. The most favorable wavelength to test this possibility is at 366 nm where the lens has an absorption maximum. Since cataract formation can be a very long term process, some difficulty may be encountered in defining an end point for threshold damage. It is suggested that for preliminary studies a possible end point is the reversible lens clouding which appears five to ten days after exposures which lead to long term cataract formation⁵. Once this clouding clears, no evidence of radiation damage is apparent until the cataract forms months or even several years later.

4) Wavelength dependence of retinal damage threshold in the near UV: As reported in Part I the threshold for retinal damage does not vary with wavelength over most of the visible. However, as the wavelength is shortened to the visible - UV border, the amount of radiation being transmitted through the anterior components of the eye becomes severely attenuated and the threshold for retinal damage will rise rapidly. Since continuously tunable lasers are now available in this range, this wavelength dependence could

and should be studied.

5) Crossover wavelengths: As a logical extension of the experiments outlined above it is noted that the cornea, retina and possibly the lens are each the most sensitive components of the eye to radiations of different wavelengths. Setting an allowable exposure standard at any given wavelength must obviously involve identifying the primary site of damage from radiation of that wavelength and further identifying the mechanism(s) for damage at that site so that the dependence on the laser beam parameters may be specified. This will involve a series of observations at wavelengths between 280 nm (where the cornea is the primary damage site and a photochemical mechanism is thought to dominate) and 450 nm (where the retina is the most sensitive ocular component and the damage mechanism is thermal in nature).

6) Repair mechanisms in the corneal epithelium: The cumulative effect predicted for photochemical damage is obviously valid only over periods of time where no measureable radiation repair occurs. For the epithelium there is (at least) an effective repair rate of the order of one day due to the normal replacement rate of epithelial cells. Whether there is any repair mechanism over and above this can only be determined by experimental observation. Threshold determinations for exposures consisting of two equivalent doses with a varying time interval between doses would be the simplest experimental approach to this problem.

7) Cumulative effect: It appears that the most straightforward experimental support for the proposed photochemical model would be verification of the predicted cumulative effect. For a series of n identical pulses, the damage threshold is predicted to be either I_{TH}/n or I_{TH}/\sqrt{n} where I_{TH} is the threshold intensity for a

single pulse. Therefore, a series of threshold determinations for a single pulse and then sequences of 2, 3, 4... identical pulses could confirm the presence of the cumulative effect and also distinguish between the two types of photochemical processes which have been described.

Finally, there are several other experiments which may eventually be of great significance depending on the results of preliminary studies outlined above. Briefly, these are:

8) Laser microbeam exposures to identify the most sensitive cellular components under various conditions.

9) Radiation damage dependence upon the direction of polarization for media which may have oriented molecular constituents (e.g., the corneal stroma and the lens).

10) Studies of lens damage resulting from heating effects from exposures of the iris to UV laser radiation.

II-G APPENDIX I

MOLECULAR ABSORPTION IN THE CORNEAL EPITHELIUM

The absorbance, A , of a solution of concentration c and optical path b is defined as follows:

$$A = \epsilon b c = \log_{10} I_0/I \quad (I-1)$$

where I_0 is the intensity of the incident radiation and I is the intensity of the transmitted radiation. ϵ is the molar extinction coefficient provided that c is in units of moles per liter and b is in units of centimeters. The quantity A is also referred to as "optical density", "extinction" and "absorbancy".

If the molecular weight of the absorbing species is unknown, it is standard procedure to report the absorbance of a 1% (by weight) solution with a 1 cm optical path. This absorbance is symbolized by $A_{1\text{cm}}^{1\%}$.

For a solution with more than one absorbing species, the absorbances are additive.

The absorbing species of the corneal epithelium have been identified as the aromatic amino acids of proteins and the bases of nucleic acids. The absorption spectra shown in Figure 12 are taken to represent the absorption spectra for all protein and nucleic acids in the epithelium. The values of $A_{1\text{cm}}^{1\%}$ for these species are presented in Table I.

The proteins and nucleic acids may be localized in particular regions of the epithelial cells. However, for purposes of calculating the absorbance of this layer on a macroscopic scale, the epithelium is assumed to be a homogeneous mixture of protein and nucleic acid. The absorbance of the layer is thus:

TABLE II-1

ABSORPTION OF THE CORNEAL EPITHELIUM

| Wavelength | Solution Absorbances | | Epithelial Absorption | |
|------------|-----------------------|-----------------------|------------------------------|--|
| (nm) | $(A_p)^{1\%}$ 1 cm | $(A_n)^{1\%}$ 1 cm | $A = A_p + A_n = \log I_0/I$ | % Absorption $= (1 - I/I_0) \times 100$ |
| 220 | 42 | 76 | 3.38 | 99.96 |
| 225 | 31 | 66 | 2.52 | 99.7 |
| 230 | 26 | 58 | 2.12 | 99.2 |
| 235 | 18 | 59 | 1.53 | 97.1 |
| 240 | 10 | 63 | .939 | 88.5 |
| 245 | 7.0 | 77 | .756 | 82.5 |
| 250 | 4.5 | 94 | .620 | 76.0 |
| 255 | 4.0 | 111 | .636 | 76.9 |
| 260 | 4.3 | 108 | .647 | 77.5 |
| 265 | 4.7 | 97 | .644 | 77.3 |
| 270 | 5.3 | 79 | .635 | 76.8 |
| 275 | 6.3 | 58 | .647 | 77.5 |
| 280 | 6.3 | 35 | .578 | 73.6 |
| 285 | 4.7 | 25 | .428 | 62.8 |
| 290 | 3.2 | 13 | .279 | 47.4 |
| 295 | 1.8 | 8.0 | .159 | 30.7 |
| 300 | 1.3 | 4.4 | .113 | 22.9 |

$$A = A_p + A_n = \epsilon_p b c_p + \epsilon_n b c_n \quad (I-2)$$

where the subscripts p and n refer to protein and nucleic acid respectively and b is the thickness of the epithelium. The quantities reported in the first two columns of Table 1 are A_p and A_n for 1% solutions, 1 cm in thickness. The thickness of the epithelium will be taken as 50 μ . The composition previously reported for the epithelium was 80% (by weight) water with 75% of the dry material being protein and 3% being nucleic acid. Therefore, the epithelium is taken to be a solution with 15% protein and 0.6% nucleic acid. The absorbance of this layer is thus:

$$\begin{aligned} A = A_p + A_n &= (A_p)_{1\text{cm}}^{1\%} \times 15 \times 5 \cdot 10^{-3} + (A_n)_{1\text{cm}}^{1\%} \times 0.6 \times 5 \cdot 10^{-3} \\ &= 0.075 (A_p)_{1\text{cm}}^{1\%} + 0.003 (A_n)_{1\text{cm}}^{1\%} \end{aligned} \quad (I-3)$$

The calculated absorbance is shown in the third column of Table I. The percent absorption is shown in the last column and plotted along with the experimental absorption spectrum in Figure 15.

It is of interest to calculate the fraction of absorbed energy deposited with each absorbing species at any given wavelength. The fraction f_i absorbed by the i^{th} species is, in general:

$$f_i = \frac{A_i}{\sum_j A_j} \quad (I-4)$$

where the summation is over all absorbing species in the solution. The fractions f_p and f_n for the protein and nucleic acid components of the epithelium are reported in Table 2. The relative absorption of the i^{th} component will then be the product of the percent absorption of the epithelium at any wavelength and the corresponding fraction f_i at that wavelength. These products are listed along with their

TABLE II-2

RELATIVE ABSORPTIONS OF PROTEIN AND NUCLEIC
ACID COMPONENTS OF EPITHELIUM

| Wavelength | Fractional Absorbances | | Relative Absorptions | | Relative Transmissions | |
|------------|------------------------|-------|----------------------|------------------|------------------------|--------------------|
| (nm) | f_p | f_n | $f_p \times \%A$ | $f_n \times \%A$ | $1/f_p \times \%A$ | $1/f_n \times \%A$ |
| 220 | .993 | .067 | 93.3 | 6.70 | .011 | .149 |
| 225 | .922 | .078 | 91.9 | 7.78 | .011 | .129 |
| 230 | .918 | .082 | 91.1 | 8.13 | .011 | .123 |
| 235 | .884 | .116 | 85.8 | 11.3 | .012 | .089 |
| 240 | .799 | .201 | 70.7 | 17.8 | .014 | .056 |
| 245 | .694 | .306 | 57.3 | 25.2 | .018 | .040 |
| 250 | .545 | .455 | 41.4 | 34.6 | .024 | .029 |
| 255 | .474 | .526 | 36.5 | 40.4 | .027 | .025 |
| 260 | .499 | .501 | 38.7 | 38.8 | .026 | .026 |
| 265 | .548 | .452 | 42.4 | 34.9 | .024 | .029 |
| 270 | .626 | .374 | 48.1 | 28.7 | .021 | .035 |
| 275 | .731 | .269 | 56.7 | 20.8 | .018 | .048 |
| 280 | .818 | .182 | 60.2 | 13.4 | .017 | .075 |
| 285 | .825 | .175 | 51.8 | 11.0 | .019 | .091 |
| 290 | .860 | .140 | 40.8 | 6.64 | .025 | .151 |
| 295 | .849 | .151 | 26.1 | 4.64 | .038 | .216 |
| 300 | .881 | .119 | 20.2 | 2.73 | .050 | .367 |

reciprocals in Table 2. The reciprocals or "relative transmissions" are plotted in Figure 16, where they are compared with the action spectrum for photokeratitis.

II-H APPENDIX II

SOLUTION OF THE RATE EQUATIONS FOR ELECTRONIC EXCITATION

The rate equations for the populations of the three level system shown in Figure 18 are as follows:

$$\begin{aligned}\frac{dS_0(t)}{dt} &= -C(\lambda)IS_0(t) + k_f S_1(t) + k_p T_1(t) \\ \frac{dS_1(t)}{dt} &= C(\lambda)IS_0(t) - (k_f + k_c) S_1(t) \\ \frac{dT_1}{dt} &= k_c S_1(t) - k_p T_1(t)\end{aligned}\tag{II-1}$$

where the rate constants for photodamage have been neglected relative to the rate constants for transitions between the three levels. At any given time, the sum of the three populations will be related by:

$$S_0(t) + S_1(t) + T_1(t) = N^0\tag{II-2}$$

where N^0 is the total number of absorbing molecules in the system.

(II-2) can be used to eliminate one of the variables (S_0 is chosen in this case) from (II-1) so that the system of rate equations reduces to:

$$\begin{aligned}\frac{dS_1(t)}{dt} &= C(\lambda)I [N^0 - T_1(t)] - [k_f + k_c + C(\lambda)I] S_1(t) \\ \frac{dT_1(t)}{dt} &= k_c S_1(t) - k_p T_1(t)\end{aligned}\tag{II-3}$$

This is a nonhomogeneous coupled pair of linear differential equations.

The general solution will be the sum of any particular solution of the nonhomogeneous equations plus the general solution of the homogeneous pair of equations¹⁸.

If a square-wave pulse is assumed so that the intensity, I , is a constant during the period of irradiation (and zero otherwise), the solution of (II-3) is simplified since the coefficients are now time independent and a pair of constants m and n will suffice as the particular solution. The solution of the homogeneous pair of equations is straightforward¹⁸ and the general solution of (II-3) is found to be:

$$S_1(t) = c_1 e^{\lambda_1 t} + c_2 e^{\lambda_2 t} + m \quad (\text{II-4})$$

$$T_1(t) = c_1 e^{\lambda_1 t} \left(\frac{k_c}{\lambda_1 + k_p} \right) + c_2 e^{\lambda_2 t} \left(\frac{k_c}{\lambda_2 + k_p} \right) + n$$

where:

$$\lambda_{1,2} = \frac{-(k_p + k_f + k_c + C(\lambda)I) \pm \sqrt{(k_p + k_f + k_c + C(\lambda)I)^2 - 4k_c C(\lambda)I - 4k_p(k_f + k_c + C(\lambda)I)}}{2} \quad (\text{II-5})$$

and c_1 , c_2 , m and n are constants which are determined by the boundary condition of the problem.

The initial conditions are that $S_1(t)$ and $T_1(t)$ are equal to zero at $t = 0$ (all molecules are in the ground state before the irradiation commences). The final conditions which must be satisfied are that if the irradiation continues for a sufficiently long time (with I constant) a steady state will be reached with populations S_1^0 and T_1^0 for the S_1 and T_1 states respectively. The steady state populations are found from (II-3) by setting the time derivatives equal to zero, thus:

$$\begin{aligned} C(\lambda)IN^0 - C(\lambda)IT_1^0 &= [k_f + k_c + C(\lambda)I] S_1^0 \\ k_c S_1^0 &= k_p T_1^0 \end{aligned} \quad (\text{II-6})$$

This yields:

$$n = T_1^0 = \frac{C(\lambda) I N^0}{C(\lambda) I + [k_f + k_c + C(\lambda) I] k_p / k_c} \quad (II-7)$$

$$m = S_1^0 = \frac{k_p}{k_c} T_1^0$$

The constants c_1 and c_2 are then found by substituting (II-7) into (II-4) at $t = 0$. The results are

$$c_1 = \frac{T_1^0 (\lambda_1 + k_p) (\lambda_2 + 2k_p)}{k_c (\lambda_1 + \lambda_2)} \quad (II-8)$$

$$c_2 = -\frac{k_p}{k_c} T_1^0 - c_1$$

In the limit of negligible population inversion of S_1 and T_1 with respect to S_0 , $C(\lambda)I$ is neglected relative to k_f , k_c and k_p . The properties of the molecules under consideration are such that k_p may be neglected relative to k_f and k_c . With these simplifications (II-5) reduces to:

$$\lambda_1 \approx -k_p \quad (II-9)$$

$$\lambda_2 \approx -(k_f + k_c)$$

and the populations become:

$$S_1(t) \approx S_1^0 [1 - e^{-(k_f + k_c)t}] \quad (II-10)$$

$$T_1(t) \approx T_1^0 [1 - e^{-k_p t}]$$

where:

$$T_1^0 \approx \frac{k_c C(\lambda) I N^0}{k_p (k_f + k_c)}$$

$$S_1^0 \approx \frac{C(\lambda) I N^0}{k_f + k_c}$$
(II-11)

Thus, $S_1(t)$ approaches its steady state value with a time constant $\frac{1}{k_f + k_c}$ and $T_1(t)$ approaches steady state with a time constant $\frac{1}{k_p}$.

The total number of molecular lesions formed directly from the S_1 and T_1 states will be proportional to the integrals of (II-10) over time:

$$\begin{aligned} \int_0^\infty S_1(t) dt &\approx \int_0^\tau S_1^0 [1 - e^{-(k_f + k_c)t}] dt \\ &= S_1^0 \tau + \frac{S_1^0}{k_f + k_c} [e^{-(k_f + k_c)\tau} - 1] \end{aligned}$$

$$\begin{aligned} \int_0^\infty T_1(t) dt &\approx \int_0^\tau T_1^0 [1 - e^{-k_p t}] dt \\ &= T_1^0 \tau + \frac{T_1^0}{k_p} [e^{-k_p \tau} - 1] \end{aligned}$$
(II-12)

If the pulse width, τ , is long with respect to $\frac{1}{k_f + k_c}$, the integral for $S_1(t)$ reduces to $S_1^0 \tau$ so that the number of lesions formed directly from the S_1 state is given by the expression:

$$\frac{C(\lambda) I N^0 \tau}{k_f + k_c}$$
(II-13)

If τ is also long with respect to $\frac{1}{k_p}$, the second integral of (II-12)

reduces to:

$$\frac{k_c C(\lambda) I N^0 \tau}{k_p (k_f + k_c)} \quad (\text{II-14})$$

which is proportional to the number of lesions formed from the T_1 state.

For the cases where photodamage occurs after absorption of a second photon the number of molecular lesions formed will be proportional to the integrals:

$$\int_0^\tau C_s(\lambda) I S_1(t) dt$$

$$\int_0^\tau C_t(\lambda) I T_1(t) dt \quad (\text{II-15})$$

which in the limits where (II-13) and (II-14) are valid reduce to:

$$\frac{C_s(\lambda) C(\lambda) I^2 N^0 \tau}{k_f + k_c}$$

and (II-16)

$$\frac{k_c C_t(\lambda) C(\lambda) I^2 N^0 \tau}{k_p (k_f + k_c)}$$

for two photon processes with S_1 and T_1 respectively as the intermediate states.

II-I REFERENCES

1. E. A. Boettner, Final Report, Contract AF41(609)-2966, Project No. 6301, University of Michigan (July, 1967).
2. V. Kinsey, Arch. Ophthal., 39, 508 (1948).
3. D. G. Pitts, et al., SAM-TR-69-10 (February, 1969).
4. G. F. Cooper and J. G. Robson, J. Physiol., 203, 411 (1969).
5. A. Bachem, Amer. J. Ophthal. 41, 969 (1956).
6. R. W. Ebbers, private communication.
7. "The Physiology of the Eye," 3rd Edition, H. Davson, Academic Press, New York (1972).
8. "Wolff's Anatomy of the Eye and Orbit," 6th Edition, R. J. Last, W. B. Saunders Co., Philadelphia (1968).
9. R. C. French and Z. Duma, Can. J. Biochem. Physiol. 41, 1005 (1963).
10. D. M. Maurice and M. V. Riley in "Biochemistry of the Eye" (C. Graymore, ed.) Academic Press, New York (1970).
11. "The Molecular Basis of Life: Readings from Scientific American," W. H. Freeman and Co., San Francisco (1968).
12. "The Chemical Foundations of Molecular Biology," R. F. Steiner, D. van Nostrand Co., Princeton (1965).
13. "The Proteins" (H. Neurath and K. Bailey, eds.) Academic Press, New York (1955).
14. "The Nucleic Acids," E. Chargaff and J. Davidson, Academic Press, New York (1955).

REFERENCES (cont'd)

15. "Photochemistry of Proteins and Nucleic Acids," A. McLaren and D. Shugar, Pergamon Press, New York (1964).
16. "Molecular Photobiology," K. Smith and P. Hanawalt, Academic Press, New York (1969).
17. "Excited States of Proteins and Nucleic Acids," (R. F. Steiner and I. Weinryb, eds.) Plenum Press, New York (1971).
18. "Introduction to Ordinary Differential Equations," S. L. Ross, Blaisdell Publishing Co., Waltham, Mass. (1966).
19. S. Siegel and K. Eisenthal, J. Chem. Phys. 42, 2382 (1965).
20. H. B. Steen, Photochem. and Photobiol. 9, 479 (1969).